ALIGNED CARBON NANOTUBE CARPETS ON CARBON SUBSTRATES FOR HIGH POWER ELECTRONIC APPLICATIONS

Betty Tun-Huan Quinton

Mechanical and Thermal Systems Branch
Power and Control Division

JUNE 2016
Interim Report

AIR FORCE RESEARCH LABORATORY
AEROSPACE SYSTEMS DIRECTORATE
WRIGHT-PATTERSON AIR FORCE BASE, OH 45433-7542
AIR FORCE MATERIEL COMMAND
UNITED STATES AIR FORCE

NOTICE AND SIGNATURE PAGE

REPORT DOCUMENTATION PAGE		*Form Approved* OMB No. 0704-0188

The public reporting burden for this collection of information is estimated to average 1 hour per response, including the time for reviewing instructions, searching existing data sources, gathering and maintaining the data needed, and completing and reviewing the collection of information. Send comments regarding this burden estimate or any other aspect of this collection of information, including suggestions for reducing this burden, to Department of Defense, Washington Headquarters Services, Directorate for Information Operations and Reports (0704-0188), 1215 Jefferson Davis Highway, Suite 1204, Arlington, VA 22202-4302. Respondents should be aware that notwithstanding any other provision of law, no person shall be subject to any penalty for failing to comply with a collection of information if it does not display a currently valid OMB control number. **PLEASE DO NOT RETURN YOUR FORM TO THE ABOVE ADDRESS**.

1. REPORT DATE *(DD-MM-YY)* June 2016	2. REPORT TYPE Interim	3. DATES COVERED *(From - To)* 01 January 2014 – 01 June 2016

4. TITLE AND SUBTITLE
ALIGNED CARBON NANOTUBE CARPETS ON CARBON SUBSTRATES FOR HIGH POWER ELECTRONIC APPLICATIONS

5a. CONTRACT NUMBER In-house
5b. GRANT NUMBER
5c. PROGRAM ELEMENT NUMBER 62203F

6. AUTHOR(S)
Betty Tun-Huan Quinton

5d. PROJECT NUMBER 3145
5e. TASK NUMBER
5f. WORK UNIT NUMBER Q0LA

7. PERFORMING ORGANIZATION NAME(S) AND ADDRESS(ES)
Mechanical and Thermal Systems Branch (AFRL/RQQM)
Power and Control Division
Air Force Research Laboratory, Aerospace Systems Directorate
Wright-Patterson Air Force Base, OH 45433-7542
Air Force Materiel Command, United States Air Force

8. PERFORMING ORGANIZATION REPORT NUMBER
AFRL-RQ-WP-TR-2017-0160

9. SPONSORING/MONITORING AGENCY NAME(S) AND ADDRESS(ES)
Air Force Research Laboratory
Aerospace Systems Directorate
Wright-Patterson Air Force Base, OH 45433-7542
Air Force Materiel Command
United States Air Force

10. SPONSORING/MONITORING AGENCY ACRONYM(S)
AFRL/RQQM
11. SPONSORING/MONITORING AGENCY REPORT NUMBER(S)
AFRL-RQ-WP-TR-2017-0160

12. DISTRIBUTION/AVAILABILITY STATEMENT
DISTRIBUTION STATEMENT A: Approved for public release. Distribution is unlimited.

13. SUPPLEMENTARY NOTES
PA Case Number: 88ABW-2016-3045; Clearance Date: 17 June 2016.

This thesis is in partial fulfillment of the requirements for the degree of Doctor of Philosophy submitted to Wright State University in 2016. This is a work of the U.S. Government and is not subject to copyright protection in the United States.

14. ABSTRACT
One of the driving forces behind nanotechnology research is the miniaturization of electronic devices. Electrical and thermal transport properties of device materials at micrometer and nanometer scales become very important in such applications. Carbon materials, especially carbon nanotubes (CNTs), have exceptionally low density and superior electrical, thermal, and mechanical properties. Vertically aligned CNTs attached to lightweight carbon substrates may hold the key to fully use these outstanding properties. However, the majority of studies reported to date involve either loosely unattached CNTs or CNTs attached to traditional electronic grade silicon, which have limited use in lightweight electronic components. Studies of CNT arrays attached to carbon substrates are extremely scarce, but if successful, such a composition could lead to unprecedented lightweight electronic devices with superior electrical and thermal transport properties. This dissertation is aimed at performing detailed investigation of such structures.

This work investigates the synthesis-structure-property relationships of CNT arrays attached to carbon surfaces relevant to power electronic applications. Several detailed investigations were performed to achieve the goal of creating multiscale combination materials and to test their feasibility as high power electronic devices. Background studies were piloted to determine the most practical growth technique and growth parameters in order to achieve dense CNT growth. Floating catalyst chemical vapor deposition was determined to be the most effective, scalable, and reliable growth method. In addition, an oxide buffer layer was deemed necessary for dense CNTs growth on carbon substrate. Several oxides were compared in order to determine the most suitable for CNTs growth while providing superior thermal properties. Among the buffer oxides investigated in this study, the ALD Al_2O_3 buffer layer provided the fastest CNT nucleation and most uniform size distribution. However, Al_2O_3 buffer layer was plagued by adhesion issues, which may limit future applications. Plasma SiO_2 offers a slower initial nucleation rate, but yields the tallest carpet height in identical growth conditions, and also appears to be the most stable and repeatable.

15. SUBJECT TERMS thermal management, two-phase flow, flow visualization, electric capacitance tomography

16. SECURITY CLASSIFICATION OF:			17. LIMITATION OF ABSTRACT:	18. NUMBER OF PAGES	19a. NAME OF RESPONSIBLE PERSON (Monitor)
a. REPORT Unclassified	**b. ABSTRACT** Unclassified	**c. THIS PAGE** Unclassified	SAR	134	Travis E. Michalak **19b. TELEPHONE NUMBER** (Include Area Code) N/A

Standard Form 298 (Rev. 8-98)
Prescribed by ANSI Std. Z39-18

Aligned Carbon Nanotube Carpets on Carbon Substrates for High Power Electronic Applications

A dissertation submitted in partial fulfillment of the
requirements for the degree of
Doctor of Philosophy

By

Betty Tun-Huan Quinton
M.S. Egr., Wright State University, 2008
B.S., University of Illinois at Chicago, 2006

2016
Wright State University
WRIGHT STATE UNIVERSITY

Abstract

Quinton, Betty Tun-Huan. Ph.D., Engineering Ph.D. Program, Wright State University, 2016. Aligned Carbon Nanotube Carpets On Carbon Substrates for High Power Electronic Applications.

One of the driving forces behind nanotechnology research is the miniaturization of electronic devices. Electrical and thermal transport properties of device materials at micrometer and nanometer scales become very important in such applications. Carbon materials, especially carbon nanotubes (CNTs), have exceptionally low density and superior electrical, thermal, and mechanical properties. Vertically aligned CNTs attached to lightweight carbon substrates may hold the key to fully use these outstanding properties. However, the majority of studies reported to date involve either loosely unattached CNTs or CNTs attached to traditional electronic grade silicon, which have limited use in lightweight electronic components. Studies of CNT arrays attached to carbon substrates are extremely scarce, but if successful, such a composition could lead to unprecedented lightweight electronic devices with superior electrical and thermal transport properties. This dissertation is aimed at performing detailed investigation of such structures.

This work investigates the synthesis-structure-property relationships of CNT arrays attached to carbon surfaces relevant to power electronic applications. Several detailed investigations were performed to achieve the goal of creating multiscale combination materials and to test their feasibility as high power electronic devices. Background studies were piloted to determine the most practical growth technique and growth parameters in order to achieve dense CNT growth. Floating catalyst chemical vapor deposition was determined to be the most effective, scalable, and reliable growth method. In addition, an oxide buffer layer was deemed necessary for dense CNTs growth on carbon substrate. Several oxides were compared in order to determine the most suitable for CNTs growth while providing superior thermal properties. Among the buffer oxides investigated in this study, the ALD Al_2O_3 buffer layer provided the fastest CNT nucleation and most uniform size distribution. However, Al_2O_3 buffer layer was plagued by adhesion issues, which may limit future applications. Plasma SiO_2 offers a slower initial nucleation rate, but yields the tallest carpet height in identical growth conditions, and also appears to be the most stable and repeatable.

Thermal investigations were conducted on the final products, which consisted of aligned CNTs arrays of different carpet heights on carbon substrates. Observations show that the thermal resistance of the CNT array varies linearly with CNT carpet height, as expected. This variation was used to estimate the thermal conductivity of multi-walled nanotube in the carpet, and found to be approximately 35W/m-K. This value shows promise that such lightweight structure can replace current commercially available products.

This dissertation will reveal key results and discuss the investigations from the following areas: comparing chemical vapor deposition growth techniques, the importance of oxide buffer layer on carbon substrates, the effect of buffer layer composition, the effect of oxide thickness and growth time on CNT carpet height, and the feasibility of such lightweight structures for power electronics through thermal analysis investigations.

Keywords: Carbon nanotubes (CNTs), chemical vapor deposition (CVD), thermal interface material (TIM), oxide buffer layers.

Acknowledgements

I would like to express my heartfelt thanks and deep sense of gratitude to the many people who have guided me through this research project. This work would not have been possible without their supports, efforts, mentorships, and friendships.

First and foremost, I would like to thank my advisor, Professor Sharmila Mukhopadhyay, for her exceptional guidance, and support throughout this dissertation work. She has been a great source of inspiration and wisdom. Dr. Mukhopadhyay's mentorship has helped me become a better researcher.

I would also like to thank the Aerospace Systems Directorate of Air Force Research Laboratory (AFRL) for the Pathways Program. This internship opportunity have provide me with a once in a lifetime learning opportunity, and allowing me to conduct and coordinate many of my experiments in a top notch laboratory facility. I have met many mentors along the way and I am forever grateful for their teachings and techniques. Furthermore, I would like to thank all my committee members for their insightful inputs on my dissertation and positive feedback during all the discussion.

This dissertation would not have been possible without the outermost support, understanding, and the backing of my family. Special thanks go to my parents, husband and TingTing for their unconditional love, encouragement, and inspiration.

I would also like to thank my colleagues and mentors whom I met at Wright State University and at AFRL for their time to discuss and exchange ideas related to research and friendship. They have made this journey much more enjoyable and memorable!

Dedication

This dissertation is dedicated to my lovely Mom
For the endless love, strength, support, and inspiration.

Table of Contents

DISTRIBUTION STATEMENT A: Approved for public release. Distribution is unlimited.

List of Figures

DISTRIBUTION STATEMENT A: Approved for public release. Distribution is unlimited.

List of Tables

List of Equations

Section I: Introduction and Background
(Materials Information and Processing Techniques)

CHAPTER 1 Introduction
1.1 Introduction

As the technology trend shows, there is an extremely high demand for lightweight materials in wide ranges of industrial and consumer electronic devices. For example, in consumer industry, the ability to reduce weight can translate to lighter and more portable computing devices. In addition, lightweight components can also benefit industrial, and defense sector such as automotive and aerospace industries, because lightweight components translates into significant saving in fuel consumption and cost of operation.

However, as device shrink in size, the amount of heat generated has less space to dissipate. Therefore thermal conduction of nanometer material places a critical role in controlling the performance of nano/micro devices. Improper thermal management can affect performance, reliability and the life expectancy of the electronic element. Exploring new material or materials combinations to address this issue is very important and can be beneficial. This research will attempt to address this issue by using materials that are both lightweight and have high thermal conductivity values.

Substituting bulk materials for lighter alternatives have evolved greatly over time. In order to properly select the optimal material for a specific task, balance among performance, reliability, cost, function and manufacturability should be considered carefully. In the earlier days, natural materials were used such as wood, bulk metal, natural rubber, and simple alloys. Next, as technology advances, engineered materials such as complex alloys, ceramics, and synthetic polymers becomes available. Furthermore, advanced engineered technology allows creations of complex engineered material such as thin films, patterned arrays, nanoparticles, foams, fiber composites and much more to be created or manufactured. Today, with the modern technology, specialized materials are engineered through precise technology processes to create customized configurations with specific dimension and geometries that ranges from nanoscale to bulk size. The advanced modern engineering process enables engineers to combine different materials together to achieve desired properties, performances and functionalities.

In recent years, technology has advanced in ways that allows electronic devices to become more robust, compact, and portable. However, to be able to continue on this trend of miniaturization, issues involving thermal management needs to be address. As electronic devices shrink in size, components are fitted closer to each other. However, the amount of heat generated by these components has less area to dissipate. Excess heat, if not rapidly dissipated away from the nanoscale electronic components, can lead to signal instabilities and rapid device degradation with time. To keep these components operating effectively and avoid damages due to overheating, there is a significant need for efficient thermal management. In addition, one common issue is failure at the device/substrate interfaces due to thermal expansion mismatch between different compositions. Therefore, optimizing thermal transport through the interface is necessary to ensure stable performance. This calls for new strategies of integrating emerging materials and/or material combinations for future thermal management devices. One of the ways of addressing the above issue is to investigate fabrication methods involving advanced materials, structures, and surface modifications for the next generation of thermal management materials suitable for high power electronic devices.

1.2 Motivation

This research is motivated by the need to create lightweight components that are efficient at addressing thermal transport properties. To accomplish this, the focus of the research will be on the investigation of carbon-based architectures that can simultaneously address the demands of lightweight materials as well as and their critical thermal management advantages. The goal is to provide insights for design and manufacturing of sophisticated multifunctional thermal interface materials in the nanoscale range. This research looks for ways to incorporate nanomaterials with bulk materials, so that innovative structures with better performances can be fabricated with specific design metrics.

Carbon is lightweight material that has very strong potential for use in future thermal management devices. Carbon comes in a variety of allotropic forms, and offers high thermal conductivity along specific planes. Combining different forms of carbon can improve thermal throughput while minimizing thermal expansion mismatches and improve device compliance. One configuration of particular interest is carbon substrate attached with vertically aligned carbon nanotubes (CNTs). It is believed that carbon materials paired in this configuration would enable higher thermal conductivity interfaces while offering interfacial mechanical flexibility.

Due to its fascinating inherent material properties, CNTs have achieved an iconic status in recent scientific and engineering research communities. These properties include high aspect ratios, lightweight, high thermal conductivity, superior mechanical properties, and attractive electrical characteristics[2]–[6]. They allow CNT to be attractive in a wide variety of advanced applications such as biological sensors[7], biological applications [8]–[10], antennae [11], purification filters [12],[13], composites[14]–[18], catalyst supports [10], [13], [19], thermal management [4], [20]–[22] and thermal interface materials [2], [22]. However, current lab-scale devices made with CNTs still struggle to demonstrate properties that are close to theoretically predicted values. Often, the discrepancies are related to the qualities of the CNTs, their arrangements, and the interfaces involved.

Previous model studies have validated that by incorporating CNTs on silicon substrates, the interfacial thermal conductivity of the composite was improved [23]. Currently, many of the CNT-based thermal device studies reported use CNTs in a dispersed manor that are loosely supported on a surface or on electronic silicon substrates. However, thermal transport properties may be improved if CNTs are attached vertically on the necessary substrate. Therefore incorporating CNTs on unconventional lightweight substrates, such as carbon-based solids, should be investigated.

Growing CNTs on carbon substrates has several advantages. Not only are they the same chemically, but they also satisfy the lightweight, chemically inert, and high conductivity requirements needed for robust devices. However growing CNTs on carbon substrate has known to be challenging, and only a few investigations were conducted in the recent years [24], [25]. In Pulikollu's dissertation work it was observed that through surface modification, the surface of carbon can interchange between an inert or reactive surface [24]. It was also found that a reactive surface can promote other carbon structures, such as CNTs, to grow on the surface thereby increasing the surface area by several order of magnitude [8], [13], [24], [25]. Investigations that utilize this new combination of CNT on carbon includes biological applications [8]–[10], water filtration [13], and phase change heat storage [25]. It is also believed that components in this configuration, CNT attached on graphite, benefits thermal applications. CNT used as thermal interface material is beneficial because it can make the

thermal interface more mechanically compliant, which reduces interface delamination. In addition, CNT does not suffer from drying, which is a common problem that thermal greases have, therefore CNT based TIM should prolongs the application usage.

One key issue not adequately investigated so far is in-depth understanding of CNT-substrate interfacial region in these arrays, and the influence of those on physical and thermal properties of the final device. Underlying this region is essential for better understanding the controllability of CNTs growth on carbon substrate as well as the effect of buffer layer usage on carbon substrate for desirable CNT growth. This dissertation research is carefully designed to address some of the above issues by investigating factors that influence CNTs growth on carbon substrates and investigating the feasibility of using CNTs-Carbon hybrid materials as thermal management devices.

1.3 Scope and Objectives

The main objective of this research is to address the emerging thermal transport issue of shrinking devices by demonstrate dense CNT structure growth on planar and porous carbon substrate and test the feasibility as thermal management material for electronic devices. This investigation will explore ways to combine lightweight materials that have high thermal conductivity values, CNT on carbon substrates. In addition, the study will explore ways to enhance CNT growth density on suitable lightweight substrates. Minimal CNT growth density should provide full substrate coverage, so that substrates are not exposed from underneath via visual examination. Other studies will focus in key issues such as growth of dense CNTs arrays on different types (allotropes and geometries) of carbon substrates, and to test the feasibility of the hybrid structure (CNT arrays on substrate) as thermal interface material. To accomplish this, several sub-tasks were studied as follows:

1. To first understand the growth of CNTs on dense sp^3 carbon materials that have high thermal conductivity and low electrical conductivity, such as diamond. This study compares different CNTs fabrication methods on diamond substrates via chemical vapor deposition (CVD) methods.
2. To grow CNTs on sp^2 carbon substrates, which are electrically conductive, lightweight, and have wider substrate geometries selections. One of the goals is to achieve dense CNT growth on porous graphitic substrates that has high specific surface area, such as carbon foam. This study was done by studying various surface treatment methods to improve CNTs growth density on porous substrates.
3. Investigation of different oxide buffer layer material (alumina and silica), oxide thickness, and growth time were performed. In order to understand key factors that affects CNTs' growth controllability in terms of array density, diameter, and height.
4. Perform high resolution electron microscopy of the CNT-substrate interfaces, and relate this region to CNTs structure and thermal transport properties.
5. Conduct thermal analysis on fabricated samples and study the influence of CNT arrays on thermal transport properties.

The following chapters explain each portions of the research in more detail.

CHAPTER 2 Background
2.1 Background and Literature Reviews

The quest of making smaller electronic devices is one of the main driving forces behind nanotechnology. As electronic devices reduce in size and weight, there is less room for heat generated to dissipate. Therefore adequate thermal conduction through the nanomaterials becomes more critical. Improper thermal management of electronics systems can dramatically decrease the life expectancy of electronic components. Electronic components often fail at the interface due to thermal stress and mismatching thermal expansion properties between materials bonded together. One way to avoid this issue is to select materials that have similar thermal expansion properties, as well as high thermal conductivity values.

Early reporting of CNT has been on common semiconducting substrates such as silicon or silicon oxide, while other reports reference using loose CNTs incorporated into polymer or grease materials for study of thermal properties. Studies that report growing CNTs on lightweight material such as carbon substrates are less common. Some have reported growing CNTs on diamond seeds [26], diamond nano-rods grown from CNT [27], and simultaneously growth of CNTs and diamond [28]. However, none of these reported growth of CNTs on bulk carbon substrates.

Part of this research effort has been to identify the best ways to grow CNTs on carbon substrates. The investigation begins by summarizing different chemical vapor deposition (CVD) methods of CNT growth on substrates that have high thermal conductivity values, such as polycrystalline diamond. Diamond substrate was chosen due to its high strength and high wearability, as well as its low coefficient thermal expansion (CTE), which matches closely with graphite. The CTE values are, 1, 2 and 17 x 10^{-6} k^{-1} for diamond, graphite, and copper, respectively [29]–[31]. Once the CNT growth on diamond substrates was characterized, the investigation followed with CNT growth on various planar and porous carbon substrates for high-performance thermal applications. Finally, the last portion of the research was defined by thermal evaluations on the CNT-substrate samples grown. The thermal evaluation is very important, as it characterizes the thermal properties of an all carbon system used in this study. By doing so, it will demonstrate the feasibility of using an all carbon system as a thermal management device.

2.2 Significance of Carbon and Its Allotropes

Carbon is the 6th element on the periodic table and it has a molecular weight of 12.01g/mole. It resides in column IV of the periodic table. In its ground state, carbon's electronic configuration is expressed as $1S^2 2S^2 2P^2$, and it has four electrons at its outer valence shell. Materials in nature tend to minimize energy in order to keep a balance and be in their most stable state. Therefore, it is natural to think that carbon will make 4 single bonds due to 4 available electrons in its unfilled outer shell. However, it was found that carbon comes in a variety of molecular structures that consist of various types of carbon-to-carbon bonds [32], [33].

Hybridized orbitals are formed by combination of 2s and 2p energy states into sp, sp^2 and sp^3 hybridization. The hybridization also determines the structure, bonding angle, bond energy, and properties of the resulting molecule. For example, due to hybridization of orbitals, carbon is able to form in a variety of allotropic forms. Stable and meta-stable forms of carbon consist of graphite and diamond, respectively. The main difference between graphite and diamond is how

the carbon atoms are bonded together. In diamond, carbon atoms are bonded in sp^3 formation where each carbon atom is tetrahedrally bonded with three other carbon atoms.

With sp hybridization, each electron in the *2s* orbital hybridizes with one of the *2p* orbital to form two sp hybridized orbitals in a straight line with bonding angle of 180°. In this configuration, the carbon has one single bond and one triple bond with 2 nearest neighbors, as in ethyne. Next, sp^2 hybridization has one *2s* orbital and two *2p* orbital hybridized to form three sp^2. In this hybridization, orbitals aligned themselves into a trigonal planar, where the carbon has one double bond and two single bond structures with a bonding angle at 120° and 3 nearest neighbors as in graphite and benzene. Finally, carbon uses one *2s* and three *3p* orbitals forming 4 sp^3 orbitals. In this configuration carbon has 4 nearest neighbors each forming a single bond with bonding angle at 109.2°. This results in the tetrahedral shape observed in diamond structures. Figure 1, illustrates several bonded carbon structures/configurations.
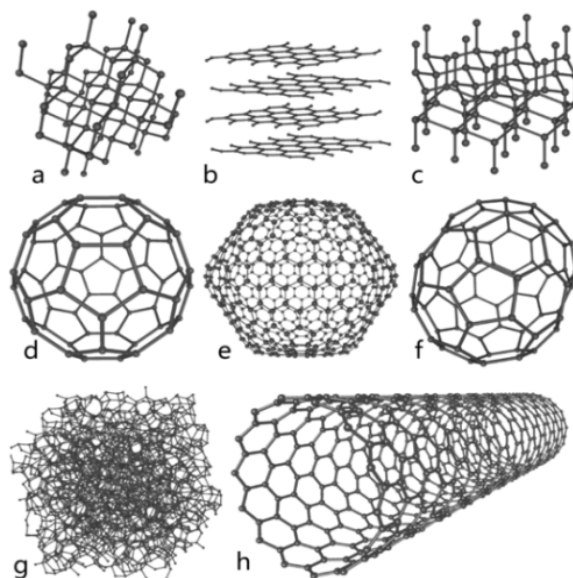
Figure 1: Allotropic forms of Carbon (Figure from Wikipedia) a) diamond, b) graphite, c) lonsdaleite d) C60 buckminsterfullerene, e) C540, Fullerite f) C70, g) amorphous carbon, and h) single-walled carbon nanotube

2.3 Diamond vs. Graphite

Diamond and graphite are the two most abundant forms of carbon allotropes. Graphite is a stable and diamond is a meta-stable form of carbon. Let us take a closer look at the differences between diamond and graphite and glassy carbon as these allotropes were the substrates that the CNT were grown on. Diamond and graphite comes from the Greek words of adamas and graphos, which means "invincible" and "to write" respectively. Although they are chemically the same, their properties are very different. Diamond is a sp^3 hybridized carbon structure, and it has 4 nearest neighbors. Each carbon atom is tetrahedrally bonded at 109.5° from three other carbon atoms with the same bond length. This bonding structure produces regular three dimensional arrays of carbon atoms. The carbon atoms in a diamond configuration are tightly bonded.

Graphite, on the other hand, is a sp^2 hybridized carbon structure that has 3 identical bonds that form in a planar configuration. The pi-bonds in this configuration are bonded cooperatively in plane, while the 4th electron on the graphite is de-localized. This configuration produces strong in-plane covalent bonds and weak de-localized bonds normal to the plane. The weak

DISTRIBUTION STATEMENT A: Approved for public release. Distribution is unlimited.

through plane bonds allow graphene planes to slide easily pass one another. This is a reason why graphite is used as a dry lubricant on locks and machineries and also for writing. In addition, the de-localized electron provides graphite's electrical conductive property. These are some important fundamental differences between diamond and graphite. Figure 2, illustrates the lattice structure and bulk appearance of diamond and graphite. In addition, Figure 2 shows some similarities and difference between the physical properties between diamond and graphite.

Diamond / SP^3
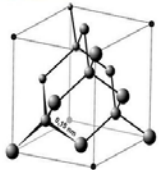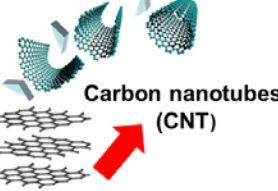
- Mohs Hardness Scale: 10
- Strong bonding, scratch and wear resistant
- Electrical insulator: S = 1 x 10^{-3} S/m
- Density = 3.51g/cm^3
- Coefficient of Thermal Expansion (CTE):
  - 1 x 10^{-6}K^{-1}
- High thermal conductivity value
  - 2000 W/mK (ref: Hone)
- High index of refraction

Graphite / SP^2 — Carbon nanotubes (CNT)

- Mohs Hardness Scale: 1.5
- Strong in-plane and weak out-of-plane bonding
- Electrical conductor: S = 1x 10^5 S/m
- Density = 2.09g/cm^3
- Coefficient of Thermal Expansion (CTE):
  - 1.5 x 10^{-6}K^{-1}
- sp^2 carbon varieties
  - Highly Oriented Pyrolyzed Graphite (HOPG)
    - Anisotropic thermal properties
  - Pressed Graphite
  - Reticulated Vitreous Carbon (RVC)
  - Carbon nanotubes
    - 3000 W/mK (ref: Hone, Drekker ENN 2004)

Figure 2: Figures of Diamond and Graphite along with Some of Its Physical Properties

2.4 Carbon Nanotube

The structure of CNT is similar to graphite. A single atomic layer (2-D sheet) of graphite is called graphene, and CNTs can be described as a graphene sheets rolled up into a tube structure. Graphite is a layered structure, where each carbon atom has three valence electrons in plane making of a net of hexagonal "honeycomb" pattern. It also has a 4th valence electron that is located perpendicular to the hexagonal plan. Due to this 4th bond, each sheet of graphene is located at a distance of 3.35 Å apart in the interlayer direction [33], [34]. These graphene bonds are connected through weak Van der Waals forces that loosely stack the graphene sheets together. Because of this, the carbons planes can easily glide pass one another as well as being cleaved easily. In addition, this is the reason why the electrons do not pass easily in the normal direction. As a result, graphene and CNTs are anisotropic when it comes to thermal or electrical conductivity.

Since their discovery in 1991 [35], CNTs can arguably be considered as another natural allotropic form of carbon. There are two main types of CNTs. One is called, single wall CNT (SWNT) and the other is multi-wall CNT (MWNT). This dissertation focuses on the latter. The first evaluation of CNTs was in the mid 70's when researchers were more focused on researching carbon fibers. It was through the work of Endo et al. that people saw the first set of SWNT and MWNT in HRTEM images [36]. However, CNTs did not become a significant research topic until Iijima published his findings on tubular carbon structures. Soon after that, other groups

published articles on different methods of synthesizing CNTs. Currently it is known that CNTs can be fabricated using a wide variety of methods such as arc-discharge, pyrolysis, laser ablation, electrolysis and chemical vapor deposition (CVD) [33]. This research uses CVD to grow CNTs, and it will be discussed in more detail in Chapter 4. Several articles have reported theoretical calculations of CNT properties, and it was predicted that SWNTs had metallic or semi-metallic properties based on tube chirality and that MWNT were only metallic [32], [37]. Mechanical testing of MWNT was done and the result demonstrated that CNTs are much stronger and more flexible than carbon fibers. From these preliminary results and publications, CNTs soon become a leading research area. It was thought that the potential applications of combined properties of CNTs were endless. Some journal articles also identified different morphologies of CNTs, such as spaghetti, bamboo or coiled shaped ones. To make coiled tubes, defects such as pentagon and heptagon shaped rings must be formed. Dekker's group named the areas with pentagon or heptagons rings 5-7 defects [38]. These defects are resulted from thermolytic process with different growth rate or agglomeration. Dekker et al, also suggested that locations with pentagon rings exhibit higher residual strain and greater chemical reactivity than hexagonal areas [38]. Other CNT morphologies have also been reported, such as cone shaped or bamboo-like shaped [39]–[42]. CNTs are unique because they have a high aspect ratio, a hollow core, high tensile strength, and they are both electrically and thermally conductive. Utilizing one or two physical properties, mentioned above, one can incorporate CNT in areas such as gas storage [43], field emission sources [44], high power capacitors [45], nano switches [46], chemical sensors [47], composites [14], thermal interface material [2], and the list goes on. However, it is necessary to understand CNT growth mechanisms and how to control and modify CNT properties in order to tailor them to a specific application. A portion of this dissertation is spent on understanding variables that affect the CNTs growth mechanism and morphology. The proposed future work addresses how CNTs could be used to enhance properties of applications.

2.4.1 Physical Properties of CNTs

2.4.1.1 Electrical properties:

It was mentioned earlier that CNTs are a rolled up sheet of graphene. It was understood that CNTs can either be a single-wall SWNT or MWNT. For SWNTs, it can be further divided into one of the three types depending on how the tube is rolled up, and they are known as armchair, zigzag, and chiral [32]. According to Dresselhaus, the armchair type of SWNT is the only one that is considered metallic, the other two are semiconductors [48]. MWNT are predominately metallic due to its metallic outer shell. According to Kordrostami, a significant benefit of CNTs is that they contain long mean free paths in the micrometer range and can handle a large current density [49]. These are favorable characteristics of material properties for future electronic devices. Furthermore, it's been suggested that the CNT preparations method can strongly affect the overall electrical property and performance [50].

2.4.1.2 Thermal properties:

Diamond and in plane graphite both exhibit extremely high thermal conductivity values. It has been reported that CNTs also exhibit high thermal conductivity that is dominated by phonons at all temperatures along the tube axis. In graphite the phonon only dominates specific heat above 20K [2]. Kim reported individual MWNT have higher recorded thermal conductivity value than diamond at room temperature with a value of 3000W/mK [2], [3], [51]. Due to the high thermal conductivity value, CNTs may be beneficial to be used in areas such as heat sinks and thermal interfaces.

2.4.1.3 Mechanical properties:

The carbon-to-carbon bond that exists in graphite is one of the strongest in nature. It has been published that CNTs are strong and flexible, which allow it to resist breaking upon bending. CNTs regularly demonstrate an average Young's Modulus of $Y = 1$-1.8 TPa, which is much higher than carbon fibers with $Y = 800$ GPa [52], [53]. The high strength and flexible nature of CNTs are perfect for areas such as lightweight composites or even atomic force microscopy (AFM) tips.

2.5 Possible Applications with CNTs

With the physical properties mentioned above, it is easy to see that CNTs have the ability to be very versatile and useful in many future applications. However, due to wide variations in fabrication methods, [arc discharge, laser ablation, chemical vapor deposition (CVD)], not all CNTs are created equal. To optimize CNT growth parameters a detailed study usually needs to be performed. However even with an optimal recipe developed for one system, it is possible that different tubes can be grown if a different system was used. In this investigation, three different CVD processes have been compared initially and one was selected as the growth method for the reminder of the investigation. The selected growth method was deeming most ideal to achieve the investigation need, while producing CNTs that are aligned and densely grown on the substrate. A detailed description on the different growth methods along with the recipes used is available in Chapter 3.

Using CNT's high aspect ratio, one can use it to enhance applications in terms of providing higher surface area without adding a significant amount of weight. Higher surface area allows more reactions to take place simultaneously, which can benefit applications that have reactions dominated by available surface area, such as in the case of a catalytic reactions. Applications that can benefit from higher surface areas are scaffolds for cellular growth, cathodes for solid-state lithium ion batteries, and thermal interface materials (TIM). The proposed work for this dissertation is interested to see if CNTs can be used as a TIM to enhance heat dissipation for power electronic devices.

The interface is an important location; it is where two different surfaces come together and meet and where all of the interactions and reactions take place. Interactions, such as energy transfer, chemical reactions, diffusion, and physical adhesion/repulsion, are of great interest and are the basic foundation for this research. Understanding the different types of interactions taking place at the interface and how those interactions progress would allow one to gain controllability for future designs. The ability to control a reaction will allow one the ability to design and engineer tailored products for a specific application. In this case, the application of interest is the thermal management of power electronics.

2.6 Carbon Materials for High Power Electronics Applications

2.6.1 sp^3 Carbon ➔ Diamond

Diamond has unmatched physical property. It is durable, high in thermal conductivity and have highest electric breakdown field. Due to these properties, diamond is said to be an excellent candidate for power electronics devices [54]. However natural form diamond is expensive, and therefor hard to justify its use in commercial grade devices. In order to make diamond more affordable for high power electronic devices, studies have shown that laboratory grown diamond films are achievable[55]. One way to make power electronic devices more robust and to address thermos-mechanical stress is incorporation of CNTs with diamond

substrate. Successful attachment of carbon nanotubes (CNTs) on diamond substrates can lead to unique/robust creation with superior thermal and mechanical properties. This concept has been demonstrated using modeling analysis. Roy etal. has shown different geometric configuration how CNT and allotropic forms of carbon can be fitted together, however this was only demonstrated through computational modeling [56]. Some has reported the growth of CNT on diamond seeds [26] or diamond films [55]. However researches that grow CNT on diamond substrates remains low. Chapter 4 addresses the insufficiencies in the area of diamond-CNT by investigating what growth techniques and growth parameters can be used to grow dense carpets (without the substrates showing underneath) of CNT on diamond substrate. This was done by using three CVD techniques to grow CNTs on polished diamond substrates.

2.6.2 sp^2 carbon ➔ Graphitic and Vitreous

Un-like diamond, graphitic material is electrically conductive. Certain high power electronic device may find this property useful. In addition, graphitic material is lightweight and is available in wider geometric selection such as bulk substrate, foam, and loose particulates. These features can be useful in areas such as aerospace, composites, and impact absorptions just to name a few. However research that incorporates CNT with graphite also remains low, because the majority of CNT research uses electronic grade silicon as substrate. This investigation will address the limited information in areas of graphite-C by providing a systemic investigation for growing CNT on planar and porous carbon substrate and test the feasibility as a thermal management material.

2.7 History of Buffer Layer Usage for CNT Growth

It was reported that certain buffer layer material, when used, can enhance CNT growth density. Therefore this section will highlight the history of buffer layer usage for CNT growth.

2.7.1 Background: Evolution of buffer layers

Although there was not a lot of information regarding investigation of buffer layer for CNT growth on carbon substrates, buffer layer investigation has been well reported for CNT growth on other substrates.

When CNT were first discovered, researchers thought CNTs can be of a great use for thermal or electrical applications. Many of these applications require a perfectly uniform contact at the interface in order to have a low (thermal or electrical) interface resistance. Therefore, in the beginning, one approach used to create a low contact resistance is to grow the CNTs directly on metallic surfaces. It wasn't long before the research groups found that growing CNTs on metallic surfaces yielded very poor quality. Mainly, the CNT growth was hindered by strong chemical activity between the catalytic particle and the substrate. Below are some of other materials that researchers have used in terms of finding an ideal material as buffer layer for CNTs growth.

2.7.2 Pure Metallic buffer:

Study done by Du et.al, grew CNT directly on nickel substrate and the result revealed CNTs nucleated from fragmentation of nickel surface and the resulting CNTs were spaghetti like, low density and poor controllability[57]. Another attempt was done by another group, by roughing up the surface with wet etching [58] or polishing [59] and ended with similar results. The next logical attempt was to grow on other type metal substrate, perhaps an alloy.

2.7.3 Alloy Metallic buffer:

Certain alloys have higher resistance to catalytic diffusion than pure metals, therefore some groups attempted to grow on alloys or alloy coated substrates. Researchers who attempted growth on alloys such as, stainless steel [60], [61], mumetal (Ni:Fe 77:14%) [62], and Inconel [63] did find an increase in growth density of CNTs forest. These improvements are said to be the cause of increased carbon precipitation rate when these alloys are used a catalyst particles. However, the resulting CNTs diameters are usually large and none uniform.

To provide a starting point for the researchers, ternary phase diagrams are often used as a way to select possible buffer layer material. These ternary phase diagrams would usually include metallic materials that are known to be good catalytic sources for CNTs growth. For example, Figure 3, is a ternary phase diagram of stainless steel made from elemental Ni, Fe and Cr. Figure 4 shows the result of CNT growth when stainless steel alloys composed of Ni, Fe, and Cr were used as catalyst layer, the result was reported from Hiraoka et al. [64]. The result indicated that Ni-based ally with Cr or Fe are excellent for SWNT synthesis, while pure metals (Ni, and Fe) and alloys made with Fe-Cr produces both SWNT and MWNT types of CNTs.
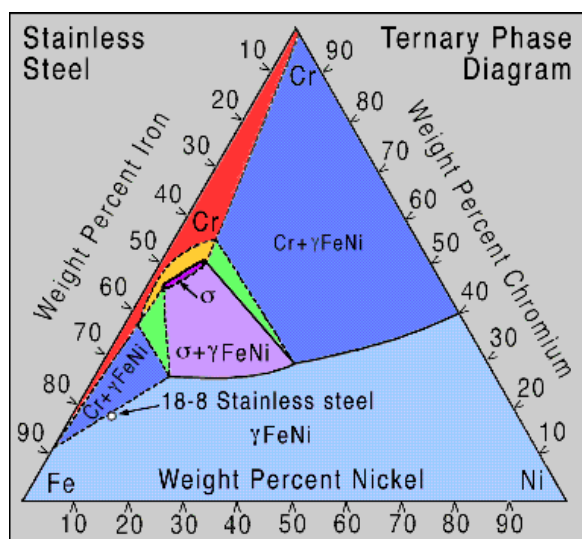
Figure 3: Example of a Ternary Phase Diagram for Alloys
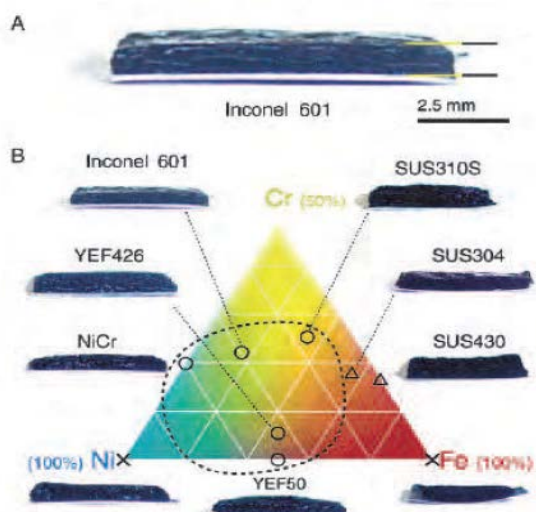
Figure 4: An Example of CNT Growth on Various Alloy Substrates

10

2.7.4 Non-metallic buffer:

There are two main groups of material that have been tried as buffer layer that are in the non-metallic family. The first is the oxide group and the other is the nitride group. It wasn't long before reporting of dense forest growth of CNTs using oxide based buffer layers. In addition the increasing the quantity of CNT, the morphology also becomes more aligned [65], [66]. Other non-oxide ceramics have also been used, such as nitrides, carbides, and carbonates. The results there still indicate that Al_2O_3 is one of the best buffer oxides used for CNT growth. There are numerous ways to grow CNT, and it is important to keep in mind that a good quality of buffer layer should restrain the diffusion reaction between catalytic particle and the substrate, while minimizing the effect of this layer on the property of the device. The investigation for Chapter 6 will be comparing the influence that alumina and silica have on CNT growth. Section 2.6 listed some of the fundamental differences observed between the two oxides.

2.7.5 Critical buffer layer thickness:

Several research groups have suggested that in order to fully prevent catalytic particles from having a reaction with the substrate, a certain thickness of buffer layer must be used [67]–[69]. Since the activation energy required for reactions between two materials are materials dependent, the figured oxide thickness will depend on which material are used. The thickness should be greater than the mean diffusion distance that catalyst material can travel during the growth time. This distance can be calculated using the diffusion coefficient equation, activation energy, and temperature.

$$D = D_o e^{-\varepsilon/kt}$$

Equation 1: Arrhenius Equation

$$\lambda = \sqrt{Dt}$$

Equation 2: Diffusion Distance (λ)

Simmons et al. gave an example such at diffusion of iron in silicon dioxide = ($D\sim 10^{-4}$ cm^2 s^{-1}, ε = 2.8 eV) [67]. Thus diffusion length should be 1.5 nm, for Co = 12nm, and for Ni = 2.5 nm [67], Figure 5. However the observation of the diffusion was observed to be longer. The longer diffusion length was due to higher concentrations of pinholes on the thin films. The table below summarizes the diffusion of different metals observed on silicon substrates.

Metal	D (cm^2/s)	ε (eV)	T (K)	λ (nm)
Fe	10^-4	2.8	900	1.5
Co	10^-7	1.7	900	12
Ni	10^-9	1.6	900	2.5

Figure 5: Chart Showing the Diffusion Distance for Different Metals on Silicon at 900K, Simmons et al. [67]

CHAPTER 3: Materials and Techniques Used In This Investigation

The purpose of this chapter is to introduce the different materials, processes and techniques used in this project.

3.1 Materials used as substrates

3.1.1 Dense carbon (sp^3) ➜ Diamond Substrates:

Diamond is a unique material that no other materials can match in terms of thermal, mechanical, chemical or optical properties. It has been thought after as an ideal material for high power electronic applications. It has been reported that diamond has a high breakdown field strength of 10MVcm^{-1} as well as high thermal conductivity values >2000 W/mK [70]. Although there are many different grades of natural and laboratory grown diamonds, a typical thermal conductivity value of a diamond substrate would have a value that is 2-5 times higher than a pure copper (385 W/mK) and almost 4 -10 times higher than an aluminum nitride(140-180 W/mK) [54]. To put it in perspective, Figure 6 shows the relative amount of diamond material required, comparing to silicon and other materials, in order to adequately block 10kV. The figure shows that the amount of diamond required is less than 10% of what is required of silicon. Therefore diamond is thought to be an excellent candidate to be incorporated in electronic devices for thermal management. In addition, due to its wear resistant properties, diamond is thought to be an excellent material choice to be used in harsh environments (corrosive and extreme temperatures.)
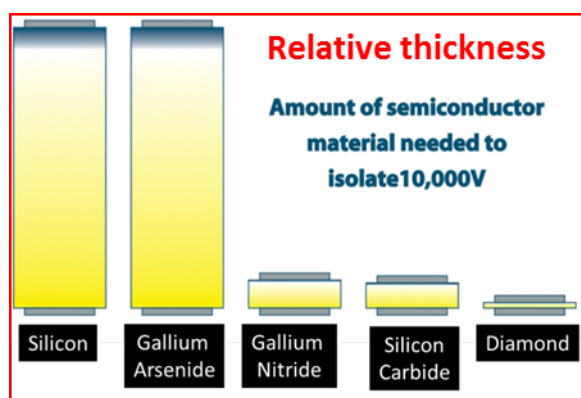
Figure 6: Relative Thickness Required to Isolate 10kV of Different Materials

However, natural form diamond is very expensive so efforts have been made to produce diamond films in a laboratory setting. Currently, a wide variety of synthetic diamond is available for commercial and consumer purchases, including (loose diamond, diamond film, polished free standing diamond substrates).

Figure 7 is an AFM image of the surface roughness of a purchased lab grown diamond substrate that was used in this study. The diamond substrate was purchased from SP^3 Inc., and the measured surface roughness has a value of 14.35 nm.
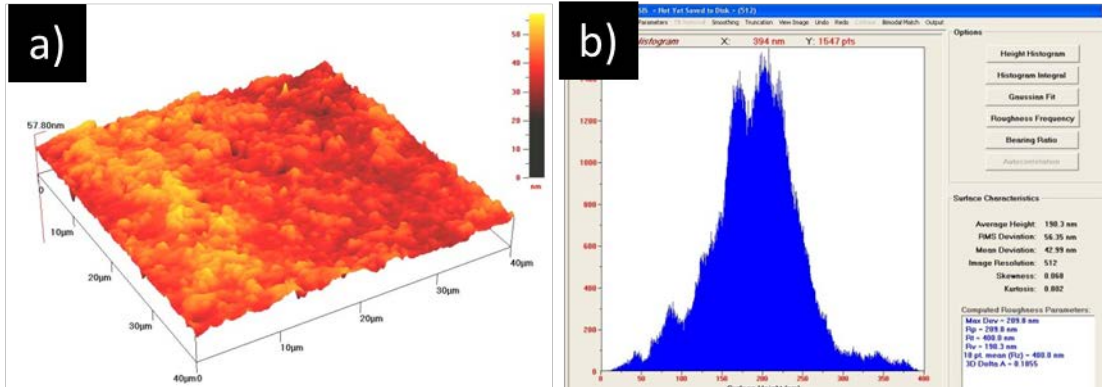
Figure 7: AFM Measurement of Diamond Substrate, a) Rough Scan, b) Height Distribution

3.1.2 Lightweight carbon (sp^2) materials ➔ graphite, CNT, carbon foams

The other allotropic form of carbon that was used in the investigation is form by the sp^2 bonding of carbon. These forms of carbon are lighter in comparison to diamond and are mostly graphitic, while some amorphous carbons can also have the sp^2 bonds. Graphitic carbons are electrically conductive and have an electrical conductivity value about $1x\ 10^5$ S/m. The combination of lightweight and electrically conductive properties can be very useful for certain power electronics in the space industries. Below is an introduction on the physical properties of a variety of sp^2 carbon used in the investigation.

3.1.2.1 Pressed Graphite:

Industrial grade pressed graphite are commercially available; and it is often used as heating strips. Pressed graphite is made up of carbon flakes that are pressed tightly together under high pressure. Samples of this material were purchased through POCO Inc., with a grade of AUX-5. The orientation of the graphite flakes are random, therefore the thermal property of the material is isotropic. The material spec sheet can be found in Figure 8.

13

POCO Graphite Grade: AXF - 5Q			
Particle size (μm)	5	Tensile Strength (N/mm2)	62
Pore Size (μm)	0.8	Psi	9,000
Total Porosity (% volume)	20	Modulus of elasticity	11,000
Open Porosity (% of total)	80	Psi x 10^6	1.6
Apparent Density (g/cc)	1.78	Tensile Strain to Failure %	0.95
compressive strength (N/mm^2)	138	Hardness (SSH)	74
(Psi)	20,000	Electrical Resistivity (μ Ω cm)	1470
Flexural Strength (N/mm2)	86	CTE (Microns/m °C)	7.9
(Psi)	12,500	Thermal conductivity (W/m K)	95

Figure 8: Material Property of POCO Graphite

3.1.2.2 RVC foam:

Reticulated vitreous carbon (RVC) foam was purchased from Ultramet, Inc. According to the manufacture, RVC foams consists of 97% open porosity, low pressure drop, and a three-dimensional interconnected network of solid struts. Each open cell can be modeled as 14-faceted polyhedral or commonly known as tetrakaidecahedron [71]. Due to the way these foams are manufactured, each strut has a triangular cross-section. Ultramet, Inc. provides carbon foam in various pore densities ranging from 10 pores per inch (PPI) up to 100 PPI. Each size of the foam is characterized by pore diameter, and relative density. For this study, as received RVC foams have a measurement of 45 PPI and a specific surface area of 3×10^3 m^2/m^3 [8]. These foams are made up of amorphous glassy carbon that provides high specific surface area, are easily machined, and are lighter than bulk carbon substrates. Figure 9 is a table from the manufacturer's data sheet, and Figure 10 is an SEM image of a RCV foam, showing the microstructures of the struts.

Riticulated Vitreous Carbon Foam, Ultramet Inc.			
Pore Size available	10,20,30,45,65, 80, and 100 ppi	Thermal conductivity, W/mK	
Ash content	0.39 wt% at 10000 ℃	at 200 ℃	0.085
Bulk density	0.045 g/cc	at 300 ℃	0.125
Ligament density	1.538 g/cc	at 400 ℃	0.18
Reistivity	0.75 Ω cm	at 500 ℃	0.252
Specific Heat	0.3 cal/g/ ℃	at 650 ℃	0.407
Maxminum use temperature	350 ℃ in air	at 800 ℃	0.625
	3500 ℃ inert	at 950 ℃	0.882
Thermal expansion, ppm/ ℃		Compressive Strength, kPa at 20 ℃	625 (10% deflection)
0-200 ℃	1.15		762 ultimate
0-500 ℃	1.65	at 1000 ℃ in argon	390 (10% deflection)
0-1000 ℃	1.65		628 ultimate
		Shear strength at 20 ℃	290 kPa
Flexual strength at 20 ℃	690 kPa		
Flexural modulus	5806 Mpa	Tensile strength at 20 ℃	690 kPa

Figure 9: Material Property of Ultramet RVC Foam
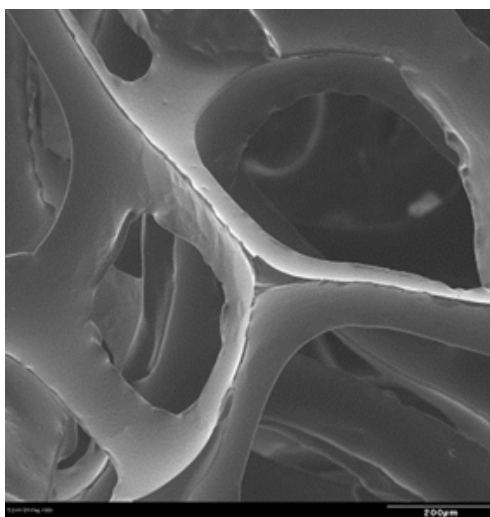
Figure 10: SEM Image of 45ppi RVC Foam

3.1.2.3 Highly Oriented Pyrolytic Graphic (HOPG) from SPI, Inc.:

Highly Oriented Pyrolytic Graphic (HOPG) was purchased form SPI, Inc. HOPG is a carbon material that is characterized by a preferred crystallographic arrangement of carbon sheets stacked in lamellar fashion where each layer of graphite is parallel to the surface of the substrate. According to company data, all of the sheets are within 1 degree of deviation from the surface. The lamellar structure provides a very strong force in the lateral direction of the plane and weak Van-der Waal forces between planes. Because of this weak bonding formed between the planes, the samples can be cleaved easily. HOPG is usually processed using a hot working technique, and then annealed under compressive stress at a high temperature near 3000K [72]. As a result, HOPG are high purity graphite, and contains less than 10 ppm of ash contents, Figure 11.

DISTRIBUTION STATEMENT A: Approved for public release. Distribution is unlimited.
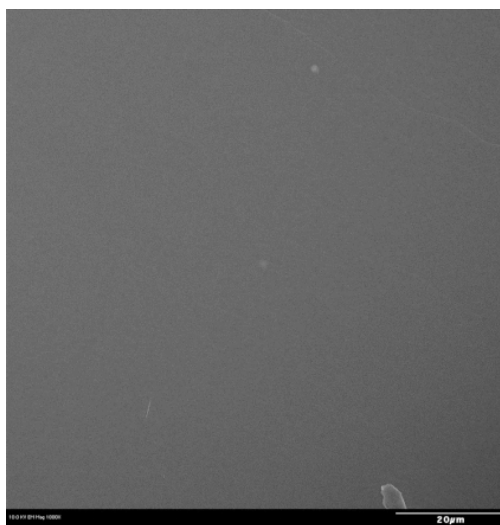
Figure 11: HOPG from SPI

The HOPG substrates used in this study are a grade 3, and were purchased from SPI, Inc. The "grading" is defined by the manufacturer, which correlates with degree of alignment between the graphene sheets. A grade of 1 being the highest grade has an $0.4° \pm 0.1°$ alignment between the graphene sheets, while a grade of 3 being the lowest grade has an 3.5° +/- 1.5° alignment between the graphene sheets. According to SPI, Inc, this material is made up of parallel oriented stacking graphite sheets, and its surface roughness is measured to be 0.2-0.3 nm in steps. Each step contains about a dozen atomic layers of graphene. Due to its highly ordered stacking nature, the thermal property of this material is anisotropic. The thermal conductivity quoted by SPI is 1800 W/mK along the basal plane, and 8-10 W/mK in the Z (through thickness) direction. This material can be used up to 500 °C in air, up to 2500 °C under vacuum, and up to 3500 °C in inert atmosphere. Figure 8 below is surface roughness image taken from AFM. The AFM scan was taken from one of the HOPG substrate used in the study, and the average RMS value was 4.36 ± 0.1 nm.
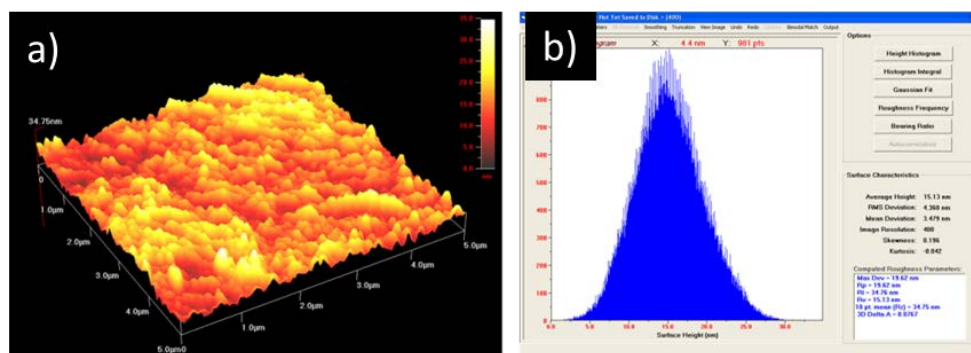
Figure 12: Surface Roughness AFM for SPI HOPG, a) Roughness Scan, b) Height Distribution

3.1.2.4 Model carbon samples

The purpose of this step is to fabricate a surface that is made of same chemical composition as carbon foam, however, on a flat substrate. This process is straight forward, controllable, and repeatable. Manufacture of carbon layer on silicon was done using the following process, and the resulting sample is named Model Carbon Sample.

16

The process began by cleaning the Si samples using a Radio Corporation of America (RCA) cleaning procedure, which is a standard wafer cleaning step. Shipley 1813 photoresist was used to graphitize the surface of a silicon wafer. Shipley 1813 is composed of electronic grade propylene glycol monomethyl, ether acetate, mixed cresol novloak resin, fluoroaliphatic polymer ether and proprietary trihydroxybenzophenone. These silicon samples were spin coated with Shipley 1813 photoresist at 5000 rpm for 35 seconds. The coated samples were cured at 150 °C on a hot plate for one minute. The samples were then annealed for 10 minutes in a horizontal tube furnace at 750 °C in argone ambient at a flow of 2 SCF/hr. The resulting vitreous carbon layer pyrolyzed on the silicon wafer surface had an average thickness of 450 nm. Figure 13 is a schematic drawing showing the development of the Model carbon sample.
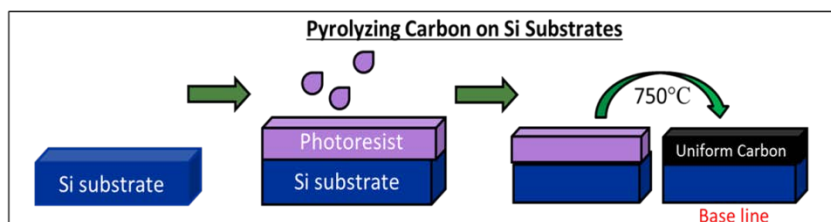
Figure 13: Schematic Drawing of Model Carbon Sample Preparation

3.2 Metals Catalysts Materials:

Iron and nickel were chosen materials as catalyst sources in this study. These two materials have been reported in the literatures to be great catalytic sources for CNT growth [73]–[76]. Depending on the growth methods used, catalyst sources can be introduced differently. For traditional growth methods, iron or nickel catalysts are sputtered onto the growth substrates. For newer and more scalable method, organometallic compound containing irons are injected into the growth chambers using a syringe pump. Ferrocene was used in this investigation as the iron catalyst source for floating catalyst CVD growth technique.

3.3 Oxide Buffer Layer Materials and Comparison:

3.3.1 Oxides Materials for the Investigation

The two oxide materials that were used in this studied were alumina (Al_2O_3) and silica (SiO_2). The oxides were used as a buffer layer to promote CNT growth density and to enhance the morphology of CNTs. It was important to know the effects of these two different oxides have on CNT growth characteristics. Here are some of the fundamental differences between these two oxides. Figure 14 shows the physical properties of these two oxides, alumina and silica. The figure shows that the intrinsic property of the oxide can change, due to different defect concentration or network former. It has been reported that different deposition methods can lead to creations of oxides with different defect concentrations [77]. Therefore it is important to not only compare the effect of oxide material differences, it is also important to compare effects associated with purity differences. The investigation for the influence of oxide buffer layers can be found in Chapter 6. Sections below introduce different oxide materials used in this investigation along with their deposition techniques.

	94% Alumina	99.5% alumina	fused silica	quartz
denisty g/cc	3.96	3.89	2.2	2.65
hardness Kg/mm^2	1175	1400	600	
thermal conductivity W/ m °K	18	35	1.4	1.3
CTE	8.1	8.4	0.55	12.3
Specific heat j/Kg °K	880	880	740	730
Dielectric strength ac-kv/mm	16.7	16.9	15-40	15-25
dielectric constant @ 1 MHz	9.1	9.8	3.82	3.8

Figure 14: Physical properties of various examples of alumina and silica

3.3.1.1 Alumina (Al$_2$O$_3$):

Single crystal of alumina has a corundum crystal structure and has a density of 3.89 g/cm^3. However depending on how the oxide films are made (deposition or growth techniques) alumina can be crystalline or amorphous. Alumina is a high dielectric material with dielectric constant of 9.8 at 1 MHz, it has a thermal conductivity value that ranges from 18 - 35 W/mK, and CTE value about 8.4.

A sapphire substrate was also used in one of the study; this substrate was purchased from University Wafers with an 001 orientation.

3.3.1.2 Silica (SiO$_2$):

Silica is made up of network formers, which means that its crystal structure is mainly amorphous. Silica has a dielectric constant of 3.8 at 1 MHz, it has a thermal conductivity value about 1.4 W/mK, and a large spread for the CTE value that ranges from 0.55-12.3.

A fused quartz substrate was also used in one of the study; this substrate was purchased from Technical Glass Products, Inc.

3.3.2 Formation of Oxide Buffer Layer Materials

This investigation uses several different deposition techniques to obtain desired thin film materials. The information about each type of thin films are listed in this section.

3.3.2.1 Thermal Silica:

These are purchased standardized commercial material readily available to the electronic device community. The silicon wafers are sold with a 1 µm thermal oxidized silica layer on top. Samples used in this investigation were purchased from University Wafers with a 001 orientation.

3.3.2.2 Alumina by Atomic Layer Deposition:

Trimethylaluminum (C$_6$H$_{18}$Al$_2$) is an organometallic compound used as a precursor chemical during the atomic layer deposition process (ALD). At room temperature this compound is primarily a dimer. Its chemical structure is made up of two aluminum atoms and each atom is attached by two free methyl groups and two shared bridging methyl groups. In this study, this precursor, when used in an ALD process reacts with the surface O-H functional group and leaves behind a monolayer of aluminum. Next, the aluminum layer will react with water vapor molecules to form aluminum oxide layer while simultaneously releasing a methane molecule back into the environment.

3.3.2.3 Silica by Atomic Layer Deposition:

Tris(dimethylamino)silane ($(CH_3)_2N)_3SiH$ is an organosilicon compound used as a precursor chemical in ALD to deposit SiO_2 thin films. This chemical is considered to be a toxic organic liquid and is a pyrophoric open air. Its chemical structure consists of a silicon atom sitting at the center of the molecule; it forms one bond to a hydrogen atom and three separate bindings to (dimethylamino) groups. The silica ALD process is also a 4 step process involving saturation of the surface with a thin layer of OH group and follow by purging of the excess chemical through a self-limiting process. However, the chemical process rate at which silicon oxide take place is much slower than aluminum oxide. Therefore, a longer precursor residence time is needed to deposit a monolayer of silicon oxide.

3.3.2.4 Microwave Plasma Silica:

Another type of silica coating used in this study was deposited by a method called microwave plasma enhanced chemical vapor deposition (MPECVD or MPD for short). The procedure used in this study was the one developed by Dr. Pulikollu as part of his dissertation work. It was published earlier that when this oxide was deposited on graphitic carbon or carbon foam, the growth density of CNT was increased [78]–[80]. Below is a recipe used in this investigation, but developed by Dr. Pulikollu's and Dr. Barney for their dissertation work [24], [25].

The silica coating deposition uses gas phase precursors in microwave plasma CVD reactor. The reactor repeats three different steps in order to build up oxide thickness. The three steps are as following:

1. Pure oxygen, O_2 (99.99%) gas, was introduced into the microwave plasma chamber for 180 sec. The gas has a flow rate of 50 ml/min. The chamber pressure was 48 Pa, and the microwave power was 225 W.
2. Pure oxygen, O_2 flow at 50 ml/min in 56 Pa. Hexamethyldisiloxane (HMDSO) flowing at a rate of 2 ml/min with microwave power of 250W for up to 300s. This step deposits the silica layer so the timing is important.
3. To stabilize the oxide coating, O_2 carrier gas flow at 50ml/min in48 Pa was introduced into the chamber at a microwave power of 150W for 60s.

By modifying step 2, in the program, the oxide coating thickness can be varied.

In Dr. Barney's dissertation, he mentioned that the coating grows by island formation and coalesces after 1 minute to form a uniform layer. At 1 minute of deposition, the film is measured to be about 4-5 nm with a roughness of less than 1 nm. The MPD method deposits silica as an amorphous layer. This silica is chemically bonded to carbon surface as a Si-C bond at the interface.

3.4 Material for floating catalyst CVD growth

3.4.1 Xylene:

Xylene ($C_6H_4(CH_3)_2$) is an organic solvent. Its chemical structure is made of two methyl groups attached to a benzene ring. The location of the methyl group can vary in one of the three available positions on the carbon thereby making isomers [ortho-, meta- , and para- xylene]. The xylene used in this work is meta-xylene from Sigma-Aldrich, but using any of the three would be fine. The purpose of the xylene is to dissolve ferrocene powder and to act as a vapor carbon

source during CNT growth. Xylene has a boiling point of 138 – 139 °C, and appears to be clear at room temperature.

3.4.2 Ferrocene:

Ferrocene ($Fe(C_5H_5)_2$) is an organometallic compound. Its chemical structure is made up of two cyclo-penta-dienyl rings attached with an iron atom in the middle. Ferrocene can easily be dissolved in organic solvents, such as one used in this study, m-xylene. At room temperature ferrocene is stable and appears to be a yellowish orange powder. The ferrocene used in this investigation is Acros Organic 98% with given melting temperature of 173 – 176 °C, boiling point of 249 °C, and molar mass of 186.04 g. This ferrocene has a sublimation point at 100°C.

3.5 CNT growth Techniques

To grow CNT, all one requires is a carbon source, a catalyst source and a heat source. This section is going to highlight some of the known techniques used to grow CNT as well as descriptions of the growth techniques that were used in this investigation.

In this investigation chemical vapor deposition (CVD) was used to grow CNTs. CVD is cost effective, and scalable which is ideal to be use for systematic investigations. However it is worth mentioning some of the other techniques that can be used for CNT synthesis.

3.5.1 Growth Methods Not Used in this Investigation

The reviews published by Terrones et al. and Kumar et al. outlines the different methods that are available for CNT growth [33], [81]. Namely they are: electric Arc-discharge, laser ablation, and chemical vapor deposition (CVD) as the most common. This dissertation focuses on CVD because it has a low set-up cost, high production yield and ease of scale-up. However, there are many different varieties of CVD technique that can be used to grow CNTs. The variation depends on the power sources, type of catalyst source, gas composition, and operating temperatures. In addition, CNTs growth is expected to depend significantly on the chemistry, morphology, and activity/reactivity of the substrate. Catalyst and substrate interactions can create differences in the type of growth mode (the root growth or the tip growth mode), size distribution, as well as the morphology of the CNT [82]–[84].

3.5.1.1 Arc-discharge:

The first CNTs were discovered while using the Arc-discharge method [85]. This method uses direct current (DC) to produce an arc between two graphite electrodes that is placed about 1 mm apart in an inert gas fill chamber with low pressure. The electrodes are usually cylindrical in shape and the arc is usually very high temperature, ~ 4000°C. The resulting CNTs from this process are usually very graphitic with minimal defects; however the entire batch may also contain products that are not CNT, such as soot or fullerenes. To obtain CNTs catalyst sources are needed, without it only soot was formed [86]. Common operation parameter includes a DC current between 50-100A, and 20 V [87]. The arc discharge vaporizes the surface of one graphite electrode and deposits the result onto the other electrode.

3.5.1.2 Laser ablation:

This method uses a laser pulse to ablate and to evaporate high-purity graphite targets at high temperature [85], [88], as a result, highly graphitized CNTs are able to grow on a sample surface. However, the production yield is very low and aligned growth is difficult. The benefit of this method is its ability to produce good quality single wall CNT (SWNT). The production of CNTs

using this method can be controlled by controlling parameters such as target composition, temperature and pressure.

3.5.2 Growth Methods Used in this Investigation

Information about growing CNT on carbon surfaces are very limited, therefore different growth methods were explored initially. Due to laboratory availabilities three CVD techniques were used to see if growing CNT sp^3 were achievable. Out of which one growth technique was selected for the reminder of the investigation in order to produce CNT that are comparable.

Since their discoveries, CNT has been fabricated by numerous growth techniques and numerous recipes, as mentioned above. However, that doesn't mean that the resulting CNTs the same intrinsic properties, due to resulting morphology differences. To start the CVD investigation, recipes used to grow CNT in this investigation was adopted from ones published in literatures that have demonstrated to be a successful in producing CNTs. The growth recipes were first replicated by using the CVD equipment, used by this investigation, to grow CNTs on electronic grade silicon substrate with thermal silica oxide layer. Once CNT growth was validated to be successful, the growth was then done on the purchased diamond substrate. This investigation of CVD growth on diamond substrate is shown in Chapter 4. The result from Chapter 4 allows us to down select the growth technique for the reminder of the investigation. Exploring successful methods of growing CNT on sp^2 carbon can be found in Chapter 5. The section below provides a description of each of the three CVD methods used in the investigation along with a description of the growth recipe used in the investigation. ****For this research, the investigation on diamond samples resulted in a proof of concept and the CNTs morphologies resulted from various CVD growth technique were compared. The growth optimization was not explored due to a limited quantity of diamond samples. More information about CNT growth on diamond substrate can be found in the Background Study Section, Chapter 4.*

3.5.2.1 Chemical vapor deposition (CVD):

This method is currently one of the more preferred methods used to grow CNTs due to its low set up cost, large CNT yield, and ability to be optimized [81], [89]. There are several different types of processes available and this investigation has chosen 3 CVD methods for further investigation. Namely the thermal CVD (T-CVD), microwave plasma enhanced CVD (MPE-CVD), and floating catalyst CVD (FC-CVD). In general CVD process starts with passing a hydrocarbon source (methane, acetylene, acetone etc.) through a horizontal tube furnace that contains a substrate with metallic catalytic material at high temperature (500 – 1200 °C). The catalytic material will decompose the hydrocarbon into the carbon source needed for CNT growth. The CNTs will nucleate from catalytic particles. CNT synthesis using this method requires controlling parameters including carbon source, temperature, pressure, catalyst, feedstock gas, substrate, buffer layers and growth time. This method is known to grow both aligned and, non-aligned CNT carpets with, high and low yields, it can facilitate tip and root growths, as well as SWNT and MWNT. Depending on the application, certain CNT morphology can be more desirable then others. The benefit of CVD growth technique is that it is versatile so that one can work to optimize the system in order to facilitate the growth of desired CNT morphology.

3.5.3 General and Specific Growth Recipes
3.5.3.1 Thermal (CVD):

Thermal CVD (TCVD) is one of the traditional growth techniques. This technique consisted of a furnace, feedstock gases, and an optional vacuum attached at the exhaust end. TCVD is a

DISTRIBUTION STATEMENT A: Approved for public release. Distribution is unlimited.

two-step process where deposition of a catalyst layer is required prior to CNT growth. Before the metallic thin films can be used as catalyst, a heat treatment step is required to coalesce the catalyst particles from the metallic films. Once the catalyst particles are formed, passing of carbon and feedstock gas into the tube furnace, in the growth temperature range, can facilitate CNT growth over time.

3.5.3.1.1Referenced TCVD Method

For the thermal CVD process, prior study by Varanasi et al. reported growing CNT on diamond film using alloy Ni-Fe-W has shown success when using acetone + Argon (10%:90%) mix bottle, and feedstock gas H_2 + Argon (5%:95%) flowing at 400 and 300 standard cubic centimeters per minute (sccm), respectively [55]. With a growth temperature ranged from 750-800 °C. The growth was performed at a pressure of 90 torr, with a growth time that ranges from 10 – 20 minutes.

3.5.3.1.2 Specific TCVD Recipe Used in this Investigation

As stated above, TCVD has a wide growth temperature range, after several growth attempts it was decided that the following is most suitable to use for this investigation. The growth parameters used in this investigation are as the following. To minimize the containments in the growth chamber, after the samples are loaded, the system was evacuated to less than 10mTorr and held there for at least 15 minutes. After which, Ar+H_2 was allow to flow for 15 minutes at 90 Torr to remove any remaining contaminates. Keeping the gas flow and the chamber pressure at 90 Torr the chamber is heated to 800 °C. Once the temperature reaches 800 °C, an annealing time of 10 minutes was used to allow catalyst particles to coalesce. Next C_2H_2 + Ar (10% + 90%) mix was introduced into the chamber, and a growth time of 20 minutes was used. After which, the carbon source was terminated from flowing into the chamber. Finally turning off the power source to the heating element, the chamber was cool to room temperature with a constant flow of Ar +H_2 gas.

Other growth temperatures (700-850 °C) were briefly explored using electronic grade silicon substrate with thermally grown oxide layer, but it was found that 800 °C provided the most uniform CNTs.

3.5.3.2 Microwave Plasma Enhanced (CVD):

MPECVD is also a traditional growth technique. This technique has two energy sources, one is a heating stage, and the other is H_2 plasma generated from a DC, Radio frequency (RF) or microwave power supply. The plasma generated can dissociate the carbon sources required for CNT growth at a lower temperature and pressure than most other CVD. Similar to TCVD, this technique is also a two-step process where deposition of a catalyst layer is required prior to CNT growth. A heat treatment process is needed to coalesce the catalyst particles from the metallic films. In general MPECVD system uses microwave power up to 1 kW, is transmitted from the generator through a wave guide to a microwave coupler that emits the radiation via the antenna into the CVD chamber. When the ideal parameters were reached, plasma can be form centered over the substrate to facilitate CNT growth for samples. Since the size of the plasma can be controlled it is possible to grow CNT over an area that is larger than 10 cm^2 [90]. Parameters controlling the plasma include the following: microwave power, chamber pressure, gas source, flow rate, and chamber temperature.

3.5.3.2.1 Referenced MPECVD Method

For the MPECVD process, Crossley et al. and Wong et al. reported growing CNT on SiO_2 coated silicon sample has shown success when using a two-step processes where a heat treatment step was performed at a lower temperature followed by growth temperature at a higher temperature [90], [91]. In this process, after samples were loaded into the growth chamber the chamber is evacuated below 10 mTorr. Then the graphite stage and substrate are heated to 400º C in a hydrogen atmosphere of approximately 20 Torr. Once the system has reached a steady state, a catalyst pretreatment phase was done to allow thin catalyst films to coalesce into catalyst, nano-particles, necessary for CNT growth. Pretreatment phase exposes the catalyst layer to a H_2 plasma induced by 400 W of microwave power for 5 minutes. The microwave power is terminated at the end of the pretreatment phase and the temperature increased to 650º C while maintaining the same gas flow and pressure. The growth phase occurs for 2 minutes at 650º C, with hydrogen and methane (CH_4) mix, and 1000 W of microwave power. The microwave power and the heating stage were terminated after the growth stage, while maintaining the hydrogen flow and chamber pressure the system was allow cooling back to room temperature.

3.5.3.2.2 MPECVD Recipe Used in this Investigation

To take a full advantage of MPECVD's capability to produce CNT at a lower growth temperature, the growth temperature was limited to 650º C. To ensure growth chamber cleanness and to minimize potential contaminants, after the substrates are loaded, the chamber is evacuated below 10 mTorr. Then the graphite stage and substrate are heated to 400º C in a hydrogen atmosphere of approximately 15 Torr. Once the system has reached a steady state, a catalyst pretreatment phase coalesce catalyst metal film into nano-particles necessary for CNT growth. Pretreatment phase exposes the catalyst layer to a H_2 plasma induced by 400 W of microwave power for 5 minutes. The microwave power is terminated at the end of the pretreatment phase and the temperature increased to 650º C while maintaining the same gas flow and pressure. The growth phase occurs for 2 minutes at 650º C, with a hydrogen and methane (CH_4) mix, and 1000 W of microwave power. The microwave power and the heating stage were terminated after the growth stage, while maintaining the hydrogen flow and chamber pressure the system was allow cooling back to room temperature.

Other parameter such as pressure ranges (5 – 25 torr) and growth temperatures (400 -600°C) were briefly explored. However it was not use due to difficulties in resulting a plasma or growth of CNT.

3.5.3.3 Floating Catalyst (CVD):

The growth system is very similar to TCVD, where 1 inch horizontal furnace tube was used. The furnace used can reach a maximum temperature of 1200 ℃. The main advantage the FCCVD process is that it is a one-step process, which introduces the carbon and the catalyst source simultaneously into the growth zone.

3.5.3.3.1 Referenced FCCVD Method

For the FCCVD growth method, the investigation uses optimized procedures reported in in Barney's dissertation [92], where substrates were first coated with plasma silica prior to CNT growth. The carbon and catalyst source used in this investigation was Xylene to Ferrocene. The xylene acts as the carbon feedstock while ferrocene decomposes at high temperature to provide the catalytic iron particles required to nucleate for CNTs growth[93] To prepare solvent solution for this task, 0.12 g of Ferrocene was dissolved in 10 ml of xylene to be delivered into the

growth chamber. Carrier gas used was Ar and H_2 from independent gas bottles flowing at a ratio of 100/50 sccm, respectively.

3.5.3.3.2 FCCVD Recipe Used in this Investigation

To prepare the growth chamber for CNT growth and to eliminate as much contaminants as possible, after the samples were loaded, the carrier gas Ar and H_2 was introduced into the chamber flowing at 100/50 sccm, respectively. This carrier gas was flown through the entire FCCVD grow process, from initial stage of preparation of the growth chamber, to elevating temperature to growth temperature of 750 °C, and finally cooling the chamber back to room temp. The carbon and catalyst source was only introduced once the temperature has reached a steady state at 750 °C, and this source was injected at a rate of 3ml/ hr for 20 minutes. Certain studies in this investigation may changes the growth time, which will be specified in the corresponding sections, but the default growth time used in the study is 20 minutes.

3.5.3.4 Sample Recipe Comparisons:

Figure 15 below is a side-by-side comparison listing of the ingredient and the growth parameter used for the three different types of CVD. Each growth technique has its pros and cons when it comes to usability and production quality. However the goal is to see which growth techniques can produce dense growth of CNT on carbon substrate, and is the most suitable method for this investigation. To read more about the background study that compares the resulting CNT using the recipes below please see Chapter 4.

	Traditional Growth Methods		Newer Approach
Growth Methods	Thermal CVD	Microwave Plasma CVD	Floating Catalyst CVD
Symbols	T-CVD	MPE-CVD	FC-CVD
CVD Process	2-steps	2-steps	1-step
Carrier Gas	Ar/H_2	H_2	Ar/H_2
Pressure (Torr)	100	20	ATM
Heat Treatment Temp (˚C)	800	400	n/a
#1 **Successful** Carbon Source	Acetylene	Methane	Xylene
#2 **Successful** Catalyst Source	Ni	Fe	Fe from ferrocene
#3 Growth Temperature (˚C)	800	650	750
Reaction Chamber	1" Horizontal	3" Reaction Chamber	1" Horizontal

Figure 15: Side-by-side Comparison of the Growth Parameters Used for the Three Different Kinds of CVD Used in this Investigation

3.5.4 Growth mechanisms

It has been observed and published that CNTs have two growth modes, a tip growth and a root growth mode[94]. It has been reported that particles > 5nm favors tip group while particles > 5nm favors root growth when grown on silica [95]. Both of which can produce CNTs that are highly crystalline in the (002) plane. In the tip growth mode, decomposed carbon feedstock reacted with the top portion of metallic catalytic particle and resulted in H_2 and C_n species. The carbon species diffuse through the metallic particles follow by precipitation from the opposite end. This process is than continued until metallic particles no longer react [96]. The root growth mode occurs when carbon moves through catalytic particle from the surface of the substrate, the catalytic particle remain anchored at the surface of the substrate.

In general CVD process can be further divided into two types, the first type is the one that require a two-step process for CNTs growth and the other type is a one-step process. Both types

were explored in this dissertation. Although, CNT growth mechanisms are still a highly debatable topic and regardless which type of growth process is used. The general consensus, however is that the following must take place in order for CNTs to grow: (1) Hydrocarbon vapor is carried by inert gas into the growth zone that is at a significantly elevated temperature. (2) The presence of catalytic particles in the growth zone will decompose the hydrocarbon into a carbon source. (3) Carbon sources then diffuse through the metal particles. (4) Formation of graphitic structures at the apex -side farthest away from the substrate- of the catalytic particle is achieved through nucleation or precipitation [81], [96]–[98].

3.6 Surface modification methods

It was observed that growing CNT directly on sp^2 carbon surfaces were challenging. Therefore some surface modification steps were taken to see which ones are effective in enhancing CNT growth density. Below is the description of different surface modification techniques used in various part of the investigation, with a majority of the comparisons made in Chapter 5. It is placed here as a common area that can be reference back to. The treatments are separated into two groups. The first group is surface oxidation method by adding oxygen containing group to the carbon surfaces. The second group is deposition of oxides onto the carbon surface.

In addition, reactive ion etch (RIE) was used in order to provide surface roughness variation. This was done as a secondary surface modification technique.

3.6.1 Surface Oxidation Techniques
3.6.1.1 Nitric acid:
Nitric acid was used as another surface modification method. It was demonstrated that nitric acid can create surface defects on carbon, it was reported that such defects can enhance CNT growth on carbon surfaces [99], [100]. This treatment uses 50 ml of 70% nitric acid at 100 °C for either a 4hr or an 8 hr interval. The samples were than dried in a vacuum furnace at 100 °C for 24 hours.

3.6.1.2 Oxygenation:
This investigation also explored the use of oxygenation treatments as a way for surface modification. The purpose of oxygenation treatment is to create surface defects (such as voids); it was believed that these defect sites can enhance the growth density of CNT. Oxygenation treatment was carried out on RVC foams. According to Ultramet, Inc. RVC foams can withstand air up to 350 °C. This means that a portion of carbon will be burn off due to combustion, at temperatures above 350 °C. This study first investigated if surface defects were created by the oxygenation process. The study was designed to determine the effectiveness of these defect sites on assisting CNT growth on carbon surfaces. RVC samples were first cut into samples sizes measured at 5 mm x 5mm x 10 mm blocks. The oxidation treatment took place for 1 hour at each of the following temperatures: 350 °C, 400 °C, 450 °C, and 500 °C. The horizontal tube furnace was first pre-heated at the set treatment temperature for 30 minutes. Pure oxygen gas was flowing at a rate of 1 liter/minute. The pre-treatment and post treatment weights were measured in order to determine how much carbon has been lost during the heat treatment process. The weight loss is due to combustion taking place between oxygen and carbon materials at high temperature.

Figure 16 shows the result from thermaogravimetric analyses (TGA) used to quantify mass loss and validate the weight measurements. The Figure shows the percent of carbon weight loss

as a function of temperature. This is good information to have, since it shows that around 500 °C, about 10 wt% of carbon has been burned off. This should mean there is a dramatic increase in the amount of defect sites on the surface of the carbon foam.
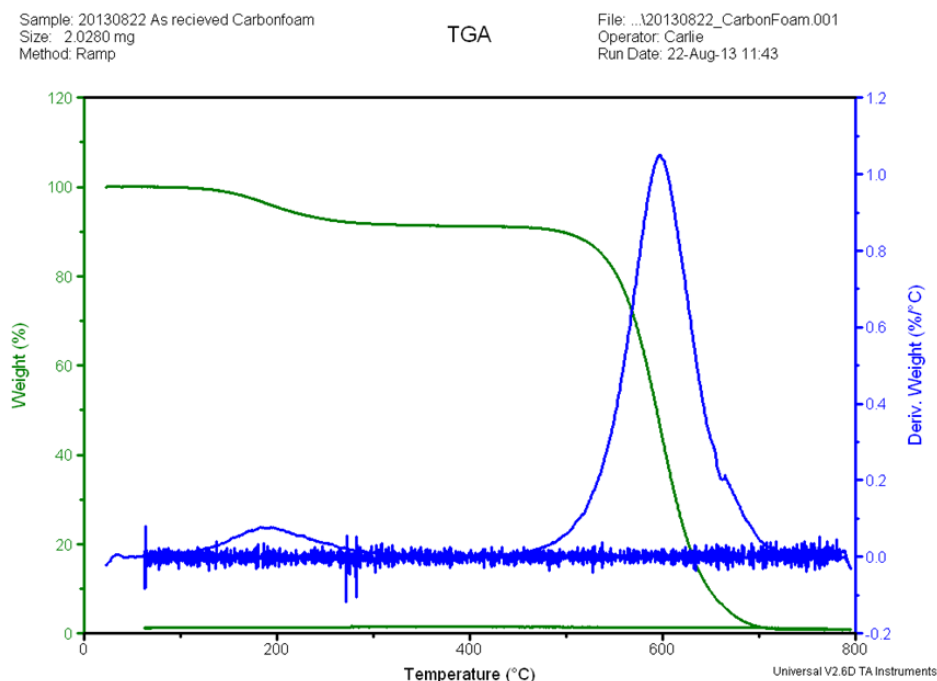
Figure 16: TGA Measurement of RVC Foam Samples

3.6.3.3 Bis(trimethylsilyl)amine (HMDS):

Figure 17, is a chemical structure of bis(trimethylsilyl)amine (HMDS). HMDS is an color less organosilicon liquid that is often used as an adhesion promoter for photoresist in lithography steps. To minimize contaminants and to enhance solvent wetting sample were cleaned with a two-stage substrate cleaning process. Acetone removes organic impurities; a subsequent rinse in isopropyl removes the contaminated acetone thus avoiding striations.

HMDS is usually applied on a substrate follow by soft bake on a hot place. When used, HMDS fragments into smaller groups by chemically bonds its Si atoms to the oxygen of an oxidized surface while releasing ammonia group and methyl groups. The methyl group of HMDS forms a hydrophobic layer on the substrate surface, thereby enhances wetting and adhesion of resist solvents. As a result of this process, a silica coating was formed on the surface of the substrate. Studies will be performed to investigate if this silica coating can boost CNT growth.
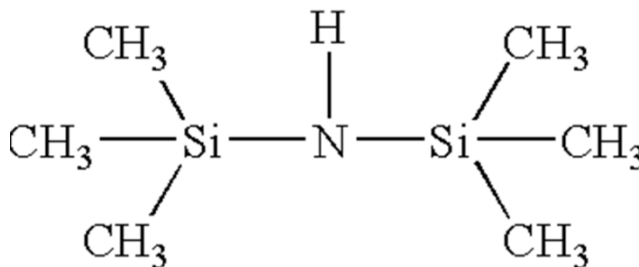
Figure 17: Chemical Structure of HMDS

26

3.6.2 Deposition Techniques
3.6.2.1 Microwave Plasma Deposition (MPD)
     The methodology of silica coating using microwave plasma CVD was adopted from the
same growth conditions that was documented in detail in Pulikollu et al. [78].   To achieve silica
coating, mixture of hexamethyldisiloxane (HMDSO) and O_2 were used sequentially in a
magnetron generated microwave plasma coating system. To build up the silica coating thickness
the process were repeated several times until the desired thickness is achieved.

3.6.2.1.1 Plasma Silica Deposition Rate
     In order to measure the deposition rate for plasma silica discrete deposition times were used
to build up different silica film thicknesses. Figure 18 shows the resulting oxide thickness vs
deposition time. The result shows that the deposition of plasma silica is linearly related to the
length of time used for film deposition. The first point on the chart is a point measured in a
previous investigation from this research group. This data point with 1 minute of deposition,
which resulted in 4 nm of film thickness has been published earlier by Mukhopadhyay et al. [80].
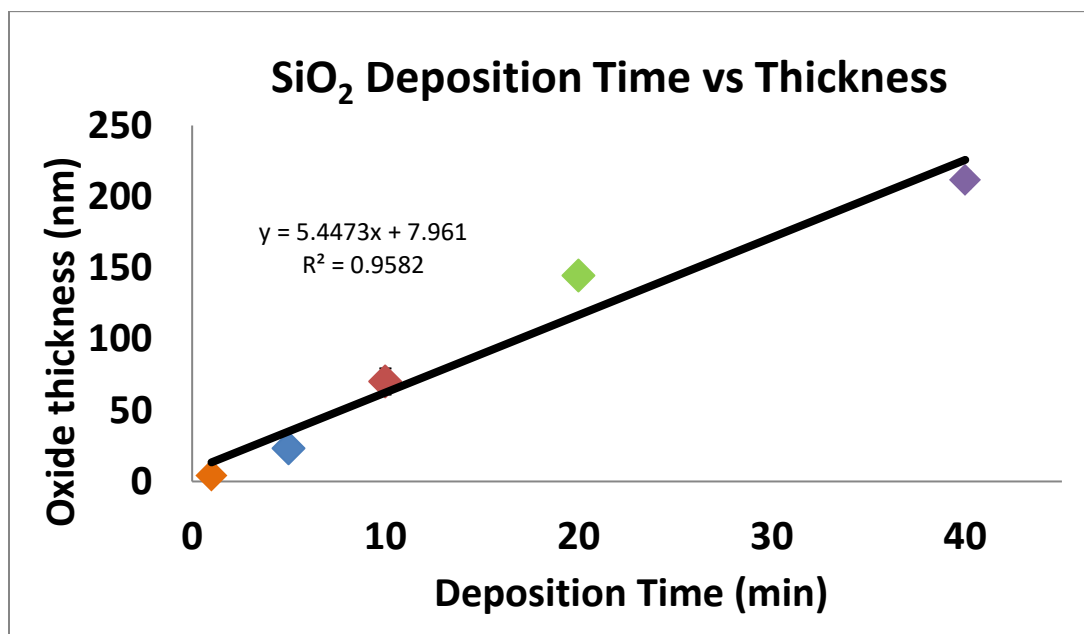
Figure 18: Plasma Silica Deposition vs. Time
(The First Point (~4 nm) is a reference point from Mukhopadhyay et al.[80])

3.6.2.2 Atomic Layer Deposition (ALD)
     ALD is a vapor phase self-limiting thin film deposition method where the reactions take
place between precursor gas molecules and the surface of the substrate. The resulting thin film is
typically pinhole free and conformal to the surface of the substrate [101]. The precursor used for
deposition of Al_2O_3 was Trimethyaluminum, and SiO_2 was Trisdimethyaluminum, both
precursors alternated with water vapor during the deposition process. The thin film growth
process was carried out at 200 °C with a deposition rate of 1 Å/s and 0.5 Å/s for Al_2O_3 and $SiO_2,$
respectively.

3.6.2.2.1 ALD Alumina Deposition Rate
     In order to measure the deposition rate of the ALD alumina, discrete cycles were deposited
to build up different alumina film thicknesses. Figure 19 shows the resulting oxide thickness vs

deposition cycle. The result shows that the deposition of ALD alumina is linearly related to the number of deposition cycle.

ALD Al$_2$O3 Deposition Time vs Oxide Thickness
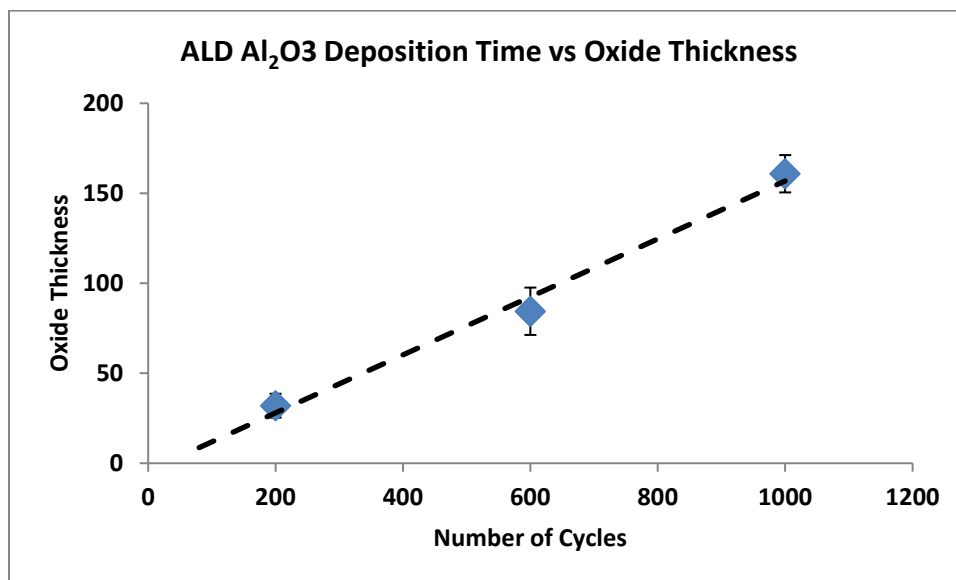
Figure 19: ALD Alumina Deposition vs. Cycle

3.6.2.3 Sputtering:

Sputtering is a technique used for thin film deposition. In this study the sputter is used to sputter thin film of nickel or iron to be used as the catalyst source for TCVD and MPECVD CNT growth techniques. The substrate that is receiving the deposited material is placed in a vacuum chamber filled with inert gas, Argon. A negative charge is applied to the target material in the sputter chamber, at which a plasma plume is formed. The free electrons from the target source will then collide with outer electronic shell of Argon gas. The positive charged Argon ions will then be attracted to the negative charged target material at a very high velocity that "sputters off" atomic size particles of the target material. The thin films are then formed by these atomic size particles that are knocked off from the bulk material and condense on the sample surface.

The sputter system used in this investigation has the following settings; 345V with 150 mA and Ar gas flowing at about 20 sccm to keep the pressure at constant about 5 x 10^{-2} Torr.

3.6.3 Surface Roughing Techniques
3.6.3.1 Reactive Ion Etch (RIE)

Certain model carbon samples used in the investigation require a variation in surface roughness. One way to accomplish that is to use reactive ion etch (RIE). RIE uses gas sources, typically oxygen or argon, to create plasma. This plasma can be used to etch the surfaces of a substrate material, thereby altering the surface morphology in terms of surface roughness or dangling bonds. Here are the operating parameters for the RIE: 50 mTorr, 5.8 sccm O$_2$ flow, 13.56 MHz, 0.71 W/cm², and the DC bias voltage was around -500 to -540 V. The chuck cooling water was set to 20°C, but the sample was not bonded to the stage.

3.7 Instrumentation Used for Characterization, Testing and Evaluation
3.7.1 SEM:

Scanning electron microscope (SEM) is a type of electron microscope. This equipment produces images by scanning the surface of the sample with a focused beam of electrons. When

electron hits the surface of the sample it interacts with the atoms on the sample and produces secondary electrons that can be detected to form a high magnification image. The signal contains information about sample's topography and/or chemical composition as well. For this study FEI SIRION SEM and JEOL SEM equipment were used to capture images using the secondary mode. These equipment allows high resolution topographical images up to 100-200k magnification, however if the sample is not highly conductive it can limit the magnification and the imaging quality.

3.7.2 EDS:

Energy-dispersive X-ray spectroscopy (EDS) is an elemental analysis tool that is often used in conjunction with SEM. Scanning electron beam excites atoms that emit X-rays and give off an unique signature peak or peaks on a x-ray spectrum. The incident beam will excite the electron in an inner shell of the sample and ejecting the electron leaving an electron behind. The energy difference between the higher energy shell and the lower energy shell is expressed as a signature peak on the x-ray chart.

3.7.3 TEM:

Transmission electron microscopy (TEM) is another form of electron microscopy. The specimen used here are ultra-thin (<80 nm). From the incident beam the electron is passed through a specimen and an imaged is formed on the other side of the specimen onto an imaging device. The TEM can magnified and focus the image on a fluorescent screen. TEM images are typically taken at significantly higher resolution and magnification, comparing to SEM images, and in optimal conditions it can achieve images of single column of atoms.

3.7.4 FIB:

Focused ion beam (FIB) is an instrument that uses an electron beam for sample imaging similar to an SEM, and in addition it has an ion beam column that can be used for thin film deposition and/or ablation of materials. This is key equipment for TEM sample preparation.

In order to view a sample using TEM, the electron beam needs to be able to transmit through the sample thickness. The thickness for "electron transparency" is usually targeted to be roughly around 75 – 150 nm; however a sample that require atomic resolution may require a thickness around 10 nm. This sample specimen was nicknamed "foil" due to the work done historically with TEM material came from material made of metal foils [102]. The term foil will be used here on after describing the sample being view under TEM.

There are multiple methods to prepare a TEM foil, with advantages and disadvantages associated with each of the methods. Traditionally TEM foils are made from thinning of bulk material to sub-micrometer dimension using mechanical cutting, grinding, and polishing with progressively finer diamond abrasives. This process is non-trivial and can be very time consuming. In addition, during the sample preparation process there are possibilities of introducing artifacts and damages to samples. With practice, these less optimal effects can be minimized, however, it is important to choose the appropriate sample preparation method for specific sample composition for a particular data collection. One of the goals for this study is to analyze the cross sections of the grown CNT samples. Since the foil has a specific orientation it needs to preserve, this makes Focused Ion Beam (FIB) an ideal method for sample preparation. The cross-sectional foils prepared in this study were prepared by using FIB technique described below.

FEI DB235 is a dual-beam FIB system that is capable of switching between electron bean mode, used mainly for imaging, and ion beam mode used mainly for surface modification. The ion beam has an output ranging from 5-30 keV. The grown CNTs samples are first mounted on a SEM pin stub using carbon double side sticky dot to stabilize the sample. This configuration allows the user to transfer the mounted sample from SEM to FIB without needing to re-mound the sample. This minimizes the possibility of damaging the sample through the imaging process. The procedure used to thin the cross-sectional sample from bulk CNT grown sample is outlined in the Figure 20. Figure 20a and Figure 20b shows the surface of the sample tilted at 52°, with respect to the electron beam. Figure 20a is taken using an electron beam (E-beam) source while Figure 20b is taken using an ion beam (I-beam) source. The differences between taking images and etching material while using I-beam is the amount of current being used. The larger the current the more damage the I-beam can do to the material in the viewing area. Figure 20c and Figure 20d is showing the surface of the sample with a protective cap made of Pt and C. The protective cap prevents ion damage to the cross section foil, which is the area of interest. Figure 20c shows trenches were cut on the front and the back face of the foil. The next step is to undercut the foil to release it from the main substrate. This under cut will cut across the thickness of the developing foil. This step is than followed by inserting a needle called Omniprob 3000, made of tungsten. The purpose of the omniprob is to first lift out the loose foil, follow by attachment of the foil to a TEM grid. The attached foil can be seen in Figure 20e (I-beam) or Figure 20f (e-beam). The final process is to thin a section of the foil to electron transparency, about 100 nm range. The foil is then ready for initial TEM analysis. From this first analysis the user can gauge the foil thickness, and see if subsequent thinning using a (Fischione NanoMill 1040) is needed. Figure 20 g-i are TEM images of the foil with increased magnification.
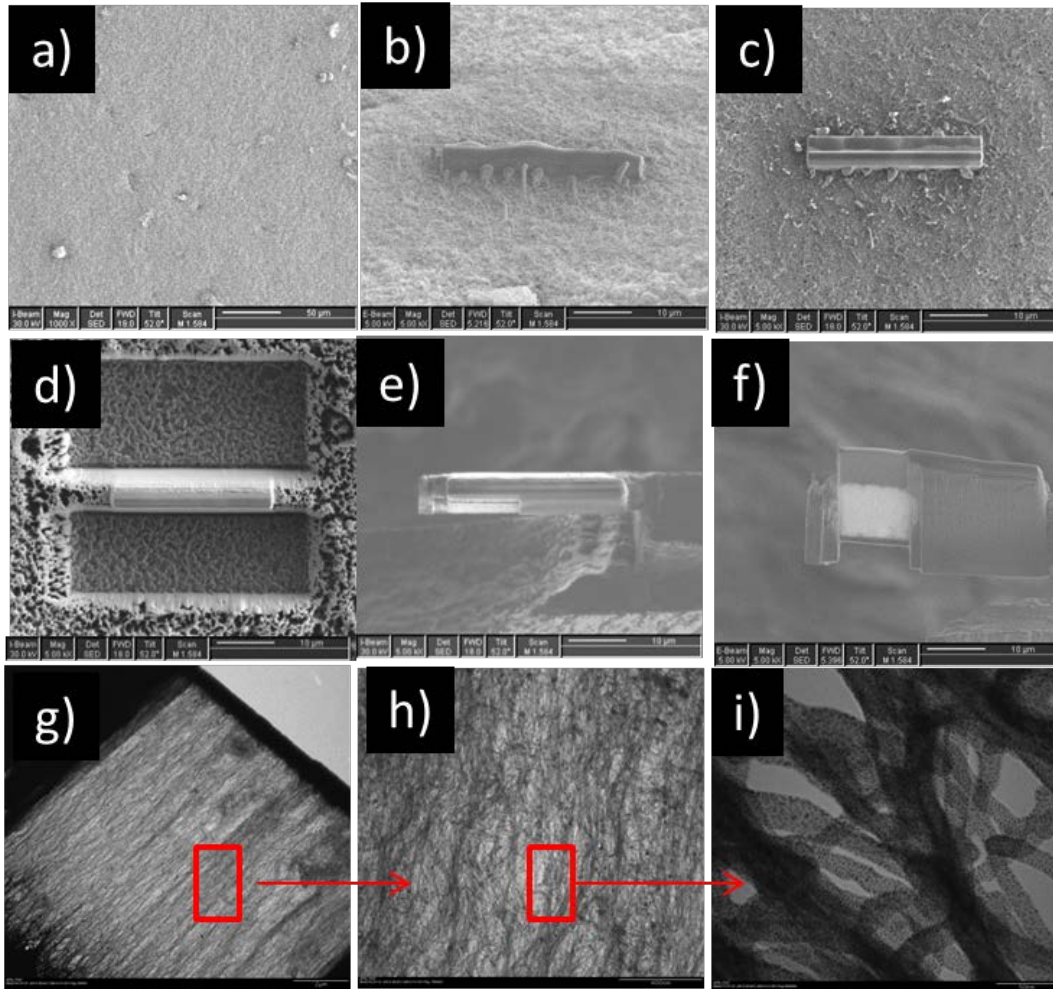
Figure 20: FIB Images of TEM Foil Making Steps

a) Initial surface, b) secondary electron view of protection cap, c) View of the protection cap (I-beam), d) Trenched section, E) Lift off attachment of the foil (I-beam view), e) Thinned foil sample (e-beam view) g) TEM low magnification view of CNT foil, h) TEM medium magnification view of CNT cross-section, i) TEM high magnification view of CNT.

3.7.5 Table Top Stylus Profilemeter:

In order to investigate surface modification treatments that deposits oxide thin films, oxide deposition rate needs to be established first. Oxide deposition rate was measured for ALD alumina and plasma silica, respectively. Knowing the deposition rate allows deposition of desirable oxide thickness. This will help in the investigation of CNT growth characteristics associated with oxide thickness.

The oxide thicknesses were measured using a table top stylus profilemeter. A screen shot of the data from the profilemeter is shown in Figure 21. The thickness of the film is taken from the difference measured from the height of the film and the baseline.

DISTRIBUTION STATEMENT A: Approved for public release. Distribution is unlimited.
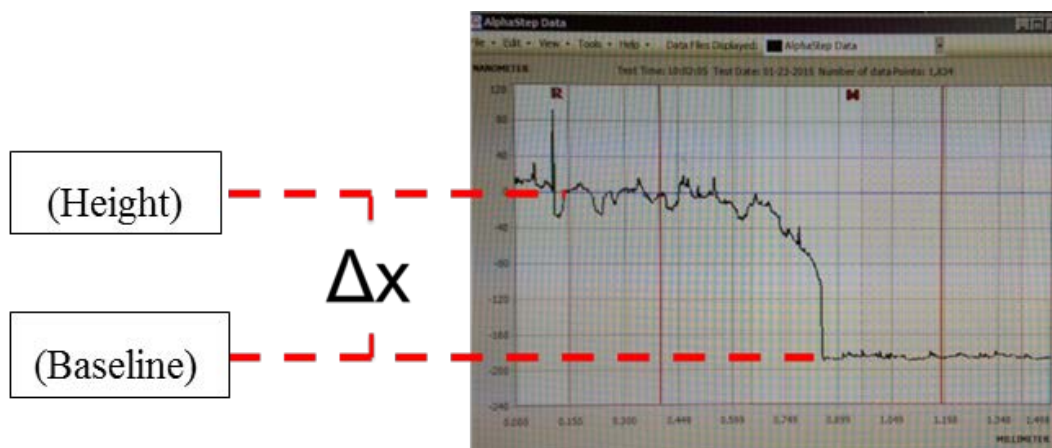
Figure 21: Screen Shot of Profilmeter

3.7.6 AFM:

In this dissertation AFM used is The Quesant© model Q-Scope 250. Atomic force microscopy (AFM) is an instrument that uses a cantilever with a scanning probe that gently surveys the sample surface. As the probe scans across a surface, it provides a feedback in the form of electric potentials or currents. AFM can be operated under three different modes and they are contact mode, non-contact mode and tapping mode. Depending on the scanning mode, the AFM can measure force in the form of contact force, Van der Waals force, chemical bonding, magnetic force, and even electrostatic forces. The probe tip is commonly made of silicon nitride or silicon with a tip radius of curvature in the nanometer range.

It is important of compare surface roughness of the growth samples, because it was believe that surface roughness can have an influence on CNT growth in terms of density and alignment. The reported surface roughness values in this dissertation are obtained using 1 Hz scan rate with 400 points per inch sampling resolution. For more information about the surface roughness measurements and the effect it have on CNT growth please see Chapter 6.

3.7.7 Raman spectroscopy:

This instrument uses a laser source to interact with phonons and electrons of a sample resulting in an energy shift of the reflected photons. Raman shift are recorded in wavenumbers (cm^{-1}) and provides information about the vibration modes of the sample and can provide chemical information and crystallinity quality. In the case of CNT, Raman spectroscopy is used to identify distinct signature modes that are commonly referred to as D-peak (I_D) and G-peak (I_G) corresponding to "disordered" carbon and "graphitic" carbon [103]. The G-peak and the radial breathing mode (RBM) are 1st order Raman scattering peaks resulted from measuring scattered phonon energy. RBM is strong feature of SWNT. It is a unique phonon mode, where it all carbon atoms move coherently in the radial direction. The presence of this peak means that you have detected SWNT, and it is located at ($200\ cm^{-1}$). While the D-peak is resulted from measuring the 2nd order Raman scattering. Both G-peak and D- peak are resulted from Raman scattering, therefore they are formed by the stoke process as appose to the anti-Stokes process where the phonons are absorbed. Raman spectra plots are formed by measuring the intensity of the scattered light as a function of frequency .The Raman Spectroscopy used in this study was a DeltaNu ExamineR 532 equipped with a green laser measured with a 532 nm wavelength.

3.7.8 Sonication:

Many reported works involving the use of CNTs, stated that the CNTs are in a loose power like form. However, it is believed that in order to fully benefit from CNT's high thermal conductivity, a strong attachment between the CNT and a substrate is required. One such configuration is to grow CNT directly on a substrate. After the growth a sonication test can be done to compare the quantitative attachment strengths of the samples. In this investigation, a Branson 3210 sonicator bath was used. This sonication device uses a frequency of 42 kHz with an output wattage of 100W. Grown CNTs samples were sonicated in water for 5 minutes.

3.7.9 Laser Flash Analysis:

Laser flash apparatus (LFA) technique was first developed in 1961 by Parker et al. [104], and has been well established and widely accepted as a thermal measurement technique. This instrument measures the thermal diffusivity of a material. The measurement set up is easy, and it only requires a small sample size. This method does require the values of specific heat and density of the material being tested. Sometimes these two values are not readily available. This method uses a short laser pulse to heat the front side of the plane-parallel to the sample. The pulse is usually in the millisecond range, and the intensity is usually in several kilowatts per square millimeter range. The heat absorbed from laser will propagated through the sample, causing the backside of the sample to rise in temperature. The change in temperature is detected by an infrared detector, on the opposed face of the sample with respect to the laser. The entire experiment was kept at an inert environment with a constant flow of argone gas at 60 sccm. The output from LFA is the thermal diffusivity (α) value measured. In many cases the specific heat (C_p) of the sample can also be measured at the same time. If the density (δ) of the material is known, than thermal conductivity (λ) can be calculated using the equation below.

$$\lambda(T) = \alpha(T) * C_p(T) * \delta(T)$$

Equation 3: Thermal Conductivity

Thermal diffusivity is defined by the Parker's equation below and has a unit of (m^2/s)

$$\alpha = 0.1338 * \frac{d^2}{t_{1/2}}$$

Equation 4: Thermal Diffusivity

Equation 4, takes account for the material's thickness and the time at which the rise in temperature has reached half of the maximum ($t_{1/2}$), see Figure 22for a plot from a typical scan.
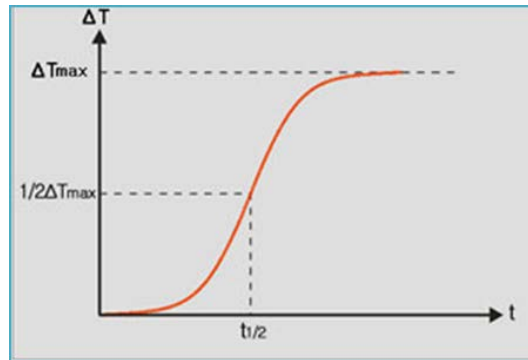
Figure 22: Half Time Rise of a Diffusivity Chart from Netzsch Equipment Manual

The laser flash system used in this study was built by Netzsch, their MicroFlash©457 model. This instrument has a high accuracy and repeatability, ±2% for standard materials and ±3% for

most materials measured. It has a wide temperature testing range of -125°C to 1100°C. It also uses a non-destructive non-contact technique, and it has multi-layer sample measurement and analysis capability. A functional diagram of the system provided by Netzsch is shown in Figure 23.
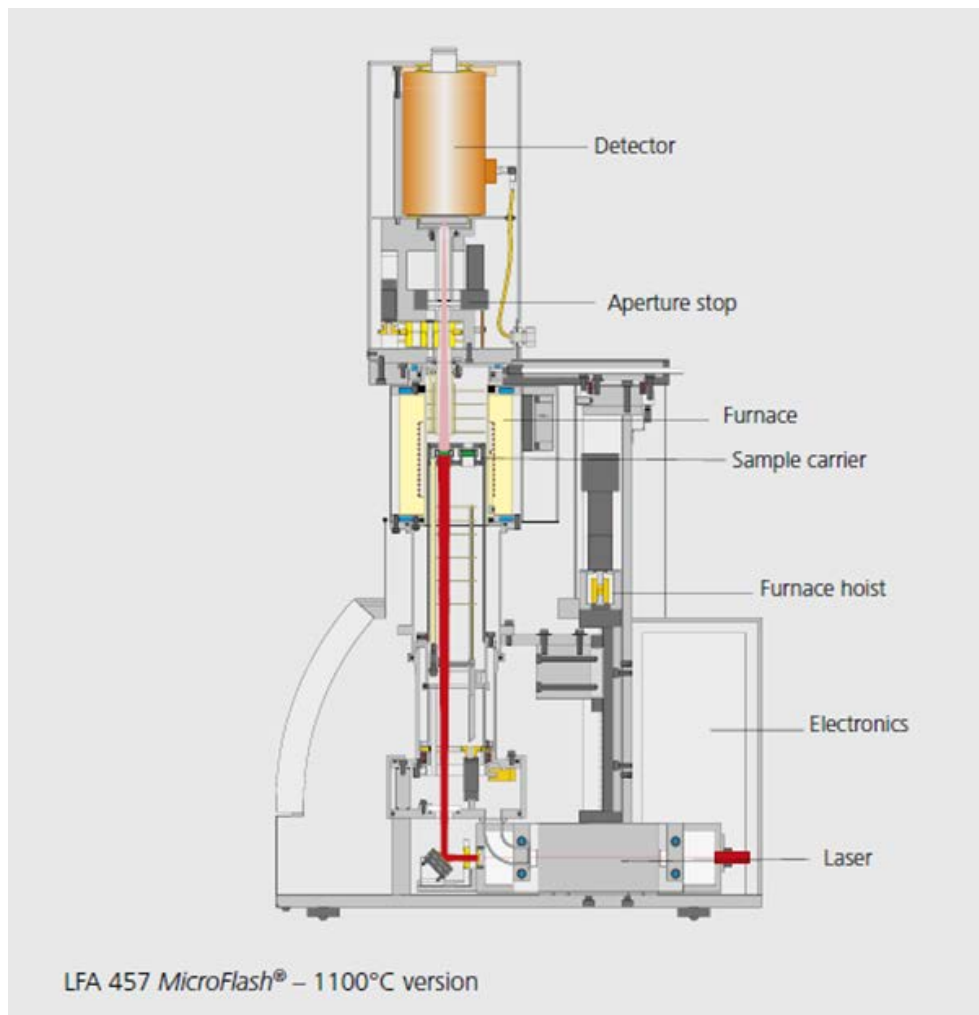
Figure 23: Drawing of a Laser Flash System

The image shows the LFA 457 is equipped with a laser, a furnace, sample stage and an IR detector, which are all controlled by a built-in data acquisition system also by Netzsch. The sample stage can rotate and is set to hold up to three samples. To take measurements using the LFA 457 system, the sample needs to be opaque to infrared. It is recommended that samples with low emissivity values can be coated with a thin layer of graphite to achieve blackbody radiation characteristics. It is also suggested that additional coating with a thin layer of gold can be applied if better heat signal absorption is required.   The samples are usually 10 mm^2 by 0.1 to 6mm in thickness. It is important to have the sample as flat as possible in order to achieve optimal signal detection. Ideally the laser should enter the sample at a 90 degree angle; this would allow heat to flow through the sample uniformly. The thermal analysis conducted using LFA will be presented in Chapter 7.

Section II: Preliminary Investigations
(Background Studies)

CHAPTER 4: *Preliminary Investigations Part I*, Growth on Dense Carbon

It was mentioned earlier in Section 3.5, that CNTs can be fabricated using a variety of growth techniques. However, it is known that the resulting CNTs are not always the same. For example some techniques are better at growing SWNT over MWNT, while others can produce coiled CNTs or vertically aligned CNTs. Due to cost effectiveness, scalability, and laboratory accessibility, this investigation selected CVD growth techniques for investigations of CNT fabrication on carbon substrates. A great majority of CNT reported thus far was done using electronic grade silicon. Growth on carbon substrates such as diamond or graphite remains low. Therefore it was not clear which of the CVD methods was are suitable at growing CNTs. Therefore, it was decided that background studies should be done to compare the effectiveness of using CVD methods to grow CNTs on diamond substrates. The following two chapters will be used for background information related to this investigation.

The background study conducted in this chapter has two purposes. The first purpose is to see if dense CNT growth (full coverage of the substrate) is achievable on diamond substrates when CVD growth technique was used. The second purpose is to provide general comparison among the three CVD growth techniques and their effectiveness of growing CNTs on diamond substrate. This background study will serve as a building block allowing more detailed studies to be conducted. The findings here will help in narrowing down selections of suitable growth technique to be used for the reminder of the research.

Due to laboratory availability three different kinds of CVD fabrication method were used. Two of which are described as traditional growth methods, T-CVD and MPECVD, while FCCVD is a newer and more scalable approach. The resulted grown samples were compared and characterized for CNTs growth density and tube morphologies, technique successfulness, and relative mechanical properties.

4.1 Objective (Grow CNTs on Diamond)

The objective of this chapter is to find out if CVD methods can be used to grow CNT on diamond substrates, in addition to compare the characteristic of the resulting tube. To accomplish this, the approach is to grow CNTs on diamond substrate using three different kinds of CVD methods, two traditional CVD methods and one newer CVD method. The results and the findings are presented below.

4.2 Preliminary Investigations: Suitable Catalyst Source For Traditional Growth Methods

The main difference between traditional growth methods and the newer and more scalable growth methods is the number of steps required for CNT growth. The traditional growth is a 2-step process where metallic catalyst thin films need to be deposited independently and a heat treatment step is often required to coalesce the metallic films in order to form catalytic particles. This creates a unique opportunity to allow investigation of the behavior of catalyst particles using the traditional method. The newer and more scalable CVD process introduces catalyst and carbon source at the same time, while heat treatment step is not need, therefore was not included in the heat treatment comparisons step.

It has been report that transition metals are excellent catalyst source for growing CNTs. However their effect in supporting CNT growth on carbon substrate, more specifically diamond substrates, has not been well understood. Due to the laboratory availability two metal sources, iron and nickel, were simultaneously investigated. Using the traditional growth methods, their effects as catalyst sources on diamond substrates were compared.

4.2.1 Thermal CVD (TCVD) – Successful Catalyst Investigations:

TCVD is a well-established technique. It has been reported that this technique is successful at growing CNTs. Several published work stated that transition metal are an excellent source for CNT growth S. However many reported studies were ones investigated using silicon as substrate. It wasn't clear if the result in terms of CNT morphology, crystallinity or areal density will be the same if diamond substrate was used. To address this uncertainty, investigations using iron and nickel as catalyst sources were conducted.

Diamond substrates were first sputtered individually with 10 nm nickel films or 10 nm iron films. These samples were grown at the same time to see which catalyst is most suitable for CNT growth. The growth parameters used for the initial TCVD investigation are listed in Section 3.5.3.1.2. Figure 24a shows the result when 10 nm nickel thin film was used for CNT growth. The SEM image shows a dense amount of CNTs were grown on the surface. Figure 24b shows the result when 10 nm iron thin film was used for CNT growth. The SEM images show that the surface did not produce anything that resembles closely to a CNT tube. These images show that using this growth parameter, nickel was better at growing CNT between the two catalyst sources. One possible reason for the differences between the results might be associated with the growth temperature and the catalyst source used. At 800°C, the temperature is above the eutectoid point for Fe-C, which is 727°C, but still below the eutectoid point for Ni-C, which is at 1326°C. This suggests that it is possible that at the CNT growth temperature, the iron thin films coalesce into nano-particles, and these particles reacted with diamond substrates or the carbon gas source. As a result, some form of carbide was more favorably formed instead of CNT. However since the eutectoid temperature is much higher for Ni-C, carbon was able to use nickel as a catalyst and precipitate CNTs out from the catalyst particles.
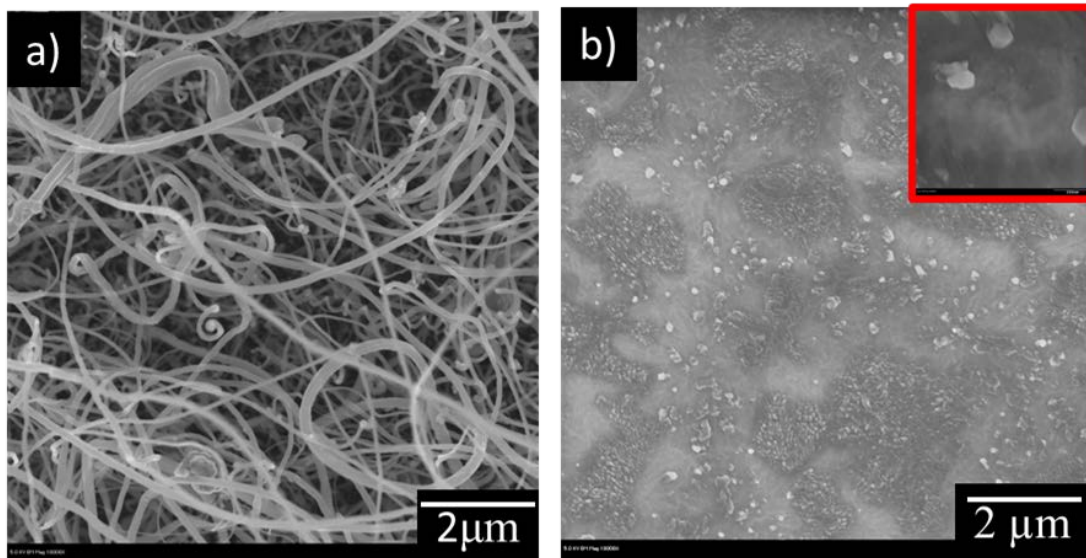
Figure 24: SEM Images
a) SEM image of post CNT growth on diamond using nickel as catalyst, b) SEM image of post CNT growth on diamond using iron as catalyst, the insert is taken at a higher magnification to show that there were no visible CNT

4.2.2 MPECVD – Successful Catalyst Investigations

Microwave plasma CVD also is a well-established CVD process; it is often used in low temperature processing of microelectronic. For CNT growth, the plasma in the reaction chamber usually dissociates the precursor even before they interacts with the catalyst particles. Thus it has been reported by Robertson et al. and Cantoro et al. that low temperature (300 °C) CNT growth was achievable when grown on substrate with alumina support [106], [107].

Diamond substrates were first sputtered individually with 10 nm nickel films or 10 nm iron films for MPECVD investigation. These samples were grown at the same time to see which catalyst is most ideal to initiate CNT growth. Growth parameter is shown in Section 3.7.2.2. Figure 25a shows the result when 10 nm nickel thin film was used for CNT growth. The SEM image shows a sparse growth of CNT on the surface. Figure 25b shows the result when 10 nm iron thin film was used for CNT growth. The SEM images show dense amount of CNT growth resulted on the surface. These images show that using this growth parameter, iron was better at growing CNT between the two catalyst sources. One possible reason is that at 650 °C, the temperature was too low to allow proper growth to take effect for samples using Ni catalyst. As a result, there was only a low CNT growth yield. Higher temperature was not explored since the goal is to take advantage of low-temperature processing technique provided by MPECVD.

Due to the results from this preliminary investigation it was determine that nickel catalyst will be used as the catalyst source for TCVD, and iron will be used as the catalyst source for MPECVD for the reminder comparison in this chapter.
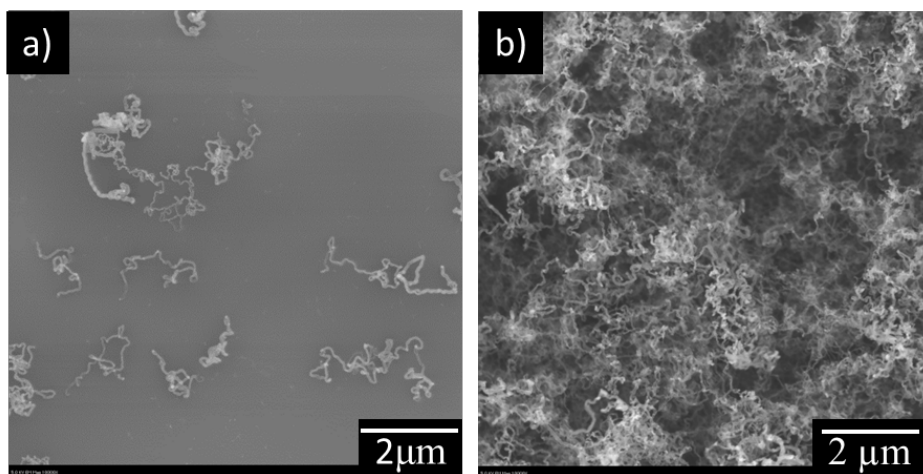
Figure 25: Nickel and Iron Thin Film SEM Images
a) result of CNT grow using nickel as catalyst with sparse, b) result of CNT growth using iron as catalyst with dense CNT growth

4.2.3 Heat Treatment – Catalyst morphology comparisons

It is well established that the underlying catalysts play a big role in the structure and the morphology of the resulting CNTs [96], [108]–[110]. The results from Section 4.2.1 and Section 4.2.2 indicated that with the growth parameters investigated, different catalyst materials are required for the two different CVD growth techniques. In this section the heat treatment step was compared to investigate the underlying catalyst morphologies. The purpose of heat treatment is to allow the catalyst films to break up and coalesce into catalytic particles for CNT growth.

For TCVD and MPECVD growth methods, samples were brought to heat treatment temperature (800 °C for 2 minutes and 400 °C for 5 minutes, respectively) and held there for the heat treatment process. Instead of continue on with introduction of carbon source to allow CNTs to nucleate, the heat sources were terminated and bring the chamber back down to room temperature. After which, the samples were removed from the growth chamber and into microscopy chamber for surface feature analysis.

Figure 26a shows the result of TCVD thermal treated 10 nm nickel film after undergoing thermal treatment. The resulting nanoislands have an average diameters of 53 nm distributed uniformly across the substrate surface. Figure 26b shows the SEM surface analysis of a sample using MPECVD to thermally treat at 400°C. The image shows that the iron catalyst agglomerated into a continuous uneven film rather than coalesced into isolated nanoparticles.
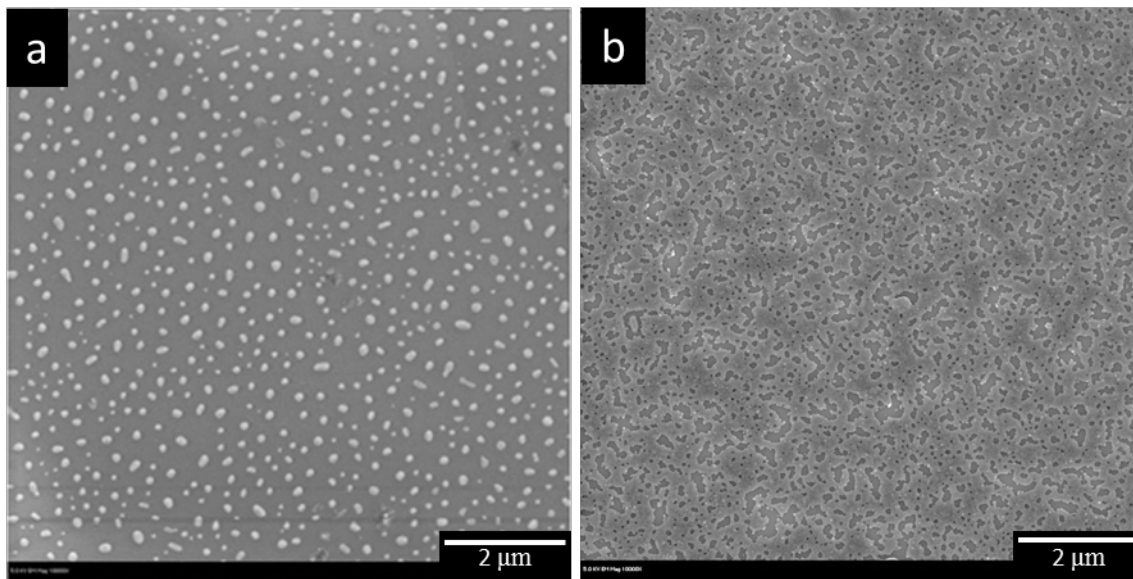
Figure 26: SEM Images of Catalyst Particles
a) Ni catalyst after thermal treatment in T-CVD. b) Fe catalyst after thermal treatment in MPE-CVD with hydrogen plasma.

4.3 Empirical investigation of 3 CVD methods for growing CNT on Diamond substrates

Now that the corresponding catalyst sources has been identified for the different growth methods a comparison of the resulting CNT using three different CVD methods were conducted.

For the growth parameters used for each of the corresponding CVD techniques please refer to the following sections. Section 3.5.3.1.2 for TCVD, Sections 3.5.3.2.2 for MPECVD, and Sections 3.5.3.3.2 for FCCVD.

In this investigation, catalyst particles size will be compared using microscopy techniques. Earlier reports of CNT growth on silicon stated that at some point CNTs will stop its growth due to inactivation of catalyst source. The inactivation of catalyst particles has been described as phenomena resulted in too much carbon built up that resulted in encapsulation of the catalyst particle. When encapsulation occurs, an immediately deactivation of the catalyst particle will occur [111]. Others mentioned that when catalyst particle changed from meta-stable phase to a stable phase it will lost its catalytic capability[109]. Furthermore, reports have shown that the catalyst activation can be extended if water vapor is introduced during growth [112]. Therefore by investigating the catalyst particles post CNT growth may reveal other notable information about the CNTs morphology and physical characteristics.

4.3.1 Characterization Methods

The grown sample resulting from each of the CVD methods were analyzed by microscopy, spectroscopy and sonication methods. FEI Sirion, a high resolution SEM, was used for microscopy analysis of CNT carpet height and nanotube morphology. In addition, to understand whether the tubes were tip or root growth, cross-sectional TEM foils were prepared. Energy Electron Loss Spectroscopy (EELS) equiped by the TEM was used for chemical composition analysis. Raman spectroscopy analysis was used to provide the qualitative comparisons for the crystallinity characteristic of CNTs. The Raman intensity ratio between the disorder peak (D-peak) and the graphite peak (G-peak) is used to determine the degree of crystallinity/purity of the CNT [113]. Finally, sonication test was performed for a qualitative analysis on the durability

and mechanical strength of the bonding between CNTs and the diamond substrate. If CNTs are present on the surface of the substrate after a sonication test, it will suggest that the bonding between CNT and the substrate is strong. The grown CNTs samples were tested in a sonicator bath that uses a frequency of 42 kHz with an output of 100W. For details of sonication see Section 3.7.8.

4.4 Results and Discussion

4.4.1 Nanotube Morphology:

Figure 27 shows SEM images of the CNT layer formed on diamond film using the three different techniques. For TCVD nickel was the catalyst source, while MPECVD and FCCVD both uses iron as catalyst source. Figure 27a is the image of T-CVD grown CNTs which have an average tube diameter of 61nm ±12nm, with uniform tubular structure. This correlates well with the uniform size distribution of nickel islands of similar sizes seen in Figure 26a.

Figure 27b is an SEM image of MPE-CVD-grown CNT that indicates that the CNTs are not uniform and contain various defects as well as variation in diameters. This may be the result of the seed catalyst layer consisting of irregular-shaped particles. The nonuniformity of individual tubes may also be influenced by defects developed during formation. The MPE-CVD method uses a hydrogen plasma that forms the growth process [27]. Some studies suggest that exposing growing CNTs to hydrogen-rich environments convert them into diamonds [28, 29]. Figure 27b shows the MPE-CVD CNTs tubes with defects similar to the ones reported by Behr et al. after exposure to the hydrogen-rich environment [114].

Figure 27c shows an image of FCT-CVD-grown CNTs. This figure indicates that the CNTs are uniform in diameter and grow as densely entangled forests. These CNTs have average diameters of 12nm ± 1.8nm, making them the smallest of the three growth methods. The image also suggests that there are particles residing on the outer surface of the CNTs. This is expected because the xylene/ferrocene mixture provides continuous source of iron particles throughout the entire process, some of which are expected to attach to the growing CNT surface. The diameter of the outer particles can provide an estimate of iron catalyst size, and they have an averaging diameter size of 12nm ±2.2nm.
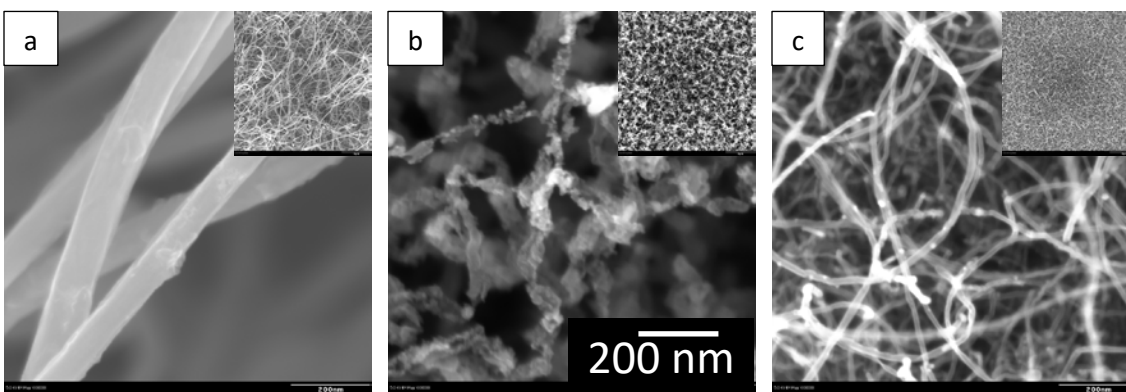
Figure 27: SEM Images of CNT Morphologies
a) T - CVD grown CNT, b) MPE - CVD grown CNT, c) FCT - CVD grown CNTs. Images are taken at the same magnifications

4.4.2 Catalyst Distribution in the Final CNT-covered Diamond Structure

Figures 18–20 show high-resolution TEM images with Energy Electron Loss Spectroscopy (EELS). Figure 28 is the TEM and EELS analysis for the TCVD sample. Figure 28a is an EELS scan for elemental carbon, the lower portion of the figure have higher carbon concentration,

therefore it was identified to be the diamond layer. The top portion of Figure 28a is highlighted by CNT. Since CNT and diamond are both made of elemental carbon the only way to tell the two apart is by comparing the pixel intensity. The whiter the pixel appears, the higher the pixel intensity for the scanned element. This is the same for Figure 29 and Figure 30. Using the pixel intensity comparison one can find the interface that separates the diamond substrate from CNTs.

Figure 28b is TEM image of the EELS scanned area, and Figure 28c is EELS scan for elemental nickel. These figures indicate that in T-CVD, nickel particles are encapsulated with a layer of carbon, and CNT growth originates from the outer carbon layer. Since the growth originates from the outer carbon layer, this image shows why the average CNT diameter is slightly higher than the average catalyst particles diameter as shown in Figure 31. The encapsulated catalyst particle remains anchored at the diamond-CNT interface implying the predominant growth mechanism is root growth. There are a few instances where the catalyst particle moved several nanometers into the CNT length, away from the interface. The interface is highlighted by the yellow dotted line. Growth patterns similar to this indicate a small probability of catalyst lift-off.

The green dotted circle in Figure 28c, circles a nickel particle, and a red arrow shows the location of this nickel particle in relation to CNT tubes in Figure 28b.
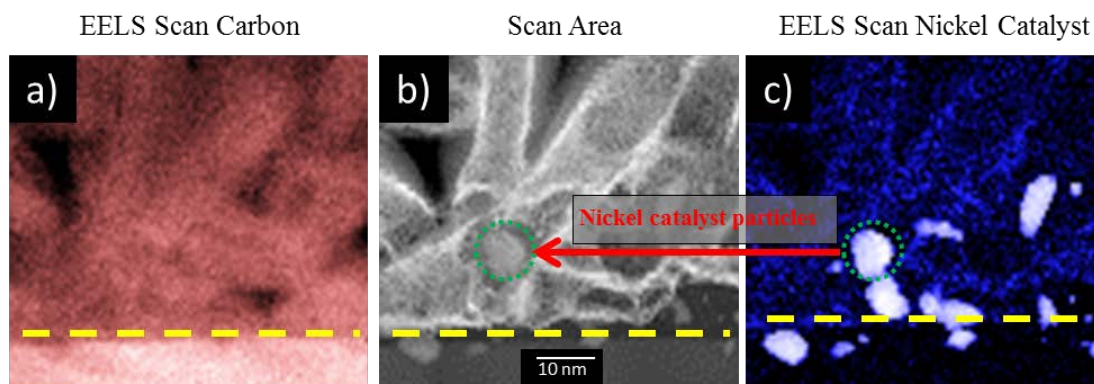
Figure 28: TEM and EELS Cross-sectional Images of a T-CVD CNT on Diamond Sample
a) EELS scan for elemental carbon, b) TEM imaged area, c) EELS scan for elemental nickel.

Figure 29 is the TEM and EELS analysis for the MPECVD sample. Figure 29a is an EELS scan for elemental carbon, Figure 29b is a TEM image of EELS scan area, and Figure 29c is EELS scan for elemental Iron. It can be seen that iron particles in this case do not reside along the interface, yellow dotted line, but rather move away from the interface and into the CNT. Figure 29b shows that the CNTs produced using MPECVD technique were defected looking. As seen in Figure 27b and Figure 29b CNT resulted in this method looked more entangled, and tube diameter were less uniform along one tube and among the tubes. It was believed that the mobility of non-anchored catalytic particles at the interface may contribute to disordered CNT growth. It has been reported that CNTs resulted from tip growth mode produced CNTs that has bamboo-like features with more defects [115]. In addition it has been reported that the catalyst morphology can change when certain growth condition were used. Irregular catalyst morphology has been observed from the TEM images. Furthermore, it has been reported that as the particles migrate more stress is build up between the nucleated CNT and the catalyst particle, as a result kinks and defects are form during the growth process [116]. Therefore, it is also possible that when particles migrate during CNT growth, some stresses can build up coupled

with irregular catalyst morphology the condition is more challenging to produce aligned CNTs. As a result CNT from MPECVD growth methods appears to be more defective. The green dotted circle in Figure 29c, circles some of the iron particles, and a red arrow shows the location of these iron particles in relation to CNT tubes in Figure 29b.
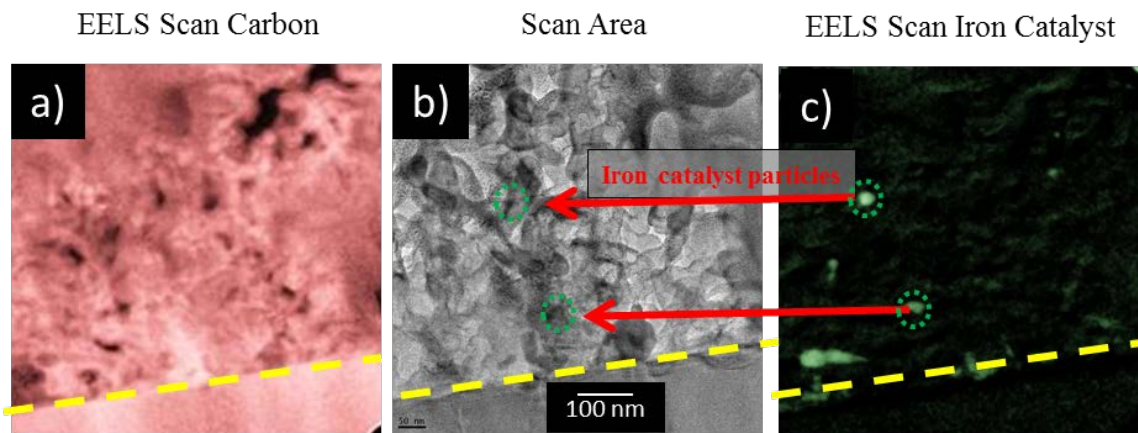
Figure 29: TEM and EELS Cross-sectional Images of a MPE-CVD CNT on Diamond Sample
a) EELS scan for elemental carbon, b) TEM scan, c) EELS scan for elemental Iron

Figure 30 shows the result from FCT-CVD growth method. Figure 30a is an EELS scan for elemental carbon, Figure 30b is a TEM image of EELS scan area, and Figure 30c is EELS scan for elemental Iron. Unlike the previous two CVD techniques mentioned, FCT-CVD technique deposited a layer of silica prior to CNT growth. These images show a high distribution of iron particles residing at the silica coated diamond CNT interface, yellow dotted line. The image suggests that silica layer has a high affinity for the iron particles. The large number of iron catalysts at the interface suggests that the silica film keeps catalyst particles anchored during CNT growth; as a result smaller and more uniform tubes were fabricated. Comparing with the previous growth methods without the silica layer, the catalyst particles appear to be larger and have higher mobility. It is believe that the oxide layer keeps the catalyst particles from agglomerating and migrating during CNT growth. In addition, Figure 30 shows additional iron particles found further away in the CNT forest. This is expected due to the continuous iron particle introduction throughout the CNT growth phase. Figure 30c, circles some of the iron particles, and a red arrow shows the location of these iron particles in relation to CNT tubes in Figure 30b.

EELS Scan Carbon   Scan Area   EELS Scan Iron Catalyst
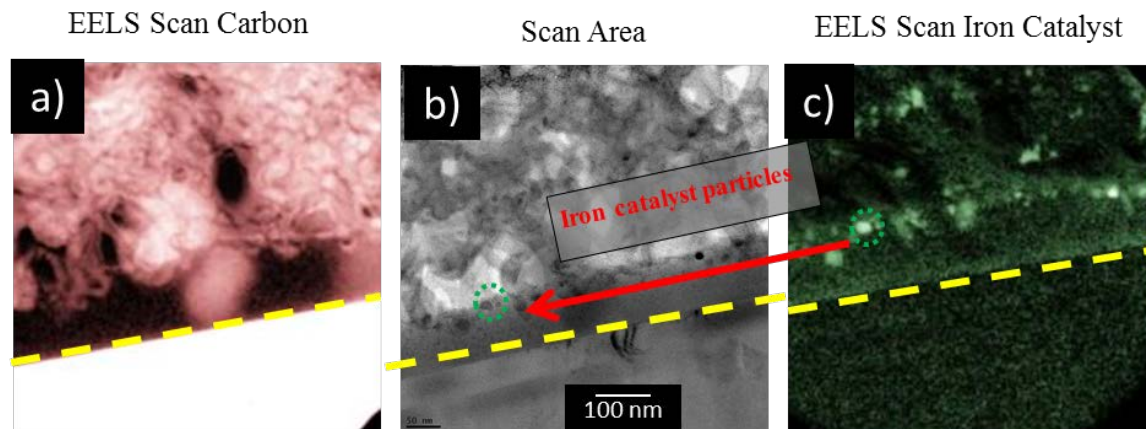
Figure 30: TEM and EELS Cross-sectional Images of a FC-CVD CNT on Diamond Sample

a) EELS scan of elemental carbon, b)TEM scan area, EELS scan of elemental Iron.

So far it was demonstrate that CNT can be successfully grown on diamond substrates. However, it was also observed that with the growth parameter used, different catalyst source were successful at growing CNTs. As a result, some features of CNT appear to be different, such as diameter and catalyst particles. These features are worth noting because they can have effects towards CNT's intrinsic physical properties. For example, it was reported that CNTs with smaller diameters have higher thermal conductivity values [117]. Figure 31 shows the average particle size distribution taken with Image J software. This software provides quantitative values for the catalyst particle size and tube diameter comparison taken from the resulting TEM images. For T-CVD, the average catalyst particle diameter was measured to be 53nm± 16nm, and the average tube diameter was 61nm ±12nm. Thus, the catalyst diameters measured using TEM images are within the margin of error with the top view images seen by SEM. For MPE-CVD, the average catalyst particle diameter was 21nm ±7nm, and the average tube diameter was 40nm ±18nm. For the FCT-CVD method, the average catalyst particle size was 12nm ±2nm, and the average tube diameter was 12nm ± 2nm. Cross-sectional TEM images provided additional information about particle location and concentration relative to the interface. It was expected that different growth techniques and different catalyst layer used will result in CNT morphology differences. Since the morphology of CNT is a dominating factor over the physical performance of the CNT. Investigating these results can reveal growth techniques required for desired CNT morphology.

It was observed that the CNT growth characteristics resulted from T-CVD, was large catalyst particles that reside close to the interface. For MPE-CVD, the catalyst particles are distributed away from the interface. This migration may be due to the fact that they are smaller in size compared to ones seen produced from T-CVD. It is possible that as CNTs nucleates it pushes smaller catalyst particles away from the interface, as a result tip growth mode more favorable in this condition [94]. However, size alone may not be the only reason why migration happened. Iron and nickel have different surface tensions (formation of particle) and surface stresses (wetting of the surface) and these could also be one of the possible reasons for migration of particles. For FCCVD growth, the images indicate that the majority of the iron particles used as catalysts are anchored along the SiO_2 layer and the iron particles that arrived later reside outside the growing CNTs. The anchoring of smaller nanoparticles may be caused by the silica functional layer and may assist in uniform CNT growth. More investigation about the role of

buffer layer can be found in Chapter 5 and 6. Figure 31 shows that the nanocatalyst particle size in each case correlates with the CNT diameters. This was also observed by SEM and TEM images, therefore it further validates the hypothesis that the CNT size is largely governed by catalyst particles.
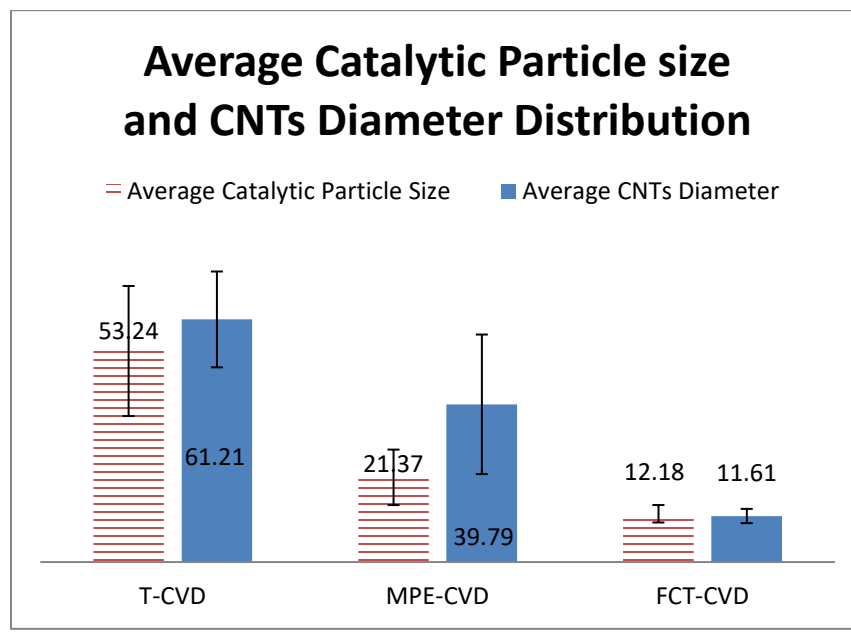
Figure 31: Particle Size and CNTs Tube Diameter Distribution Chart

4.4.3 Raman Spectroscopy Results:

Raman spectroscopy was performed on samples produced by the different growth methods. The results are presented in Figure 32. According to the Handbook of Raman Spectroscopy and Dresselhaus et al., Raman spectroscopy can be used as a guide to describe different carbon structures, such as diamond-like carbon which has C–C sp^3 bonding, graphitic carbon which has sp^2 bonding, and glassy/amorphous carbon which has C–H and disordered mixed bonds [113], [118], [119]. The peaks found around 1350-1365 cm^{-1} are called D-peaks, resulting from the disorderly network of sp^2 and sp^3 carbon clusters, whereas the peaks found around 1580-1620 cm^{-1} are called G-peaks as a result of graphite, and finally the peak found at 1332 cm^{-1} is the diamond peak [118]–[120]. In this experiment, it was observed that samples produced uniform tubes resulted in lower I_D/I_G ratio, while ones produced in kinked looking tubes produced high I_D/I_G ratio. The I_D/I_G ratios are given as follows: T-CVD = 0.30; MPE-CVD = 1.94; FCT-CVD = 0.84. Note that the T-CVD has the lowest I_D/I_G ratio; its SEM images, Figure 27a, indicated that this tube structure looks the most uniform. In contrast, the I_D/I_G for MPE-CVD is the highest and its SEM images, Figure 27b, indicated that the tube structure appears damaged and full of defects. Earlier, it was stated that hydrogen may etch the CNT surface and introduce defect sites. The presence of the defects can raise the intensity of the D-peak. Another possibility that causes a high D-peak is when CNT is introduced to a hydrogen rich environment; the hydrogen alters CNT's C-H bonding and transforms them into diamond or disordered carbon [114], [121].

Since the CNTs were grown on diamond substrates, one might suggest that the high intensity of D-peak resulted from signals coming from the diamond substrate underneath. However, the recorded D-peak intensity lies around (1354 cm^{-1}), whereas known diamond -

peaks are detected at (1332 cm^{-1}), indicating that the peak signal did not result from the diamond substrate. For confirmation, a razor blade was used to scrape away the CNTs from a sample and expose the diamond substrate underneath. The Raman spectra taken from the exposed diamond surface has a peak intensity at (1338 cm^{-1}), which closely matches the published Raman peak for diamond (1332 cm^{-1}). This additional test further indicates that the (1354 cm^{-1}) peak is indeed the -peak from the disordered CNT and not from the diamond substrate.
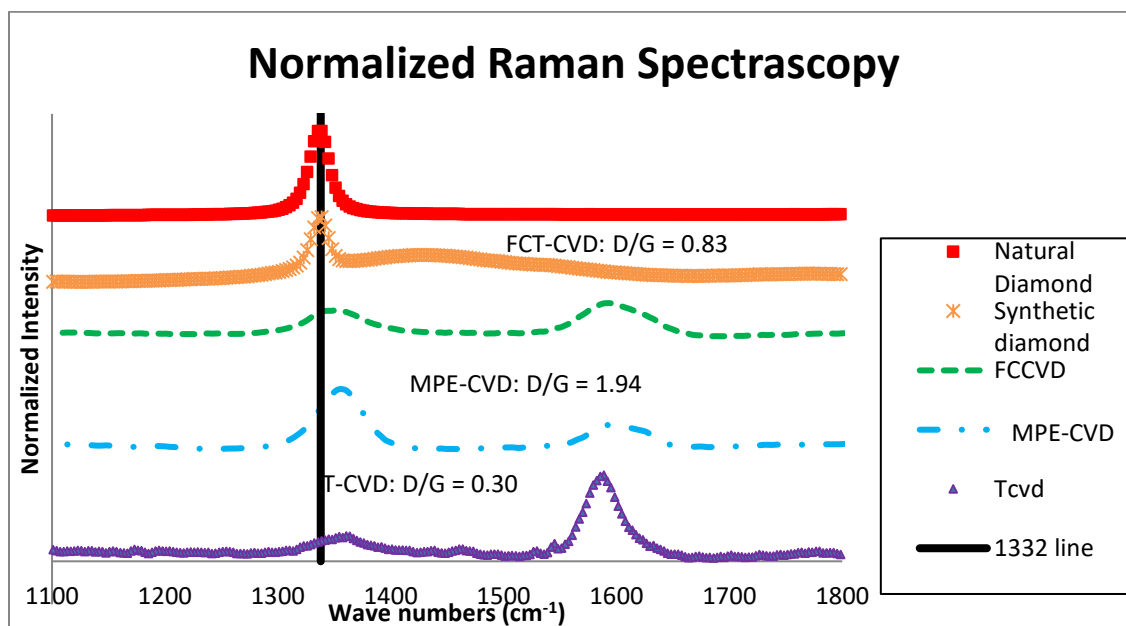
Figure 32: Raman Spectroscopy Signals for Natural Diamond, Synthetic Diamond, and CNTs from the Three CVD Methods

4.4.4 Sonication Results:

    If the sample was used in a commercial device, it would be important to know if the CNTs had the strength to stay intact within the substrate. The sonication system was used in a brief comparison study to see if the resulting CNTs were strong enough to withstand volatile vibrational condition, which may be required in certain electronic packaging.

    For the sonication test, SEM images were taken before and after the sonication treatment as shown in Figure 33. The images in the top row of Figure 33 were taken prior to sonication, and the bottom row images were taken after the test. Figure 33a were form the T-CVD, Figure 33b were from the MPE-CVD, Figure 33c were from FCT-CVD, and Figure 33d were optical images taken from MPE-CVD sample. The before sonication image seen in Figure 33d can also be used to represent T-CVD and FCT-CVD, because there were no visual differences observed after the sonication test. It can be seen that the nanotubes were intact even after sonication and that there were no noticeable differences seen in the before and after images from SEM. The low-magnification optical images show a difference for the MPE-CVD sample. Before sonication, all samples look identical at this magnification as seen in Figure 33d top image. The optical images after the sonication test were unchanged for T-CVD and FCT-CVD which are also represented by Figure 33d top image. The MPE-CVD after sonication sample was different as shown in Figure 33d bottom image. While postsonication SEM images of MPE-CVD sample show that CNTs were present on the scanned regions, the low-magnification optical images show exposed diamond substrate on the corners of the sample. This indicates detachment of CNTs at the

corners of this sample, implying that the bonding between CNTs and substrate may be the weakest in this fabrication method. It must be noted that because of the extremely high length/diameter ratio of the nanotubes, agitation in an ultrasonic bath produces concentrated stresses at the root of the CNT. Survival under these conditions indicates that these materials will be robust in many service conditions. Among the three samples, MPE-CVD specimen may be the weakest, and detachment begins to occur at the corners, which are the most vulnerable regions of the sample. Possible reasons that MPECVD growth technique resulted to be the weakest has to do with the fact that the CNTs contains the most defects, kinked tubes, and another possible reason is that the catalyst particles were not anchored on the substrate as evident by TEM images represented by Figure 29.
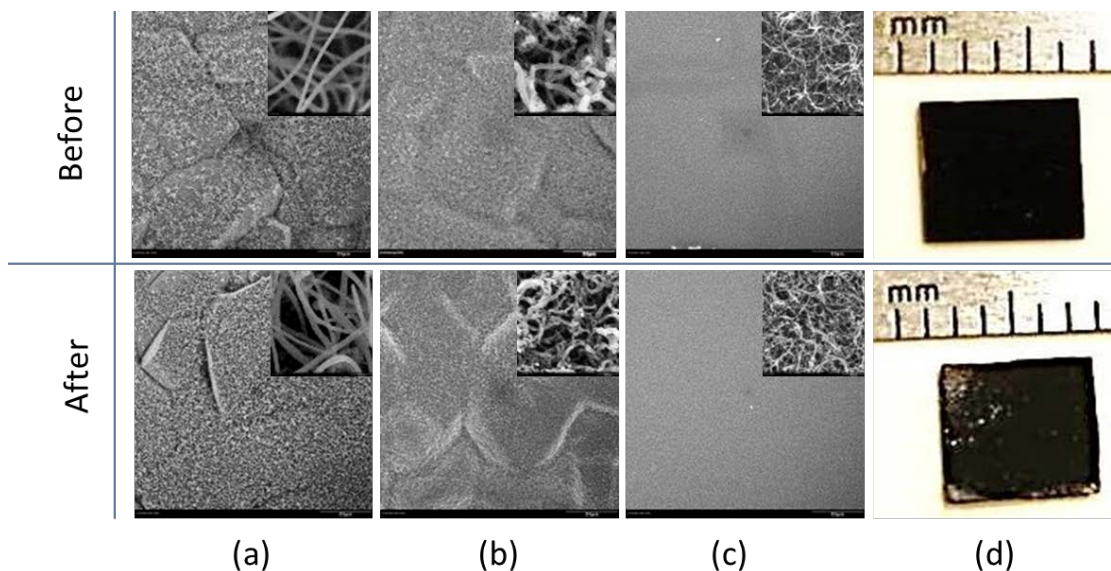
Figure 33: (a), (b), and (c) SEM Images, and (d) Optical Image
The images in the top row were taken prior to sonication, and those in the bottom row were taken after the test. (a) is the T-CVD sample. (b) is the MPE-CVD sample. (c) is the FCT-CVD sample, and (d) is taken from MPE-CVD Sample. There were no visual changes seen after the sonication test for the T-CVD and the FCT-CVD sample. Therefore, the before image from (d), can also be used to represent before and after sonication test for T-CVD and FCT-CVD sample

4.5 Overall comparison:

It is seen that very different types of CNT layers can be grown on diamond film by different techniques. It must be noted that T-CVD and MPE-CVD are multistep processes that separate the catalyst deposition step from the CNT growth step. The catalytic particles in the T-CVD growth are found to be the largest of the three types of growth for the conditions used. These particles were found to reside at the interface with minimal migration into the CNT layer. The resulting CNT diameters were the largest, and were found to be uniform, with lowest Raman I_D/I_G ratio. The uniform structures are thought to be ideal since they have less defects, which means that the intrinsic property of the tubs have higher thermal and electrical properties. It was reported that defects in CNTs can reduce thermal conductivity values [122]. In addition, it has been reported that defects on the surfaces of CNT can decreases electrical conductivity and effectiveness of ballistic charge transport [123]. Furthermore, defects in CNT can degrade thermal properties, which affect the thermal dissipation in electronic packaging [124].

The SEM images show the CNTs that resulted from the MPE-CVD method contains kinks and defects on the individual tubes. As discussed previously the CNT defect may be a result of

DISTRIBUTION STATEMENT A: Approved for public release. Distribution is unlimited.

plasma etching [125], stress formed between CNT and catalyst particles during growth [116], or migration of catalyst particles due to tip growth mechanisms. Evidence of particle migration was captured from TEM images. It is believe that migration is a reason as to why those CNT structures are kinked. It can be proposed that as the CNTs are growing with the migrating catalytic particles, a straight path for growth was not provided, which resulted in a kinked-type growth. Furthermore, since the particles were found not anchored at the interface, the resulting sonication test shows CNTs can be knocked loose from high frequency conditions. Therefore, this approach which is suitable for large area growth or low temperature growth will be useful only in situations where defective, kinked CNTs that have low mechanical bonding to the interface are acceptable. Certain post CNT growth processing such as surface functionalization of CNT might benefit from tubes that are more defective. The benefit of using FCT-CVD is that it is a one step process where catalyst and carbon source are introduced together. The resulting CNTs grown by this process had the smallest diameter, averaging 12 nm, with uniform and dense growth patterns. While this may be a very suitable approach in many applications, the technique also contains more iron particles arising from continuous catalyst deposition. This may be mitigated by modifying the process to cut off ferrocene during the latter part of CNT growth. This was not possible due to the configuration of the syringe used for the investigation. To investigate such hypothesis, one will require a different syringe adaptor else the growth procedure must be interrupted to accommodate syringe change. Since each method has its unique advantages and dis-advantages, these studies highlighting the fact that the selection of the CNT growth method is heavily influenced by the intended application.

4.6 Summary

In this empirical study, we compared the growth of CNTs forests on synthetic diamond substrates using three different CVD growth methods. The CNTs were characterized using electron microscope imaging (SEM and TEM), EELS, Raman spectroscopy, and the sonication test. Despite of different catalyst sources and interface composition used, the SEM and TEM images were able to reveal CNT and catalyst particle diameter and morphology differences. Raman spectroscopic analysis showed that T-CVD had the lowest disordered carbon to graphite intensity ratio of 0.3 followed by FCT-CVD of 0.83 and the highest by MPE-CVD of 1.94. T-CVD also produces large diameter CNTs that are otherwise clean, with minimal tubular defects or additional catalytic contaminants. MPE-CVD is sometimes the preferred method for low temperature or larger scaled applications; however, the excess hydrogen plasma energy during growth may cause surface etching, and defective CNTs that may be detrimental to precision applications. MPE-CVD has the highest probability for catalytic mobility, the most defective CNT structure morphology, and the weakest interfacial bonding strength. It may be possible to improve this situation through processing parameter changes, but not certain. FCT-CVD has the advantage of being a one-step CNT growth method that does not need a separate catalyst deposition step, yet produces dense uniform CNTs. This technique provided the smallest CNT diameter, and intermediate diamond/graphite ratio in the Raman signal. It was mentioned earlier that the diameter of CNT is a factor that determines the physical property of CNT, where thinner CNTs has higher thermal conductivity values. In this investigation, FCCVD technique produces the smallest CNT in size, and the benefit of using this technique is its ability to produce carpet s of CNT with a uniform morphology. This method does produce some excess metal particles due to continuous catalyst nucleation. It has been reported that CNT are commonly contaminated by excess metal particles, and a large research effort is say to be underway to develop a way to purify CNTs post processing [126]. Alternatively, excess metal particles can be useful for

applications that require surface functionalization of CNT, but that is not the scope of this investigation. Furthermore, one possible way to minimize the amount of excess metallic particles is by stopping the catalytic source after a certain growth time. However this was not investigated due to requirement of different system configuration. Finally, this study validated there is a correlation between the size of catalyst particle and the CNT diameters when growing on diamond substrates, which can be very useful for future application design requirements. However investigation using diamond substrates was not continues due to cost and substrate limitation.

CHAPTER 5: *Preliminary Investigations Part II*, Growth On sp^2 Carbon (Effective Surface Modifications To Enhances CNT Growth Density)

In Chapter 4, it was demonstrated that CNT growth was achievable on SP^3 carbon, diamond substrate. However, even though that diamond has excellent thermal properties, certain applications may favor substrates that are also electrically conductive. Therefore, CNT growth on sp^2 graphitic carbon should also be investigated. Sp^2 carbons are lightweight, electronically conductive, and available in a wide selection of substrate geometries. The lightweight and conductive aspect of carbon substrate may be useful for some power electronic applications that are suitable for aerospace or composite industries. Substrate geometries of a particular interest are the ones that have high specific area, such as carbon foam. Carbon foam is a high surface area material. The increased surface area offered by carbon foam and attached CNTs would greatly benefit the thermal dissipation since the heat lost via convection is proportional to the surface area (and temperature difference).

In the previous chapter, it was observed that techniques such as TCVD and MPECVD would require a pre-deposition step for catalyst source prior to CNT growth. Such task may be difficult to achieve for complex structures that require equipment that is not limited to line of sight. FCCVD growth technique is simple, scalable, and able to fabricate CNTs with uniform diameter ranges from 10-20 nm. This technique is also the most feasible technique to grow CNT on complex structures, because it is not limited to line of sight processing. Therefore this technique was selected as the growth technique for the reminder of the research.

In recent years, some research groups have identified ways to grow CNT without catalyst particles. However, the results often yields sparse CNT growth with controllability issues. The most common way to grow controllable and dense CNT still requires the use of catalyst particles. These catalytic particles are usually made of transition metals such as Fe, Ni, Pd and Au[74]. Growing CNTs directly on sp^2 carbon surfaces is challenging, and there are a few known solutions. First, it is possible that the selected transition metals will react with the carbon substrate. This leads to a formation of secondary carbide products. Some carbides have shown to inhibit CNT growth due to catalyst poisoning [127]. Secondly, certain growth conditions are favorable to many allotropes of carbon formation simultaneously. For example, different forms of carbon such as diamond, diamond-like carbon, and carbon nanotubes have been shown to grow simultaneously on a substrate [128]. Finally, catalytic particles may diffuse into the substrate during high temperature, and becomes unavailable for CNTs growth [129]. With all these known possibilities, investigation of surface modifications are needed in order see which modification are efficient in enhancing CNT growth on sp2 carbon substrates. This will then allow fabrication of better CNTs in terms of (growth density, growth morphology, and uniformity). Sections 3.6 have a description for each of the surface modification treatment used in this chapter.

The samples used in this chapter were reticulated vitreous carbon (RVC) foams. As received carbon foams were cut into sample size measuring 10 mm x 5 mm x 5mm. These samples were cleaned using sonication with a 42 kHz. Samples were first cleaned using sonication for 5 minutes in acetone followed by 5 minutes in isopropanol. After which the samples were taken out of the solution and an air gun equipped with Argon gas was used to blow dry the sample. For images of as-received RVC foams please see Figure 10. For each of the treatments described in the sections below, 3 samples were prepared. Each of the samples went

through the surface modification treatment process follow by the CNT growth process. The growing process used was FCCVD process described in Section 3.5.3.3.2

5.1 Pre-experimental study: Direct Growth without modifications (Baseline)

In Chapter 4, it was demonstrated that the FCCVD recipe described in Section 3.5.3.3.2 was successful at growing dense CNT on diamond substrate. This was then used to see if dense CNT can grow on sp^2 carbons. To begin, a baseline growth was done, using as-received foam sample without any surface modification treatments. Figure 34 is SEM image showing that the growth was low and sparse. The CNTs were clustered and randomly orientated. This result shows that it is a challenge to grow dense CNT carpets directly on as-received carbon foams.
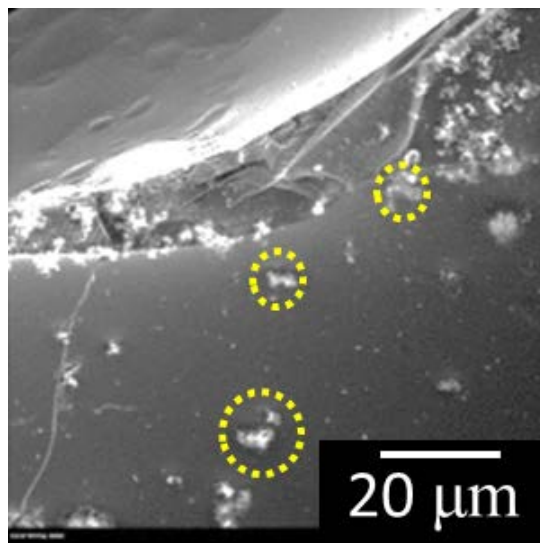
Figure 34: CNT Grown on Bare As-received Carbon Foam

Due to this finding, it was believed that CNT growth on sp^2 carbon can be improved if proper surface modifications were performed. Surface modification that oxidizes the surfaces has been shown to be effective in enhancing CNT growth on loose graphite [99].

5.2 Objective: Surface Modification to Improve CNT Growth on Carbon Foam

The objective of this investigation is to demonstrate dense growth of CNT on porous carbon surfaces. The approach to accomplish this is to look into five different surface modification techniques and to see if any of the treatments options are effective. This is a preliminary comparison in order to differentiate methods that are effective and ones that are not. No optimization of the technique will be performed. A successful growth will be the one that allows dense CNT growth, coverage without substrate showing, on sp^2 carbon substrates. The surface modification includes two main types. In the first approach, oxygen containing groups were added to the substrate surface using the following techniques; nitric acid, oxygenation, dip coating with Hexamethyldisilazane (HMDS). The second approach deposits oxide thin films on the surface of carbon substrate. The deposition techniques with corresponding oxides were plasma SiO_2, and ALD Al_2O_3.

5.3 Experimental: Surface Modifications Options

5.3.1 Surface Modifications

For each of the surface treatment options mentioned below, three test samples were prepared. After the samples receive surface treatments, CNT growth was attempted on the treated samples. Additional information about the surface modification techniques mentioned below can be found in Section 3.6.

5.3.1.1 Surface Oxidation by Addition of oxygen groups on the surface carbon substrate
5.3.1.1.a) Nitric Acid

It has been report that nitric acid has the ability to break the strong covalent carbon bonds; thereby adding oxygen containing groups as well as creating defects on the surface of carbon substrates. It has been reported that such defects were successful at allowing CNTs to grow on graphitic particles[130]. The nitric acid treatment is a slow process. It began by soaking batches of carbon foams, in a 70 % concentration nitric acid, for either 4 hours or 8 hours at an elevated temperature of 120℃.

5.3.1.1.b) Oxygenation

Carbon starts to decompose in air when temperature rises above 350 °C. Therefore one of the ways to modify the surface of the carbon foam is by exposing it to an oxygenated environment above the decomposition temperature. An experiment was setup to treat the carbon foam at various high temperatures (350, 400, 450, and 500°C) for 1 hour, in order to produce a range of defective surfaces on RVC foam. Treatments above 500°C were not pursuit because the resulting carbon foam crumbles under normal sample handling.

5.3.1.1.c) Bis(trimethylsilyl)amine (HMDS)

The literatures have suggested that CNT grows very well on oxide surfaces such as silica or alumina[129], [131]. HMDS was used to modify the surface of carbon foam. When used, HMDS, bonds its Si atoms to the oxygen of an oxidized surface, thereby creating a silica layer on the surface of RVC foam. To create this silica coating on carbon foam samples, the RVC foams were dipped into HMDS solution and set off to dry on a hot plate at 100℃. EDS shows that there were 1 atomic % of silicon present on the foam surface after the coating process.

5.3.1.2 Deposition of Oxides

Initial investigation uses carbon foam samples deposited with 4 nm of plasma silica and (2, 5, 10, 50 nm) of ALD alumina for comparisons. For oxide deposition parameters see Section 3.6.2, and for comprehensive investigation of the effect of oxide thickness on CNT growth see Section 5.4.2.2.a, and Chapter 7.

5.3.2 CNT Growth Parameters

FCCVD was used to grow CNT on the surface treated samples. The growth recipes used were ones from FCCVD mentioned earlier in Section 3.5.3.3.2.

5.4 Results and Discussion

5.4.1 Addition of oxygen groups on the surface carbon substrate (physisorption)
5.4.1.1 Growth on Nitric Acid modified sample

Figure 35 shows the image of nitric acid treated samples grown with CNTs. It was observed that clusters of CNT were present on the surface of the foam sample, however large area of substrate are still visible. As a result, it was determined that nitric acid treatment is insufficient at greatly enhancing CNT growth density on carbon foam.
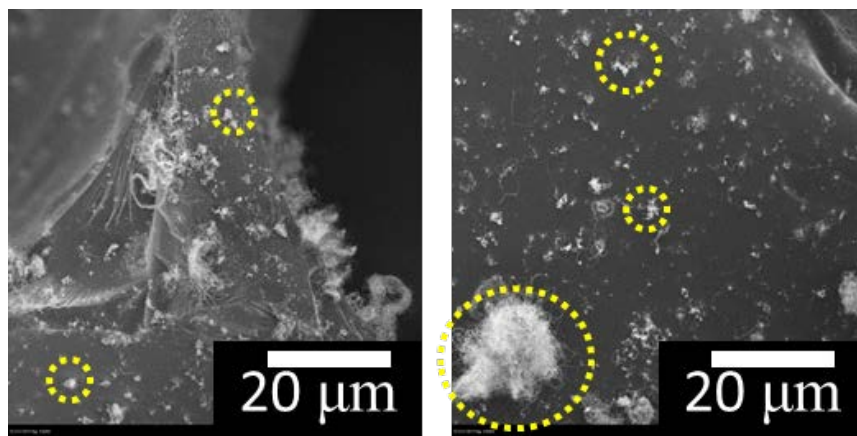
Figure 35: CNT Grown on Nitric Acid Treated Carbon Foam
A) 4 hrs treatment, B) 8 hrs treatment

5.4.1.2 Growth on sample modified by oxygen at elevated temperature

Figure 36, shows the results of CNT growth on oxygenated carbon foams. These images show varying degrees of CNTs clusters grown on the surface of carbon foam. It can be seen that larger clusters of CNTs were grown on foams that were treated at higher temperature during oxygenated environment. However, it wasn't clear if this was a result of more defect sites or larger defect sites created at those locations. Nonetheless, the overall growth yield remains low; therefore this method was not pursuit further.
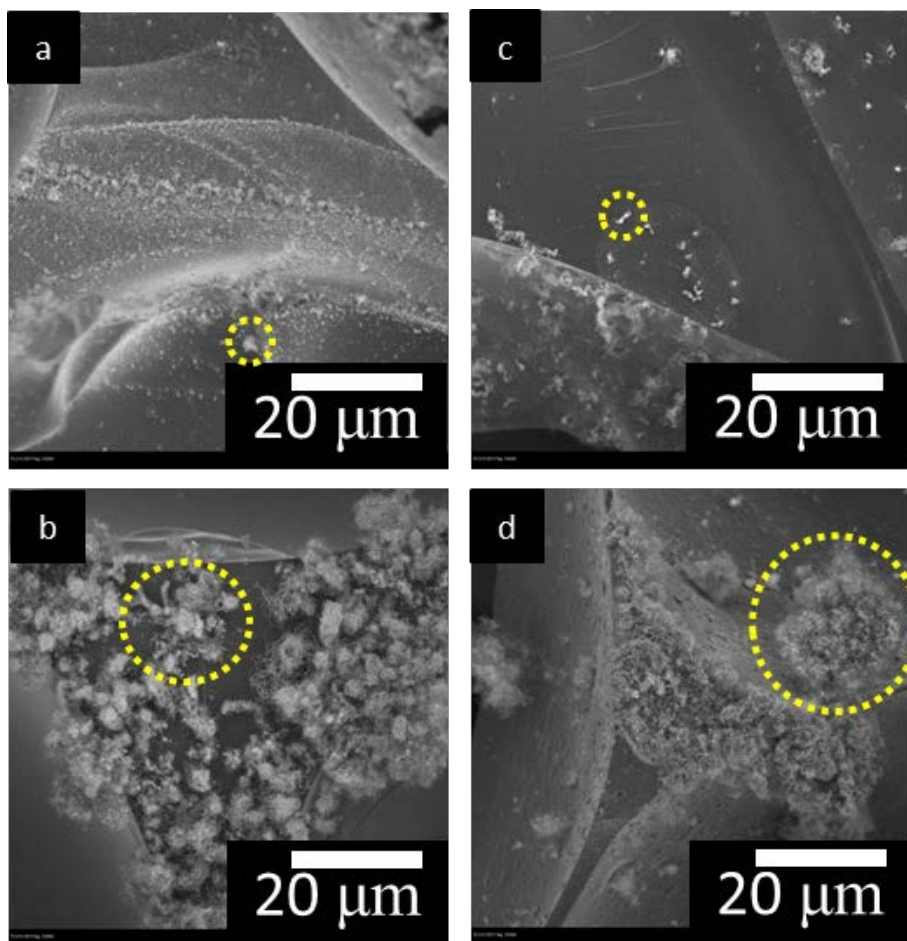
Figure 36: CNT Growth on Oxygenated Carbon Foam
A) 350, B) 400, C) 450, D)500

5.4.1.3 Growth on HMDS modified samples

The result of CNT growth on HMDS treated samples shown in Figure 37. As indicated by the figure, the result also did not show a signification improvement for CNT growth using this treatment, Figure 37 shows that the majority of substrate below is still visible. Perhaps denser CNT coverage can be achieved if thicker HMDS coating was provided; however, this method was not pursuit further at this time because other methods (oxide deposition) have shown to be more effective.
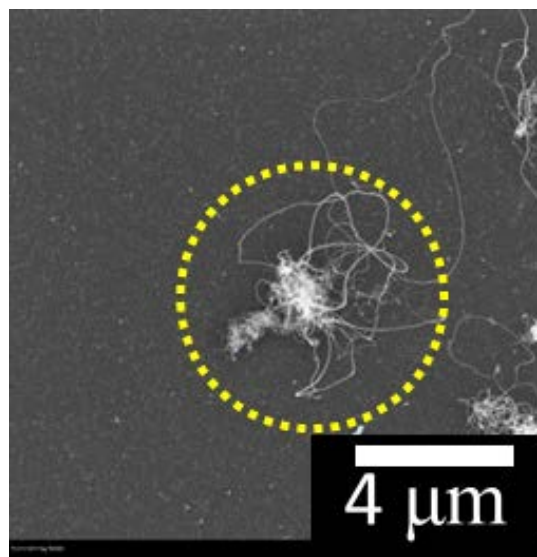
Figure 37: CNT Growth on HMDS Treated Carbon Foam

5.4.2 Deposition of Oxides

5.4.2.1 Growth on Plasma SiO₂ modified sample

Figure 38, shows the result of CNT growth on plasma SiO_2 coated samples. This image demonstrated that the qualities of growth (in terms of density, alignment, and tube uniformity) have finally increased significantly. It was the first time, in this investigation, that the results showed aligned CNT growth was achieved on the surface of the carbon foam. Earlier reports of CNT investigation conducted on electronic grade silicon, also reporting of CNT growth enhancement when oxide buffer layer were used [67], [69], [131]. The enhancement observed from this preliminary investigation prompted interest to investigate CNT growth using this surface modification technique. Investigations using plasma silica treated sample along with effects of oxide thickness will be investigated further in Chapter 6.
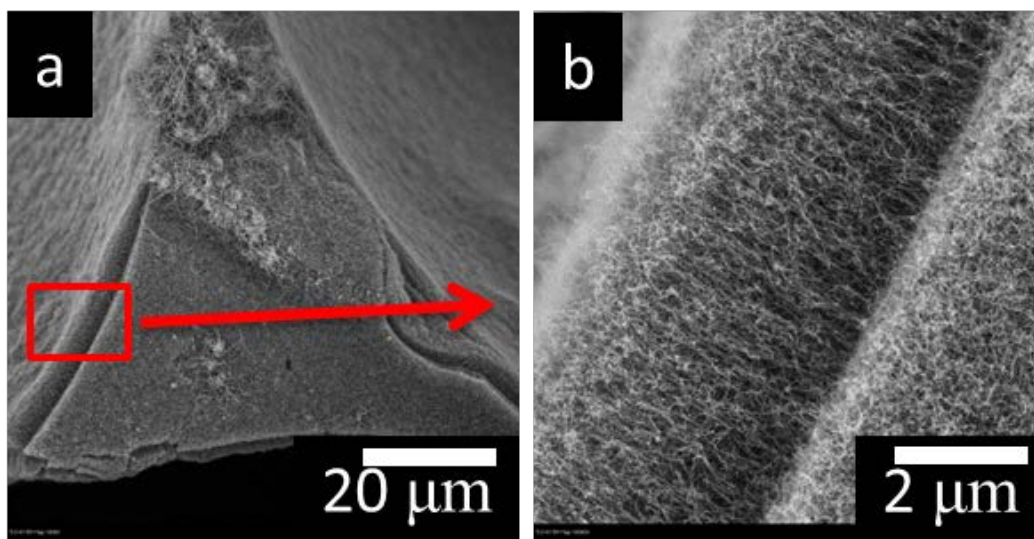
Figure 38: CNT Growth on MPD SiO₂ Modified Foam

5.4.2.2 Growth on ALD Al₂O₃ modified samples

Figure 39a, shows the result of a sample coated with 2 nm of alumina that received CNT growth, and Figure 39b is a sample coated with 10 nm of alumina also received CNT growth. Figure 39a shows that uniform distribution of CNT clusters can be seen throughout the carbon foam, however the growth was not dense nor aligned. When the alumina buffer layer was increased to 10 nm, it shows that CNT growth becomes dens and aligned. Therefore this demonstrates that proper selection of oxide thickness is required to achieve desired CNT growth density and uniformity. Simmons et al reported that there is a critical oxide thickness required for CNT growth and enhancement, however this was conducted using electronic grade silicon [67]. With the results observed here, investigation using ALD Al₂O₃ treated sample will be investigated further in Chapter 6.
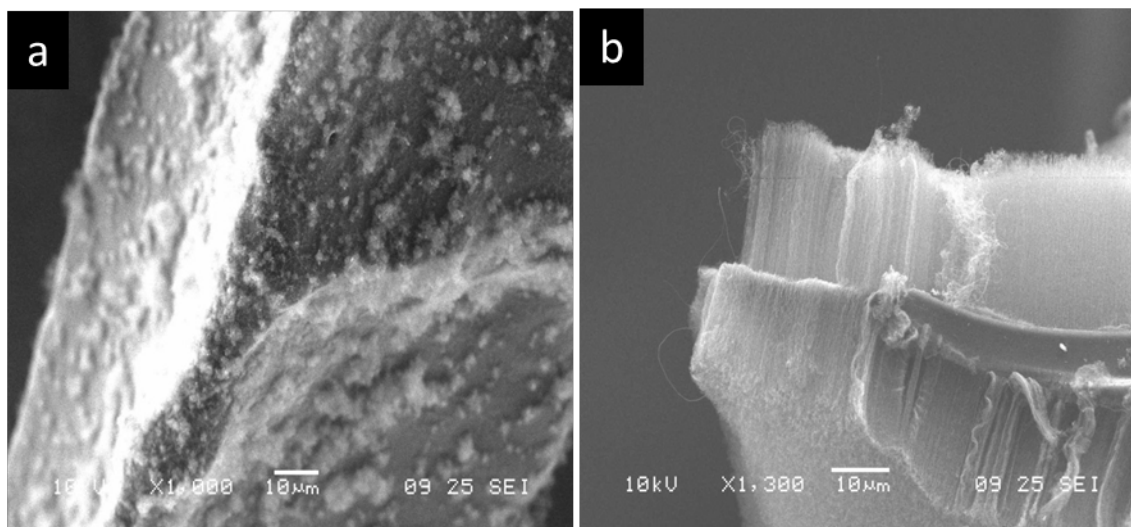
Figure 39: CNT Growth on ALD Al₂O₃ Modified Carbon Foam
A) 2nm, B)10 nm

5.4.2.2.a. Extended Growth Investigation on ALD Al₂O₃ modified samples (thickness variation)

Samples with discrete oxide thickness were prepared and grown for investigation, (5, 10, and 50 nm). The 2 nm result shown in Figure 39 was too sparse, so it was not used. Figure 40 indicated that as the thickness of the buffer layers increases the carpet height also increases, currently with an oxide thickness of 50 nm the CNT growth observed was also the longest. For SEM image see Figure 40, for plotted carpet height vs oxide thickness see Figure 41. However, it was observed that in certain areas alumina films were also "lifted-off" on these samples, highlighted by orange dotted lines, Figure 40. Note, the carpet height is measured from the entire visible length of CNT, including the lifted-off section. Therefore it wasn't clear how the carpet height will change if "lift-off" did not occur. In addition these SEM images were taken on carbon foam samples. It was realized that theses height can change or inaccuracy in measurements can occur due to the viewing angel. Therefore it was decided that detailed study will be conducted on a flat substrate. Chapter 6 will address the "lifted-off" issue by trying other deposition procedures and to investigate growth on flat substrate so that better measurements and comparisons can be made
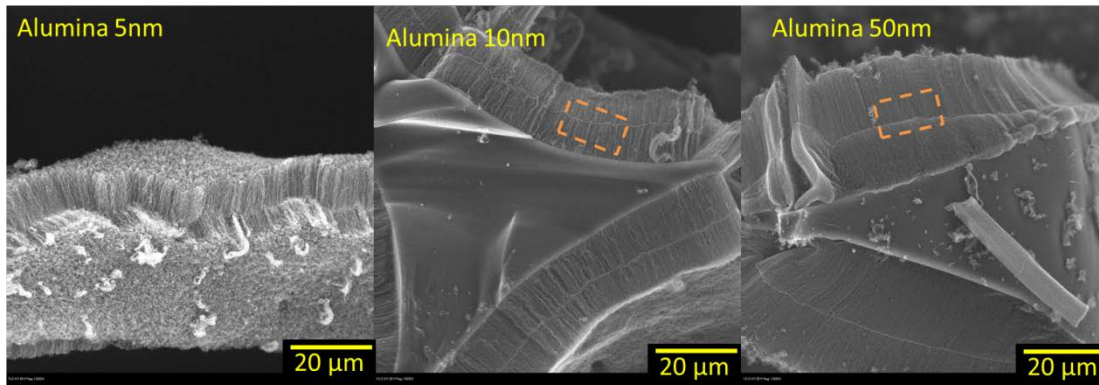
Figure 40: Oxide Thickness Effect on Carpet Height, Al$_2$O$_3$ on RVC Foam
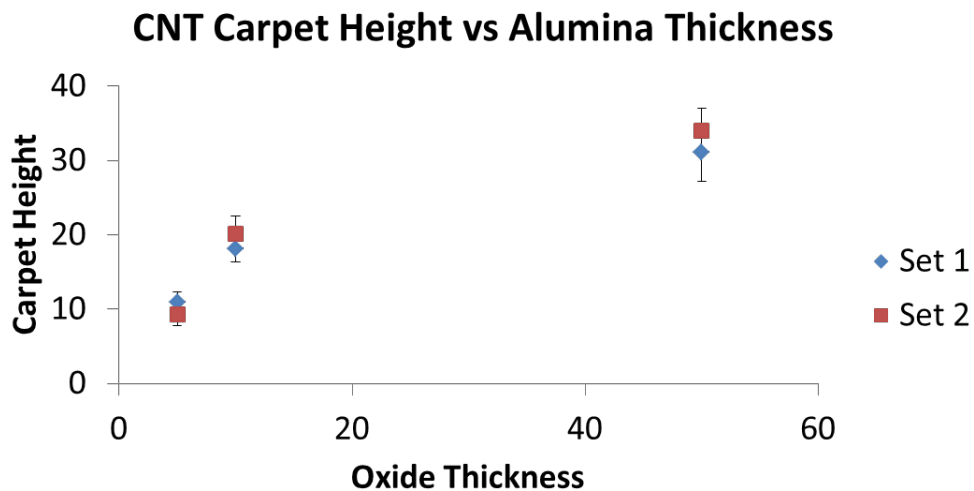
Figure 41: Observed Height vs. Oxide Thickness

It was interesting to know if CNT growth were achieved through out the foam samples. Therefore, samples grown with CNT were sawed in half, width wise, resulting a sample size of 5 mm x 5 mm x 5mm cube. The cut surfaces were investigated with SEM. Figure 42 shows a representation of the investigated area. The images from Figure 42 validated that CNT growth did take place well into the depth of the foam.
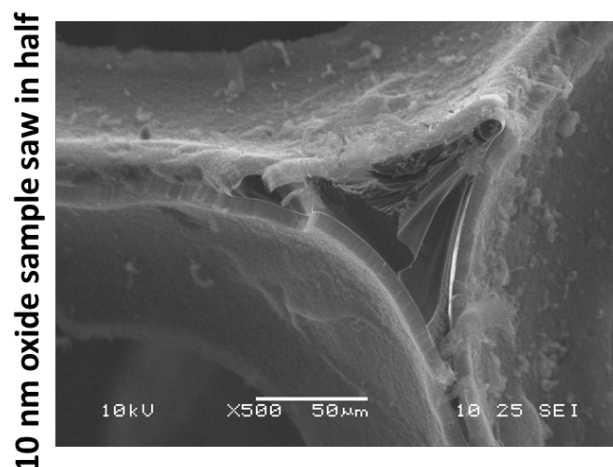
Figure 42: SEM of a Broken Interface, RVC Foam Sample Sawed in Half

5.5 Summary

Surface modification techniques investigated in this chapter indicated that only ones that use oxide buffer layer were shown to be effective in improving CNT growth density on carbon foam. It was determined that surface oxidation methods such as nitric acid treatment, oxygenation, HMDS did not improve the CNT growth on the surface of carbon foam significantly as they were used. The improvement was only observed when oxide deposition was used on RVC samples. The results show when carbon foam coated with 4 nm plasma silica the CNT growth was improved in terms of growth density, alignment and uniformity. Similar growth improvement was observed when carbon foam was deposited with (>2nm) ALD alumina film deposition. At 2 nm the growth on alumina was still sparse, however the amount of CNT cluster increased more uniformly throughout the foam. When thicker alumina was deposited, 10 nm, major improvement of CNT growth in terms of density, alignment and uniformity were observed. In addition, ALD alumina with a wider film thickness selection also show that as the film thickness increases the appeared carpet height also increased. However, it appears that certain growth using ALD alumina resulted in oxide film separation from the substrate, while the separation was not observed for sample deposited with silica with the three samples tested. However the separation issue will be investigated in a later chapter. Resolving the separation issue will allow better investigation to see the effect between oxide thickness and carpet height. The separation of the oxide film may be a result of CTE differences between the oxide layer and the carbon substrate. The CTE value for carbon is about $1.5 \times 10^{-6}K^{-1}$, for alumina is 8.1-8.4 x $10^{-6}K^{-1}$, and silica is $0.55 \times 10^{-6}K^{-1}$. As the values suggest the CTE values between carbon and silica are much closer than the difference observed between carbon and alumina.

In this chapter it was observed that two different oxide materials were successful at enhancing CNT growth on carbon substrates. It was reported that similar buffer effects were observed when silicon samples were coated with an alumina oxide, where increases of CNT growth in terms of density were reported [131]. Therefore, it is essential to investigate the effect of different oxide material and their influence on CNT growth. This will be the scope for Chapter 6, influence of oxide on CNT growth.

Section III: Experimental
(Focused Studies)

CHAPTER 6: Buffer Layer Investigation

In Chapter 5, the result shows that in order to enhance the density of CNT growth on carbon foams a pre-coating of oxide buffer layer material were required. In this study, two promising oxide materials, alumina and silica will be used to investigate their effects to CNT growth. In addition, different deposition techniques, alumina (ALD Al_2O_3, Sputtered Al_2O_3) and silica (thermally oxidized SiO_2, ALD SiO_2 and Plasma SiO_2), will be used to deposit the oxide buffer layers. It is believed that oxide deposited using different deposition techniques will result in oxide films with different stoichiometry. Figure 14 shows that oxide films made with different stoichiometry resulted in different intrinsic physical property (thermal conductivity, density, CTE… etc). It is possible that intrinsic properties difference, can potentially influence CNT growth, and therefore should be investigated.

The study investigated in this chapter will use modeled flat carbon substrates mentioned in Section 3.1.2.4, instead of carbon foams. The flat substrate geometry would allow a better experimental control and more amenable microscopy comparisons for CNT growth characteristics on buffer layer variations. In addition, the flat carbon substrates are made of the same chemical composition as the carbon foam.

6.1 Oxide Buffer material for this investigation: Al_2O_3 and SiO_2

Section 2.7 shows the history of buffer layer usage to grow CNT on silicon substrate. Initially it was thought that one of the ways to minimize interface resistance is to grow CNTs directly onto metals; however this method has resulted in a low growth density. As studies progresses, using silicon as substrate, it was found that aligned CNTs can be grown on oxide buffer layer supported substrates. It was suggested by Simmons et al. that in most cases, using iron or nickel as catalyst source, a critical buffer layer thickness of ($\sim$4nm SiO_2) is required for dense growth [67].

More recently, carbon becomes an interesting material for substrate choice due to its lightweight and excellent thermal properties. There are many great physical qualities about carbon that can potentially be useful in future space applications that find lightweight materials useful. However, growing CNTs directly on carbon is also challenging due to several factors. First, during high temperature annealing, the metallic particles can diffuse into the substrate and, depending on the distance traveled, it may no longer act as a viable catalyst to promote CNTs growth [112]. Secondly, carbon has low surface reactivity, which makes it difficult for anything to bond to the surface, including many known transition metals used as catalysts for CNTs growth[79]. There have been many attempts at surface modification to increase surface reactivity of carbon [23], [79], [119], [132], [133]. However, the most successful way is by modifying carbon surface with an oxide buffer layer. This is because the oxide layer is an effective buffer that prevents catalytic particles from being absorbed into the substrate; it also allows particles to agglomerate into islands that promote CNTs growth [67], [69], [126].

In Chapter 4, it was demonstrated that CNT morphology is very sensitive to the combination of material selection and growth techniques used for synthesis. In this chapter, the goal is to investigate how oxide buffer layers play a role in CNTs growth mechanisms; it is important to keep in mind some of the observed growth behavior already reported. For example, it has been reported that, using TCVD growth method, samples coated with Al_2O_3 as a buffer layer have

yielded the best grown CNTs in terms of tube density and alignment [112], [129], [131], [134]. This may or may not be true if a different growth method was used. With the success observed in the previous chapters, this investigation will use FC-CVD method to grow CNTs. In this investigation, it is crucial to pay special attention to the interaction between the metal particle and the buffer layer, because the reaction taking place between the metal particle and the buffer surface can simply be altered due to slight changes in environment such as (temperature, and water vapor) [135]. For example, improper growth condition, such as extreme high temperature, in certain instances, would result in excess amorphous carbon produced. In other words, any alteration in growth conduction will require detailed investigation of the resulting CNTs. It has been reported that even when the same type of catalyst was used, however on different oxide buffer layer, the resulting CNTs was different [89]. For example, Amama et al. reported seeing a difference in growth characteristics when CNTs were grown using the same conditions but upon different oxide buffer layers[129] . In addition, by comparing how the oxide buffer layer were deposited, - sputtered vs evaporated - Ohashi's group reported that CNTs grew better on sputtered oxide, which is attributed to it being more thermodynamically stable [134].

Recent studies reported by this group have shown that direct growth of CNTs on carbon is challenging and tends to result in sparse clusters [136], [137]. This is possibly due to the chemical inertness of graphite [79], [138]–[140], which results in a low affinity for the transition metal precursors that allow nano-catalyst formation [141]. In other words, transitions metals does not seed well on graphite surface [142], and as a result very limited amount of catalyst particles were available on graphite surfaces for CNT nucleation. In an attempt to address this issue, this group recently studied the effect of several surface treatments on porous carbon foam which is summarized in Chapter 5. It was found that buffer layers composed of either (5-50 nm) of alumina or 4 nm of silica largely enhanced the density of CNT growth on the foam surfaces [136], [137]. However, detailed studies have not been performed to determine the influence of buffer layer chemistry on carbon substrates with respect to CNT growth and controllability. Some general characteristics of a good buffer layer have been outlined by Rodriguez-Reinoso [141], but few additional requirements should be noted for growing them on carbon substrates: stability under reaction conditions, adequate mechanical properties, strong bonding to the substrate, and coating via a process that would not be limited by line-of-sight.

6.2 Objective: Understanding the effect of oxide materials on CNT growth

The objective of this study is to better understand the suitability of oxide materials as buffer layers used for CNT growth. To accomplish this, oxides (Al_2O_3 and SiO_2) will be deposited on flat modeled carbon substrates.

It is hypothesized that different oxide material will influence CNT growth differently and oxide deposited using different deposition technique would result in different oxygen deficiencies of the resulting oxide film. These deficiencies results in different oxide film quality and stoichiometry. Figure 14 shows those oxides results in different intrinsic properties when they have with different stoichiometry. It is possible that these properties will influence CNT growth differently. It is the goal of this study to see what those effects are. In order to study these effects, several different oxide deposition techniques will be used. The resulting oxide film will be compared for its influence on CNT growth and for its suitability as buffer layer. Here are the areas of investigation relating to the effect of buffer layers that will be investigated.

1. Surface roughness effect
2. Oxide thickness effect

DISTRIBUTION STATEMENT A: Approved for public release. Distribution is unlimited.

3. Growth time effect
4. Oxide Material effect (Alumina vs. Silica)

The influences of the different oxide materials and their surface interactions on CNT growth will be revealed in this study.

6.3 Experimental:

Model substrates of geometrically flat carbon were generated by pyrolysis of polymeric precursors on silicon wafers, Section 3.1.2.4. The vitreous carbon samples represent the same chemical structure as carbon foam but in simple planar geometry, which is much more suitable for quantitative analysis via microscopic and spectroscopic techniques. The alumina and silica was selected as buffer layer material due to the results observed from Chapter 5, where CNT growth density and uniformity were both improved when these oxides were used. Microwave Plasma Enhanced - Chemical Vapor Deposition (MPE-CVD) and ALD were selected as surface pre-coating methods, and the FCCVD technique was selected to grow CNTs on the surface. This investigation uses the FCCVD growth technique found in Section 3.5.3.3.2 for CNT growth. However the growth time has been modified to be either a 1 minute or a 20 minute growth run.

6.3.1 Preparation of Vitreous Carbon on Si (model carbon substrate):

In order to effectively compare the resulting growth morphology of the CNT carpet, the substrate used should be flat (RMS < 5nm). Such substrate requirement can be fabricated in the lab using the process described in Section 3.1.2.4. Essentially the carbon layer is created by pyrolyzing a photoresist coated silicon sample. The vitreous carbon had an average thickness of 450 nm and average RMS value about 0.4 nm.

Some modeled carbon substrates were treated with reactive ion etcher (RIE), Section 3.6.3.1, in order to provide surfaces roughness variation needed for certain comparative analysis investigated in the study.

6.3.2 Substrate and Buffer Layer Preparation

This study was conducted using flat substrates. The use of flat substrates enabled a direct comparison between samples with various oxides deposited on it. Ideally, the results from this study could be applied in future studies, where carbon substrates with complex structures are preferred.

The majority of the oxide thickness deposited in this study was 5 nm. Certain studies investigate the effect of oxide thickness on CNT growth. Those studies will have different oxide thickness, and it will be specified. The oxides deposited are of the following: ALD SiO_2 (ALD SiO_2), MPE-CVD SiO_2 (plasma SiO_2), ALD Al_2O_3 (ALD Al_2O_3), and sputtered Al_2O_3 (S Al_2O_3). In addition to these, several purchased commercially-available samples were used, and they are thermal SiO_2 (1 mm thick) on Si, sapphire substrate and fused silica. These commercially available samples were selected because it is a standardized material readily available to the electronic device community and has been used by various research groups to successfully grow dense, aligned CNTs.

6.3.2.1 Atomic Layer Deposition (ALD) of Al_2O_3 and SiO_2:
ALD is a vapor phase, self-limiting, thin film deposition method in which the reactions take place between precursor gas molecules and the surface of the substrate. The resulting thin film should be pinhole-free and conformal to the substrate surface [143]. The organometallic

precursors used for deposition of Al_2O_3 and SiO_2 were trimethylaluminum, and trisdimethylamino-silane, respectively. Water vapor was used as the oxygen source for both films. The thin film growth process was conducted at 200 °C with deposition rates of 1.5 Å/cycle for Al_2O_3 and 0.5 Å/cycle for SiO_2.

In Chapter 5, it was discovered that certain area on the samples show signs of alumina films "lift-off" post CNT growth. To address this point, some samples were deposited with the following modified ALD alumina recipes to see if film adhesion improvements could be made.

1. Pre-oxygenation of the substrate surface follows by oxide deposition at 200 ℃.
2. Pre-annealing the sample at a higher temperature (500 ℃) in Argon for 3 minutes, prior to oxide deposition at 200 ℃.
3. Depositing the alumina films at a higher temperature (300 ℃).

*** *However none of the treatments performed solved the "lift-off" issue, which was observed post CNT growth. As mentioned earlier there is a large CTE difference between C–Al_2O_3, and this difference is probably one of the main driving factors for film lift off. The lift-off issue can be undesirable for certain electronic applications, especially electrical or thermal applications, because it can disrupt transport properties at those locations. Other oxide deposition technique might be able to produce films that have stronger adhesion to the substrate, but due to the intended substrate requirement such deposition technique must not be limited to line of sight techniques. Therefore other suitable ways for improvements should be investigated in the future studies.*

6.3.2.1.1 Oxide Thickness:

ALD alumina technique mention in Section 3.3.2.2 was used to deposit the following alumina oxide thickness: (5, 10, 25, 50, 100, and 200 nm). In addition, a purchased sapphire substrate sample was used to represent a sample with infinite alumina thickness. *6.3.2.1.2 Reactive Ion Etch (RIE) with Oxygen Plasma:*

In order to provide surface roughness variations, some standard carbon samples were first treated with RIE prior to ALD alumina oxide deposition. RIE parameters used are ones mentioned in Section 3.6.3.1.

6.3.2.2 Microwave Plasma SiO_2:

MPE-CVD deposition technique mentioned in Section 3.3.2.4 was used for silica deposition. A mixture of hexamethyldisiloxane (HMDSO) and O_2 was flowed into a vacuum chamber equipped with an 850 W microwave generator with magnetron assist.

6.3.2.2.1 Oxide thickness:

Plasma silica technique mentioned in Section 3.3.2.4 was used to deposit the following silica oxide thickness: (4, 14, 23, 43, 70, 145, and 212 nm). In addition, a purchased fused quartz substrate sample was used to represent a sample with infinite silica thickness.

6.3.2.3 Sputter Alumina:

In order to provide alumina samples with different surface roughness, 5 nm of sputtered alumina was deposited. This resulted in a surface roughness with RMS value about 4 nm. The deposition technique used was mentioned in Section 3.6.2.3.

6.3.3 Samples

Section 6.3.2 shows the processing steps available for making the samples used in this investigation. This section will specify how those samples are used in the investigation. In addition, this information is shown in Figure 43.

In this investigation there are four baselines. In the first baseline growth, samples were grown on untreated carbon (standard carbon sample) to see if direct CNTs growth were achievable. The second, third and fourth baseline growth was done with xylene alone (no ferrocene), on standard carbon, and oxide coated (ALD Alumina and Plasma Silica) standard carbon substrate. Using only xylene to grow CNT, allows the study to check if CNTs can grow without metallic catalytic source.

Each sample set listed in Figure 43 were run several times in order to establish experimental uncertainties.

Base Line Samples	Growth Chemical	Surface Pre-Treatment Prior to Oxide Deposition	Growth Time (minutes)	Oxide Thickness (nm)
Standard Carbon	Xlene and Ferrocene	n/a	20	n/a
Standard Carbon	Xylene only	n/a	20	n/a
Standard Carbon with ALD Alumia	Xylene only	n/a	20	5
Standard Carbon with Plasma Silica	Xylene only	n/a	20	5
Experimental Samples	Growth Chemical	Surface Pre-Treatment Prior to Oxide Deposition	Growth Time (minutes)	Oxide Thickness (nm)
Thermal Silica on Si	Xlene and Ferrocene	n/a	1, 20	1000
Plasma Silica on Standard Carbon	Xlene and Ferrocene	n/a	1,5,10,20,40,60,80,100,120	4, 14, 23, 43, 70, 145, 212
ALD Silica on Standard Carbon	Xlene and Ferrocene	n/a	1,20	5
Fused Quartz	Xlene and Ferrocene	n/a	20	∞
ALD Alumina on Standard Carbon	Xlene and Ferrocene	n/a	1, 20, 40	5, 10, 25, 50, 100, 200
ALD Alumina on Standard Carbon	Xlene and Ferrocene	Pre-oxygenation	20	5
ALD Alumina on Standard Carbon	Xlene and Ferrocene	Pre-annealing at 500 °C	20	5
ALD Alumina on Standard Carbon	Xlene and Ferrocene	Oxide deposited at 300 °C	20	5
ALD Alumina on Standard Carbon	Xlene and Ferrocene	RIE 20s	1, 20, 40	5
ALD Alumina on Standard Carbon	Xlene and Ferrocene	RIE 60s	1, 20, 40	5
Sapphire	Xlene and Ferrocene	n/a	20	∞

Figure 43: Sample Sets Prepared for the Investigation

6.3.4 CNT Growth Parameters

FCCVD was used to grow CNT on the surface treated samples. The growth recipes used were ones from FCCVD mentioned earlier in Section 3.5.3.3.2. However, the growth time was varied between 1-120 minutes for this study.

62

6.3.5 Sample Characterization:

Scanning Electron Microscopy (SEM) and Transmission Electron Microscopy (TEM) techniques were used as part of the image analysis for this study. The catalyst diameters, tube diameters, and carpet heights were determined by measuring either the CNTs or the catalyst particles in the images. The SEM was a FEI model XL30 Sirion, operated at a 10 kV bias. SEM images were taken of at least three different regions of each sample. The TEM used was a Philips model CM200 LaB6, operated at 200 kV. The TEM samples were prepared by scraping across the surface of each 20 minutes growth sample with a clean glass slide. The scraped-off material was transferred onto a 200 mesh TEM grid. A grid sample was made for each of the sample types (Standard SiO_2, ALD SiO_2, Plasma SiO_2, and ALD Al_2O_3) after each run. Images were taken from at least three different areas per grid. Atomic Force Microscopy (AFM) was used to quantify the roughness of pre-CNT growth surfaces of the various buffer layers, as well as the model carbon layer prior to buffer deposition. A Quesant© model Q-Scope 250 AFM was operated using the non-contact mode at a 1 Hz scan rate. All sample scan areas were 5x5 μm. Scandium and ImageJ v1.48 software was used for distance measurement analysis on the microscopy images. These software packages have tailorable pixel-to-distance settings and zoom functions for better accuracy in measurement.

6.4 Results and Discussion
6.4.1 Baseline Study of CNT Growth
6.4.1.1 CNT growth on untreated carbon surface (baseline1)

To establish a baseline, CNT growth was tested on the as-formed model carbon sample without a buffer layer. Figure 44a shows a cross-section view of a cleaved model carbon sample before CNT growth. The image shows the carbon layer residing between the two yellow arrows. Figure 44b and Figure 44c are aerial views of the model carbon sample taken after brief and extended growth times of one minute and 20 minutes, respectively. Figure 44b shows that the surface of the sample contains a minimal amount of catalytic particles. Figure 44c demonstrated poor CNT growth, clearly showing that the growth takes place in few random areas. The insert on the top right corner is a higher magnification image taken from the outlined square, and it shows that each surface particle is made of randomly-oriented CNT clusters.
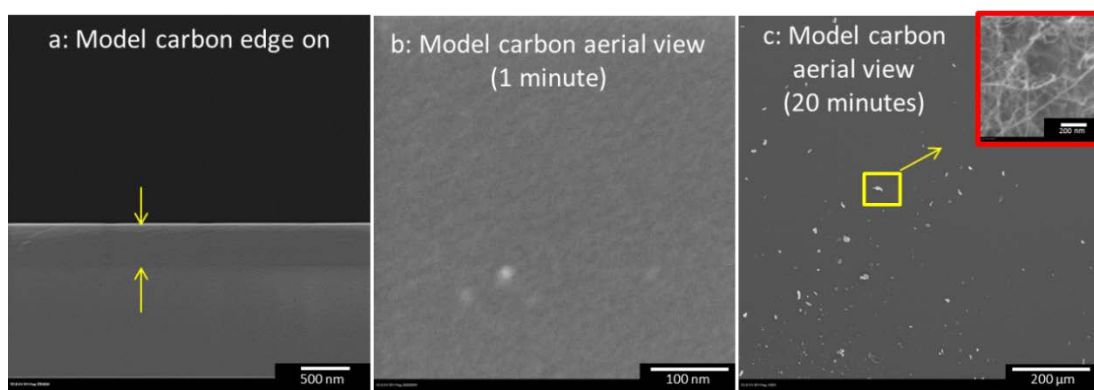
Figure 44: SEM Images Showing Cross-section and Aerial Views of CNT Growth on Samples without Oxide Buffer Layer
(a) cross-section of the model carbon sample, where the yellow arrows highlighted the carbon film. (b) high magnification of an aerial view of a sample after one minute of CNT growth. (c) sample after 20 minutes of CNT growth. The scale bars are.

Figure 44 shows that CNT growth directly on the model carbon surface was scant and disordered. This condition may be due to the fact that carbon surfaces are chemically inert and may not offer sufficient reactive sites for catalyst particle formation. Figure 44b shows that the

surface was essentially bare and contained only a few identifiable patches of catalytic particles, and Figure 44c shows random clusters of CNT growth. Figure 44b suggests that metallic particles do not condense or nucleate readily on the carbon surface. In Figure 44c, the higher magnification insert shows that catalytic particles that do attach to the carbon surface may grow nanotubes in a random and nonaligned manner.

The nonaligned CNT growth is possibly due to low CNT growth density in the local area. This allows the CNTs to grow freely in any direction, instead of being forced to grow vertically [144]. In other words, the CNTs are not confined by adjacent tubes. This experiment validated the need for suitable buffer layers to grow densely aligned CNTs.

6.4.1.2 CNT growth without catalyst source (baseline 2, baseline 3, baseline 4)

Another baseline was established for the study by introducing only xylene (without ferrocene) during CNT growth period. This growth was done using Standard Carbon substrates with and without buffer layer. This was done to clearly determine if the metallic catalytic source is necessary on these buffer layers. After repeated CVD deposition without ferrocene and SEM imaging of the surface in each case, it was clearly determined that no CNT were growing on these samples.

The role of buffer layer and catalyst source for CNT growth on carbon substrate is important for this research. It has been reported in some studies [145]–[148] that single-walled CNTs may grow directly on oxides such as alumina or silica without the usage of metallic source. In those situations, the oxides are in the form of nanoparticles. However, in this study, the oxides deposited were in the form of thin films and the result indicated no CNT could grow without the usage of ferrocene. It is therefore important to note that the mere presence of oxide is not enough to support CNT growth. In other words, CNT growths can only occur in the presence of nanoparticle catalysts, which are provided by ferrocene in this study.

6.4.2 Surface Roughness of Buffer Layers

Figure 45 shows the AFM measurements of pre-CNT growth on the four buffer layers as well as the model carbon layer. It can be seen that the surface roughness RMS values vary from 0.201 nm to 3.861 nm. In order from smoothest to roughest, the samples fall in the following order: Standard SiO_2 < ALD Al_2O_3 < model carbon < ALD SiO_2, and then Plasma SiO_2.
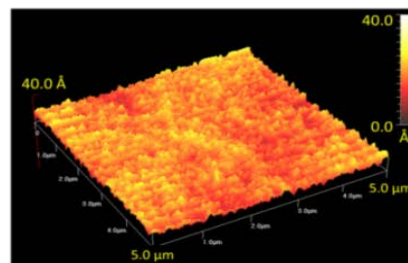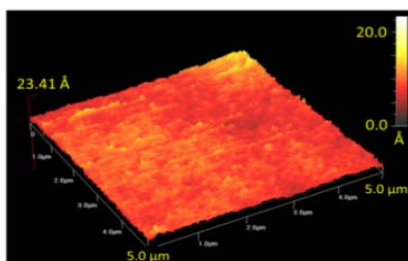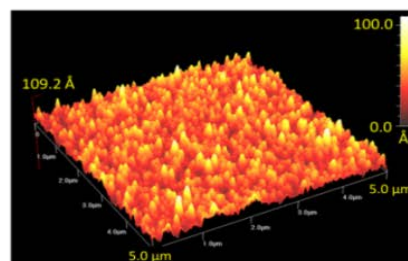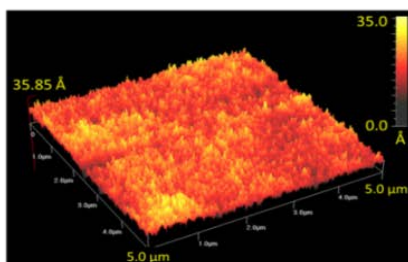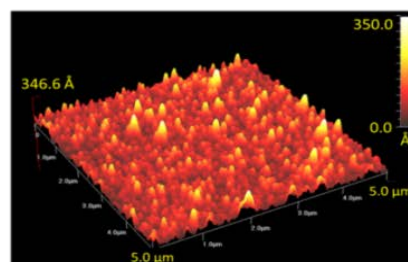
Figure 45: AFM Images Showing Surface Roughness of Samples before CNT Growth
*(Each image shows a scan taken from a represented 5μm by 5μm area at 1Hz. *Scale bars of the images are not uniform from one to another.)*

It is possible that surface characteristics such as roughness would influence CNT growth on carbon substrates. Therefore, surface roughness was measured for each type of buffer layer along with particle size, density and extent of initial CNT growth. Mock carbon samples were measured as a baseline reference, and the RMS value was found to be approximately 0.4 nm. The surface roughness increased with the addition of an oxide layer, with an exception of ALD ALD Al_2O_3, where the surface roughness actually decreased slightly. The roughness of the ALD Al_2O_3 was almost equal to that of the vitreous carbon layer, measuring at at 0.405 nm. The roughness of the ALD SiO_2 layer was more than three times higher at approximately 1.45 nm. The SiO_2 deposited via MPE - CVD had the highest surface roughness value at approximately 4 nm; this was expected, because plasma-deposited SiO_2 films have been reported to grow as 3 to 4 nm islands, which merge to form complete films [149]. The Standard SiO_2 on silicon yielded the smoothest surface, with an RMS surface roughness value of 0.2 nm.

The ALD method is normally expected to provide a conformal thin film morphology [35]. However, as stated above, the result shows that the surface roughness of ALD SiO_2 was about 3x

higher than the roughness of ALD Al_2O_3. This can be attributed to the reaction between the ALD SiO_2 precursor and the carbon film for obtaining silica. During the deposition process, the carbon film was degraded, and as a result rougher surface was measured. Another possible reason might due to incomplete saturation of active sources on the substrate surface during film growth. As seen in Figure 47b, the ALD SiO_2 surface shows irregular holes in the top view SEM images. Furthermore, the carbon layer was not clearly distinguishable in the cross-sectional SEM imaging. To help resolve this issue, an additional test was performed in which the thickness of the vitreous carbon layer was measured by electron microscopy before and after ALD SiO_2 deposition. It was confirmed that a significant portion of the carbon layer does deplete during the ALD deposition process. This depletion may have resulted in surface roughening and void formation issues. At this point, it is not known if there are other possible ALD precursors for SiO_2 growth that may prevent this damage to the underlying carbon. All that can be concluded is that the present ALD SiO_2 precursor will be of limited use in practical applications, since it can cause noticeable degradation of the underlying carbon substrate.

6.4.2.1 Surface Roughness: Surface Variation for Alumina Coated Samples

In order to offer different surface roughness for oxide sample coated with alumina, a few standard carbon samples were first modified with RIE treatment with oxygen plasma. The oxygen plasma created by RIE has the ability to etch the carbon surfaces within a few seconds of processing time, thereby creating a surface with different roughness. Since the ALD is a conformal deposition process it should deposit oxide films with similar modified roughness. Figure 46 shows the surface roughness of samples that were deposited with ALD Alumina post RIE treatments. The result shows the surface roughness increased from 0.45 nm – 0.70 nm when RIE etch time increased from 0 seconds to 60 seconds.
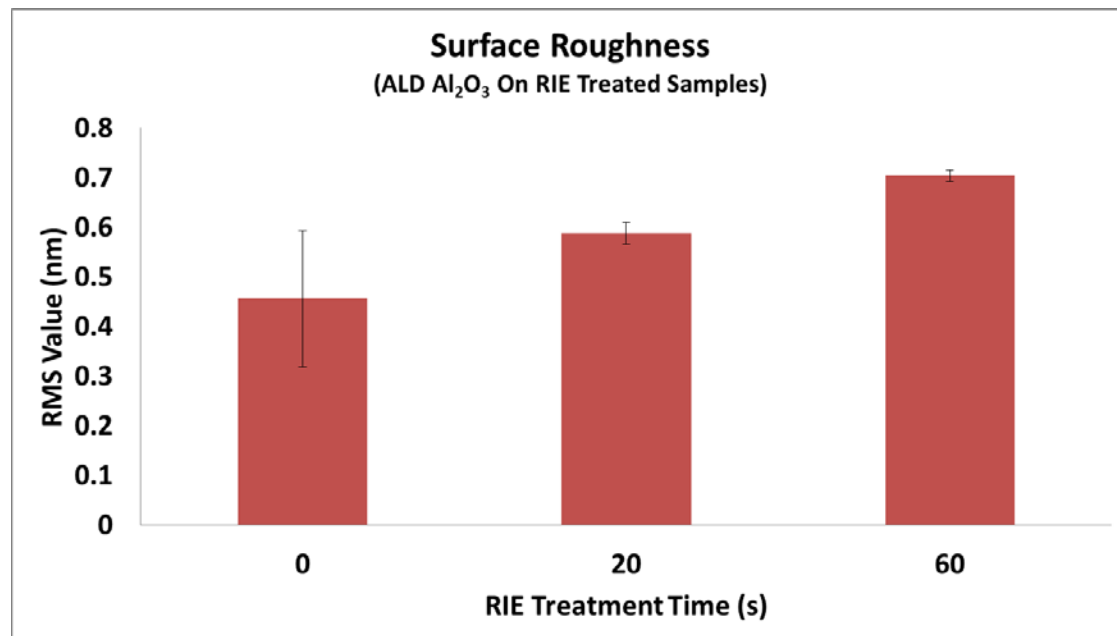
Figure 46: Surface Roughness of RIE Treated Carbon Sample that were Coated with 5 nm of ALD Alumina

Sputtered alumina samples were also prepared; the film roughness was measured with an average RMS value of 4.44 nm. However, it was later determined from SEM images that the roughness was resulted from high number of voids present on the oxide film. These surface voids could potentially be unfavorable for certain electronic application as it will increase local

DISTRIBUTION STATEMENT A: Approved for public release. Distribution is unlimited.

thermal resistance. As a result it was decided that samples with sputtered alumina will not be used in this investigation, but could be considered for future studies.

6.4.3 Growth of CNT arrays on oxide buffer layers

6.4.3.1 Brief growth: analysis of particle density, size, and CNT count

For this portion of the study, SEM images were taken of different oxide buffer layer surfaces after one minute of growth. The one-minute interval was selected to allow sufficient amounts of catalytic particles to be deposited onto the substrate. This interval also prevents CNTs from growing too long and obscuring the catalytic particles. Figure 47 shows representative SEM images taken from all the samples with buffer layers after one minute. All of the images have a viewing area of 450 nm x 450 nm and were taken at 200k magnifications. These figures clearly show the particle distribution as well as the catalytic particle sizes. As seen in the Figure 47, CNTs had started to grow on the samples, but by varying amounts.
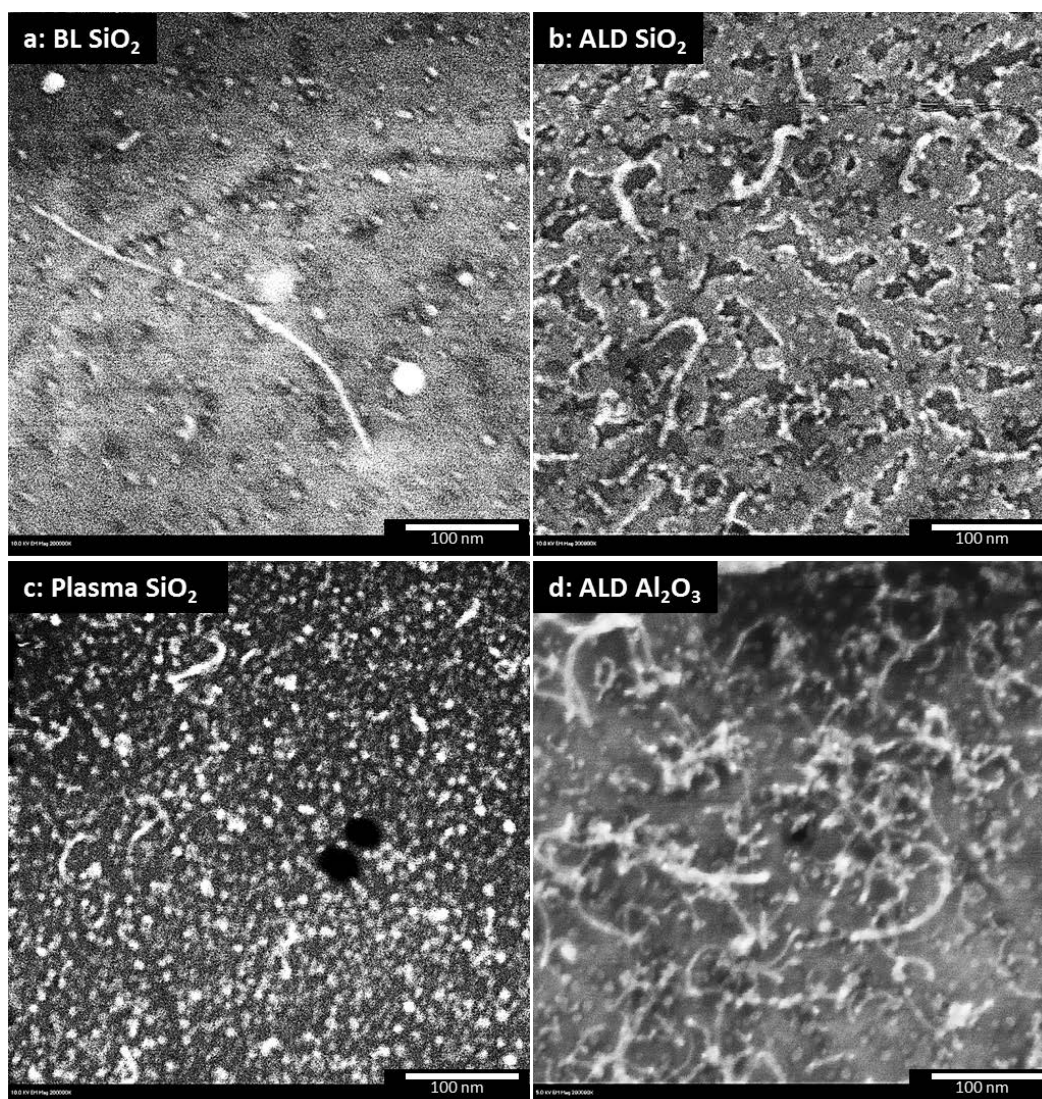
Figure 47: SEM Images after One Min Growth
(These images were processed with enhanced contrast.)

DISTRIBUTION STATEMENT A: Approved for public release. Distribution is unlimited.

Figure 48 shows the measured values for catalyst particle densities, average particle diameters, and number of CNTs per square micron after one minute of growth as obtained from the SEM images in Figure 47.
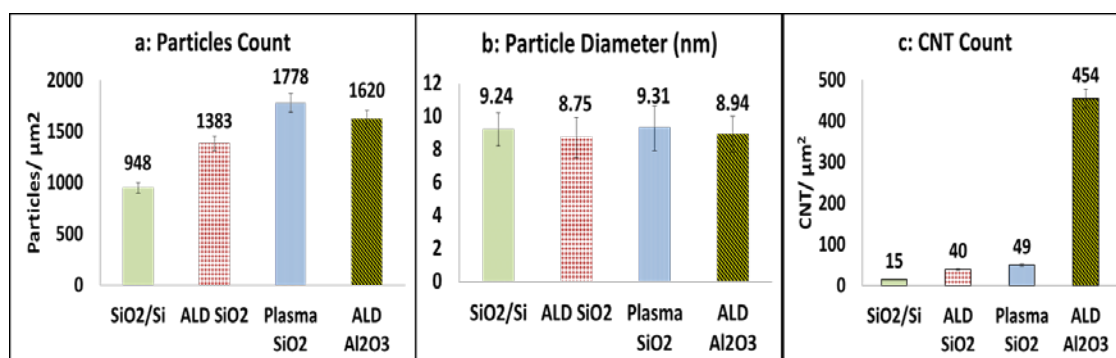
Figure 48: Data Collected after One Minute Growth
(a) particles per square micron observed after one minute for samples with different oxide buffer layers (b) average measured particle sizes after one minute and (c) number of CNTs present on the surface of each sample after one minute.

One important aspect of CNT growth is the aerial density of the nanotubes. However, as the CNTs grow, they become entangled, increasing the difficulty in determining the absolute aerial density from images. One way to compare CNT densities is to compare the number of catalytic particles on substrates before significant CNT growth. It has been suggested that each catalytic particle can produce at most one CNT [92], [109], hence particle count may provide an upper limit prediction of CNT density. Figure 47 shows an aerial view of the different samples. Figure 48 shows the average measured values as seen in the one-minute snapshots. These values serve as qualitative indicators of initial stages of growth, since it is expected that the actual quantities of catalytic particles will continue to change beyond the one-minute time frame. Figure 48 a and b suggest there were variations in terms of particle density on different buffer layers, but no significant difference in particle sizes. In addition, it is important to note from Figure 48c that, even within the first minute, there were significantly more CNTs grown on ALD Al_2O_3 than on the SiO_2 samples. The presence of more CNTs suggests that iron particles stabilize on the ALD Al_2O_3 surfaces more readily than on the silica surfaces, allowing for rapid nucleation and faster growth of CNTs. These differences may be attributed to the higher packing density of ALD Al_2O_3 and/or stronger catalyst-substrate interaction on the more ionic Al_2O_3 compared to SiO_2. Furthermore, Jadaun et al. suggested that the way that dangling bonds terminate on oxides surfaces would provide charge imbalances [77]. This may result in significant differences in the stability, surface charge densities, and chemical catalytic activities of the particles deposited on them. These atomic level differences on the oxide surfaces may be contributing to the differences in CNT nucleation.

Another way to compare the resulting information is by comparing the number of catalyst particle to surface roughness. AFM results shown in Figure 45, reveals that the three different silica buffer layers resulted in three surface roughness's measurements. Using the data collected on the samples, a trend can be seen by plotting surface roughness from the RMS values versus particle count. Figure 49 shows samples that uses SiO_2 shows a proportional increase between the surface roughness and the density of deposited nanoparticles. The fitted line has a R^2 value of 0.9721.

68
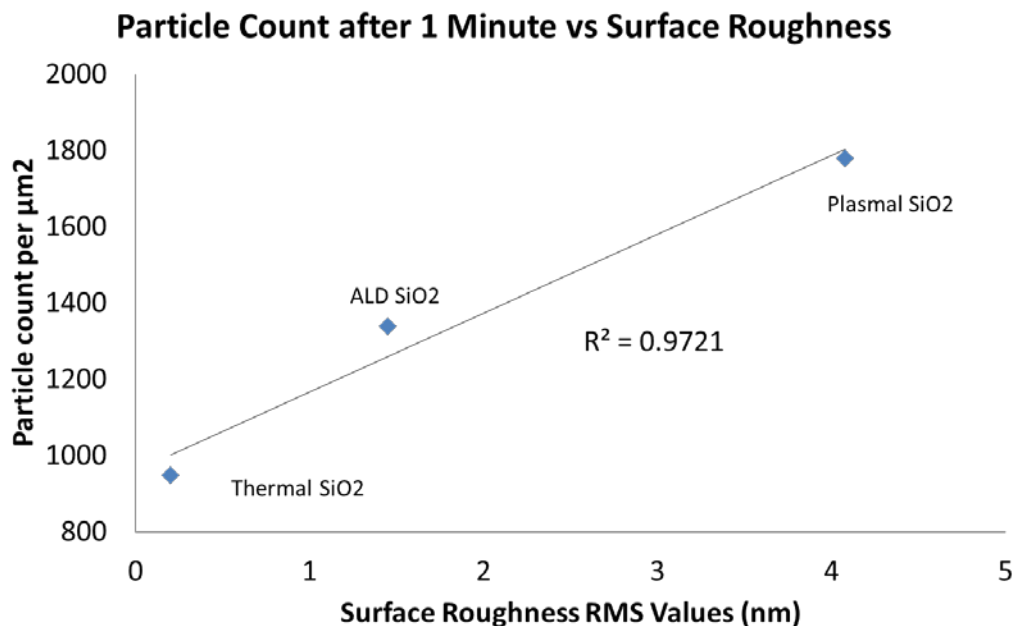
Figure 49: Catalyst Particle Count vs. Surface Roughness

6.4.3.1.1 Brief Growth for Surface Variation for Alumina Coated Samples

Similarly comparisons were attempted for the ALD alumina oxide coated samples with varying surface roughness. In this study, due to limited successful deposition technique available for alumina oxide, it was decided that surface can be modified with RIE prior to oxide deposition in order to create surface roughness variations. Figure 50 shows the SEM result of samples treated with RIE and coated with 5 nm of ALD alumina after 1 minute of CNT growth. It can be observed that the CNT growth density increases for samples receiving longer RIE treatment times. The samples that were treated with longer times have higher RMS values. It is possible that the increase observed in CNT growth density is related to rougher substrate surfaces. The SEM result shows that it is difficult to conduct particle count analysis on these samples due to the overwhelming presences of CNTs. However, it is visible that the density of CNT growth increases with rougher surfaces. Due to the overwhelming CNT coverage on the substrate surface, at this point, it is unknown if rougher surfaces contributes to higher number of particles received on the oxide surface, or does it contributes to a faster CNT nucleation rate. This might be an interesting area to investigate in the future study. However, from the results observed in Section 6.2.3, higher surface roughness did receiving higher catalyst count, therefore it is hypothesized that rougher RIE treated surfaces also received more catalyst on the substrate surface. Since CNT nucleation rate was faster on samples using alumina buffer layer, the higher visual density observed in Figure 50 is a result of more CNTs grown simultaneously from higher density population and not from faster growth rate.
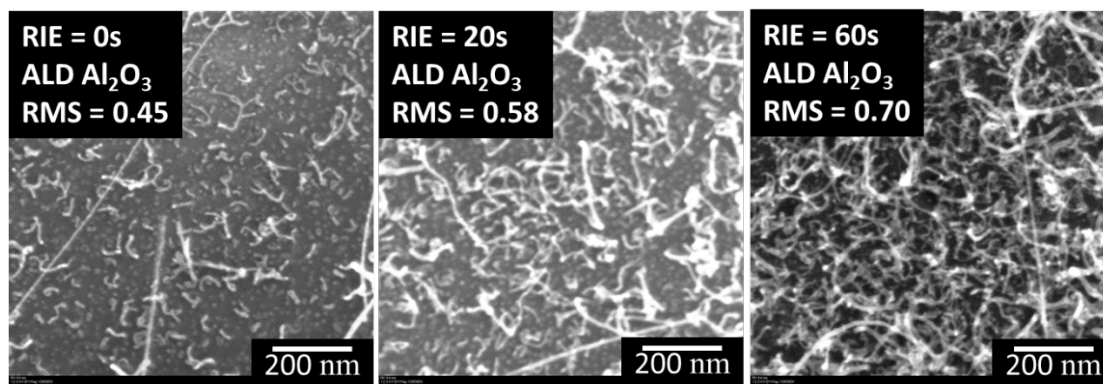
Figure 50: One Minute CNT Growth on Alumina Oxide Coated (RIE treated) Samples
(CNT growth density increases with increase of surface roughness.)

6.4.3.2 Extended growth: analysis of tube diameter, carpet height and growth rate

In order to see the influence of different oxides have on CNT growth an extended CNT growth time of twenty minutes was used. Twenty minutes of CVD growth time was selected to allow for a detailed comparison of CNT carpet height on each buffer layer. Cross-sectional SEM images were taken from all the post-growth samples once they were cleaved in half. Figure 51a–d shows the side-by- side interface comparisons of the samples grown. SEM shows that that the carbon layer appears to be missing for Figure 51b and Figure 51c, however it was visible for Figure 51d. Using EDS it was identified that indeed the carbon layer was not detected for Figure 51b, but was detected for Figure 51c. The inserts for Figure 51a–d show significant differences in the carpet height among the samples. The lower insert in Figure 51c is a low-magnification image showing the visible carbon layer for the plasma SiO_2 coated sample. Furthermore, the insert for Figure 51d shows a faint line in the middle of the CNT carpet, EDS identified this is a ALD Al_2O_3 buffer layer. This suggests that during CNT growth, ALD Al_2O_3 was detached from the interface.
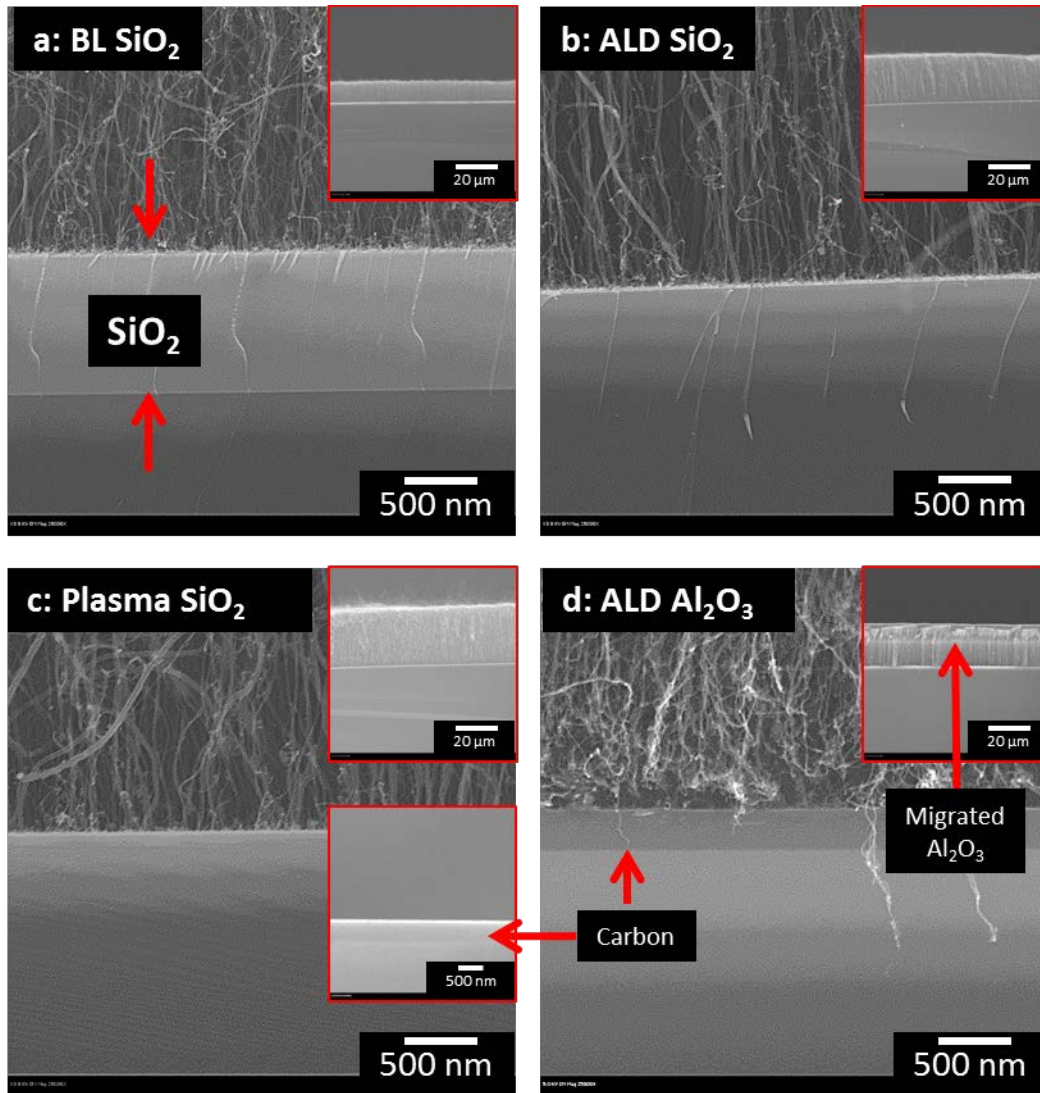
Figure 51: (a-d) SEM Images of 20 Minutes Growth Samples
(Highlighted scale bar is 500 nm .)

Figure 52a is a plot of the average height measurements, and Figure 51b shows the proportional increase trend of carpet height versus particle count, measured from one minute, for the silica samples. The linear relationship between the two can be seen from the fitted line with a R^2 value of 0.9736.
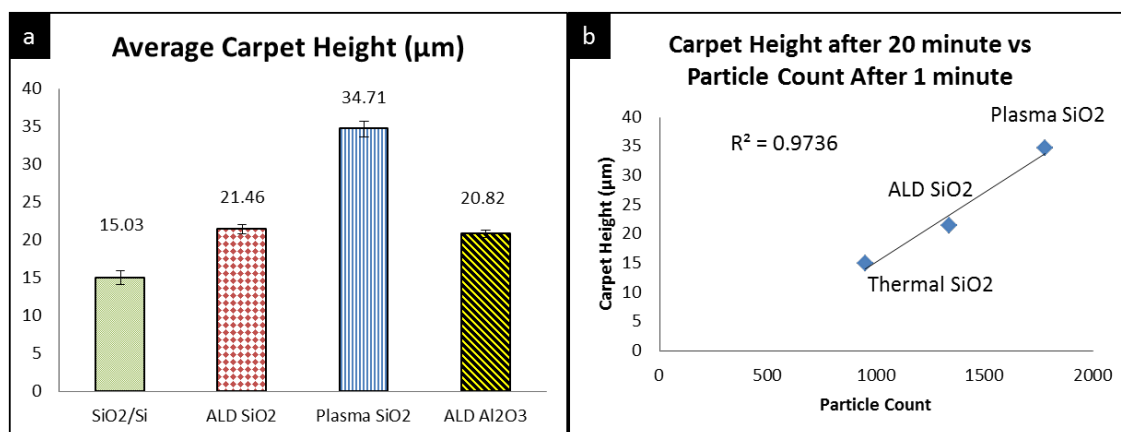
Figure 52: Carpet Height Measurements
(a) average carpet height determined for each sample, and (b) correlation between particle count (value after one minute) and carpet height (value after 20 minutes) for all the samples

As seen in Figure 51, all of the samples grew self-oriented CNT carpets, much like those described by Fan et al. [144]. However, there were variations in carpet height. The results show a clear trend for the silica buffer-layer samples. Figure 51f revealed that as the particle count increased, the carpet height also increased. This observation is important because it points to the possibility that the packing density of catalyst particles can be used to influence the carpet height obtainable under identical conditions. In other words, for a given chemical composition of the buffer layer, increased particle density as a result of increased surface roughness can influence the carpet height of the CNT array. Earlier studies have mentioned that the surface roughness has been a factor for CNT growth efficiency and lengthening [151], [152]. In addition, Xu et al mentioned that CNT alignment is a result of "crowding effect" [153]. However, some may argue that the length of the CNTs are the same, they just appear to be shorter because of the curliness difference from one batch of CNT verses the other. As a result, they are visually shorter from one SEM viewing angle. Although this might be true, and one possible way to prove this is to place the individual CNTs next to each other for comparisons, however, currently isolating individual CNTs is not a possible task. Figure 51 shows the comparative cross-section images of CNT morphology. However, it is also hard to determine the actual degree of alignment of the CNT carpet since the image was taken post cleaving, and there is no way to determine how much disturbance was done during cleaving.

6.4.3.2.1 Extended Growth for Surface Variation for Alumina Coated Samples

Extended growth studies were also performed on RIE surface modified samples. The idea is to see if rougher samples will also produce longer CNT carpets for samples coated with ALD alumina. Figure 53 shows the result of extended growth runs (20 minutes) on sample treated with and without RIE follow by ALD alumina coating. It is unclear why samples receiving RIE treatment results in a shorter CNT carpet initially when compared to sample that was never treated with RIE. However, when comparing samples treated with RIE, the samples that are rougher were able to grow taller CNT carpets. This result is similar to the ones observed when silica sample was used, were rougher samples produced taller CNT carpets. However more investigation is needed to identify the effect of RIE treatment to explain the possible negative impact that RIE treated sample have on carpet height.
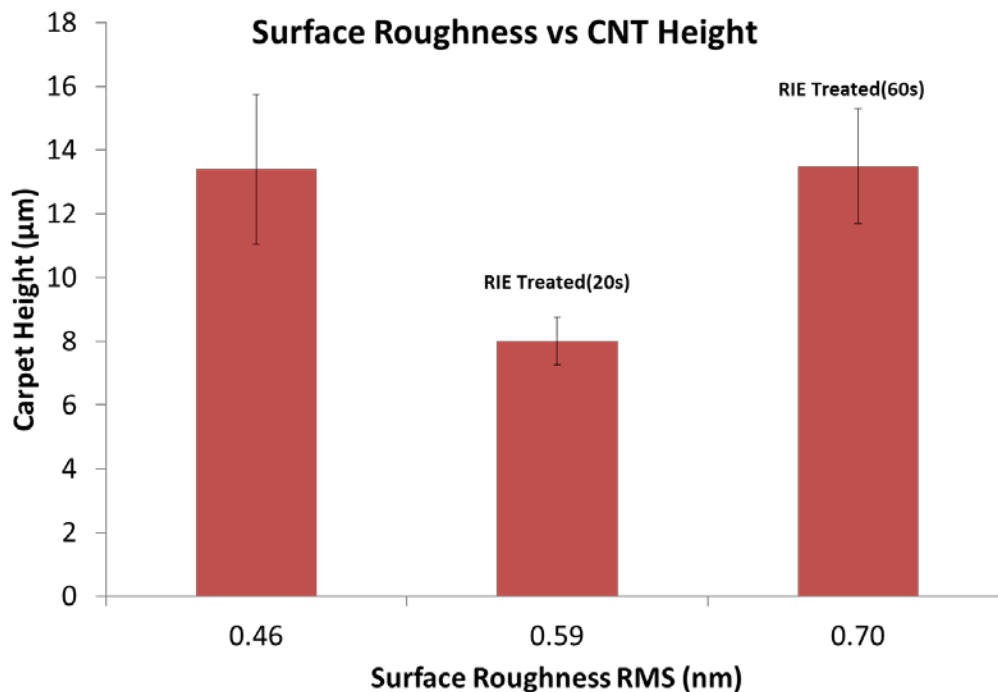
Figure 53: CNT Carpet Height on RIE Treated/Untreated Samples with ALD Alumina, 20 Minute CNT Growth

6.4.4 Thickness Effect

6.4.4.1 ALD alumina thickness effect on modeled carbon samples

In the earlier chapters, it was noted that certain growth, using ALD alumina would resulted in oxide buffer layers being "lifted-off" sometime during CNT growth.

This lifting phenomenon also raises concerns about the mechanical integrity of such structure. To address this issue, several pretreatment techniques were subsequently conducted to see if the "lift-off" issue can be corrected. The pretreatment techniques included the following.

1. Pre-oxygenation of the substrate surface
2. Pre-annealing the sample at a higher temperature (500 ℃) for 3 minutes
3. Depositing the alumina films at a higher temperature (300 ℃).

However none of the treatments performed solved the "lift-off" issue, which was observed post CNT growth. As mentioned earlier there is a large CTE difference between $C–Al_2O_3$, and this difference is probably one of the main driving factors for film lift off. Furthermore, it has been reported by George et al., that deposition of ALD alumina on CNT and graphitic surfaces is difficult, which is caused by the inert carbon surfaces [150]. However, there has been a report of successful film growth by Xuan et al. The location of the successful film growth took place along step edges, where the origin of nucleation site was believe to be located [154]. In this study, the substrate used is glassy carbon, therefore, it is possible that alumina oxides film only form a weak bond with the carbon substrate, as a results "lifted-off" of the film was observed post CNT analysis.

The lift-off issue can be undesirable for certain electronic applications, especially electrical or thermal applications, because it can disrupt transport properties at those locations. Other oxide

deposition technique might be able to produce films that have stronger adhesion to the substrate and should be invested in future studies.

Figure 54 shows the results from samples that were grown on samples deposited with various ALD Al_2O_3 thicknesses and grown for 20 minutes. These images show that the oxide layers did lift-off in certain samples. However, the image does not indicate when the lift-off occurs during the CNT growth.
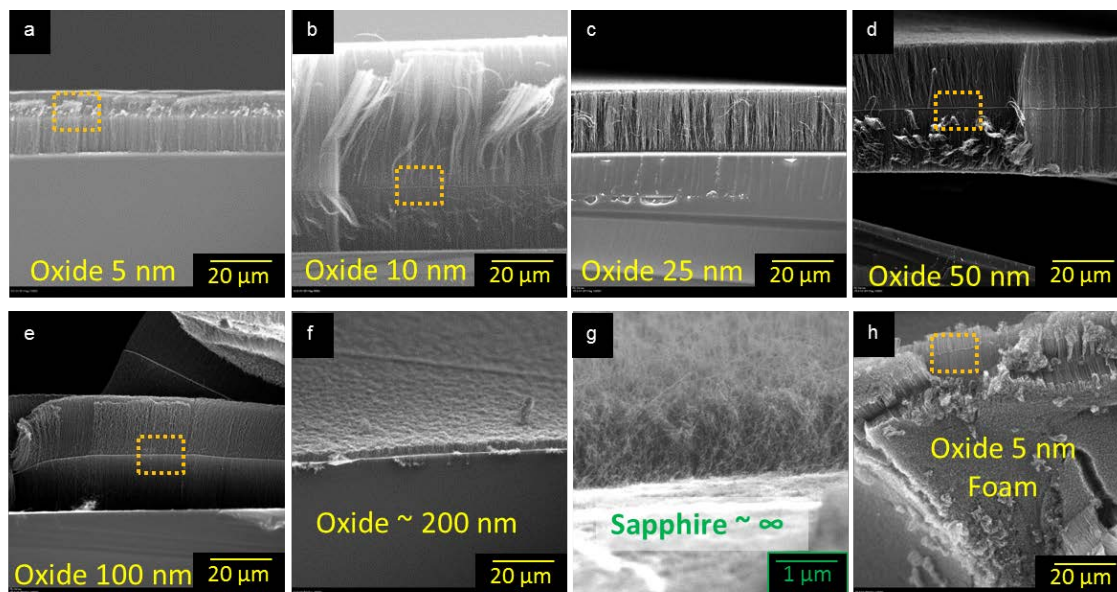
Figure 54: CNTs Grown on Various ALD Alumina Thickness Deposited on Standard Carbon Sample (unless specified otherwise)
a) 5nm, b) 10 nm, c) 25 nm, d) 50 nm, e) 100 nm, f) 200 nm, g) Sapphire, h) 5 nm oxide on carbon foam. The orange dotted rectangel highlighted the alumina that were lifted away from the sufstrate.

Figure 55 shows the SEM images of two different locations of one sample. These images show that in some area of the sample the oxide film did not "lifted-off" and in other locations the film "lifted-off" did occur. However, when comparing the carpet height of un-lifted sample to just the top portion of the lifted sample, the carpet height was measured to be within the standard deviation of error. It was believe that the top portion of a "lift-off" sample received continued growth from the beginning, regardless if the oxide peels off during the CNT growth. As a result, it was decided that measuring the top portion of a "lifted-off" sample, one can capture the effect of oxide layer thickness.
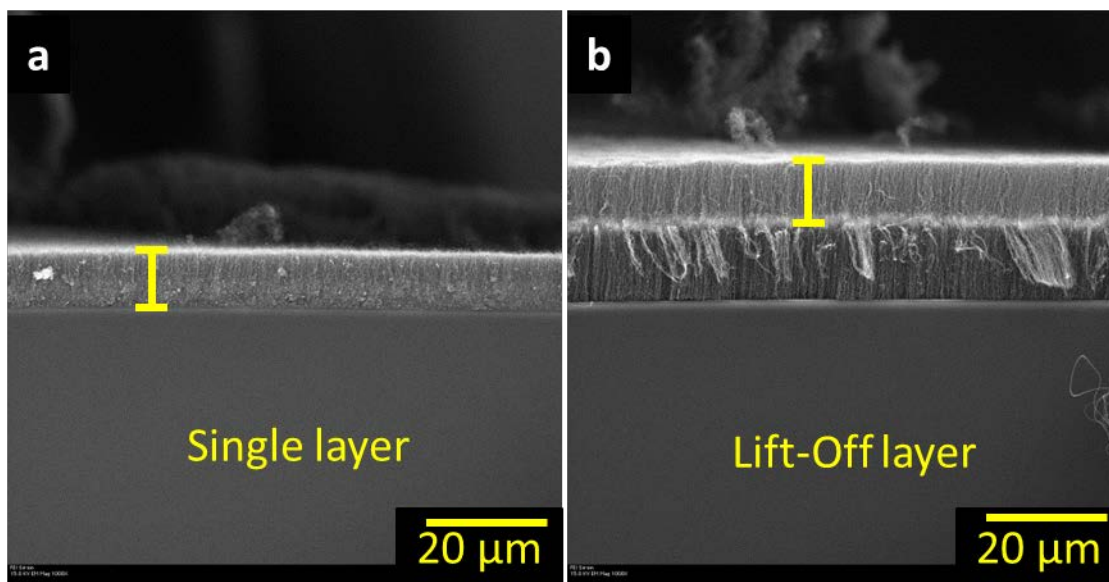
Figure 55: SEM Images Comparing the Carpet Heights
(not lifted vs "lifted-off" sample locations)

Figure 56 is a graph showing CNT carpet height as a function of oxide thickness. The feature of the graph shows that CNTs grew the fastest when oxide thickness is about 10 nm, and it resulted in tallest carpets when the same amount of time was use to grow CNTs. In addition, the images show that initially as the thickness of the buffer layers increases (up to 10 nm) the CNTs array height also increases, and further increase in thickness a reduction in height was observed. The "lifted-off" portion of the film was highlighted with an orange rectangle with dotted line in Figure 54 (a, b, d, and h). It was observed in Figure 56 that when a sapphire sample was used as a substrate, representing an infinite oxide thickness, the CNT carpet height reached a maximum around 3 µm. This result further validating that a thicker oxide thickness does not necessary yield taller CNT carpets in a given growth time. Figure 54h is just showing that the lift-off issue is not limited to flat substrate geometry, it also occurs on complex carbon geometry such as foam. This observation was mentioned earlier in Chapter 5; however since it was more difficult to conduct detail microscopy analysis on carbon foams, this investigation was repeated on more thorough by using flat carbon substrates.
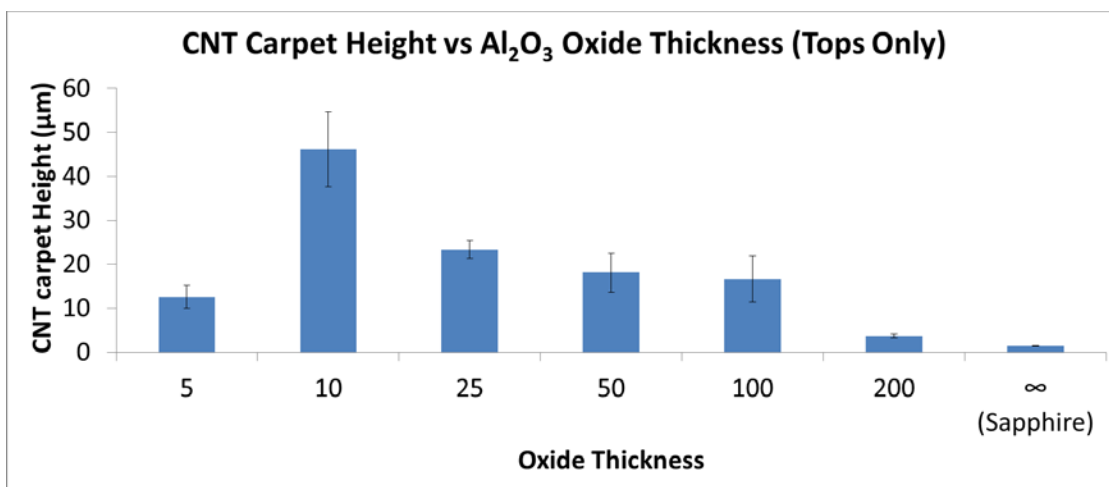
Figure 56: Chart Showing the CNT Carpet Height vs. ALD Al_2O_3 Oxide Thickness

75

6.4.4.2 Plasma SiO$_2$ thickness effect on modeled carbon samples

Similarly, to investigate the effect of silica oxide thickness have on CNT growth, samples with various oxide thicknesses were prepared using the plasma SiO$_2$ deposition technique. The ALD silica was not used due to defects created on carbon surfaces mentioned earlier. Using a 20 minutes FCCVD growth technique the result of CNT growth on those oxide thicknesses are shown Figure 57. The images indicated that the thickness of the CNT array height first increases as the oxide thickness increase, from 4 nm to 23.2 nm, however further increase in oxide thickness (> 23.2 nm) resulted in a shorter CNT array height. Figure 58 is a plot of CNT carpet height vs plasma oxide thickness. The feature of the graph shows that CNTs grew the fastest when oxide thickness is about 23 nm, as it resulted in tallest carpets when the same amount of time was use to grow CNTs.

It was also observed in Figure 58 that when a fused quartz sample was used as a substrate, representing an infinite oxide thickness, the CNT carpet height reached a maximum around 3 µm. This result further validating that a thicker oxide thickness does not necessary yield taller CNT carpets in a given growth time. This result is similar to the ones observed when alumina oxides were used for CNT growth.
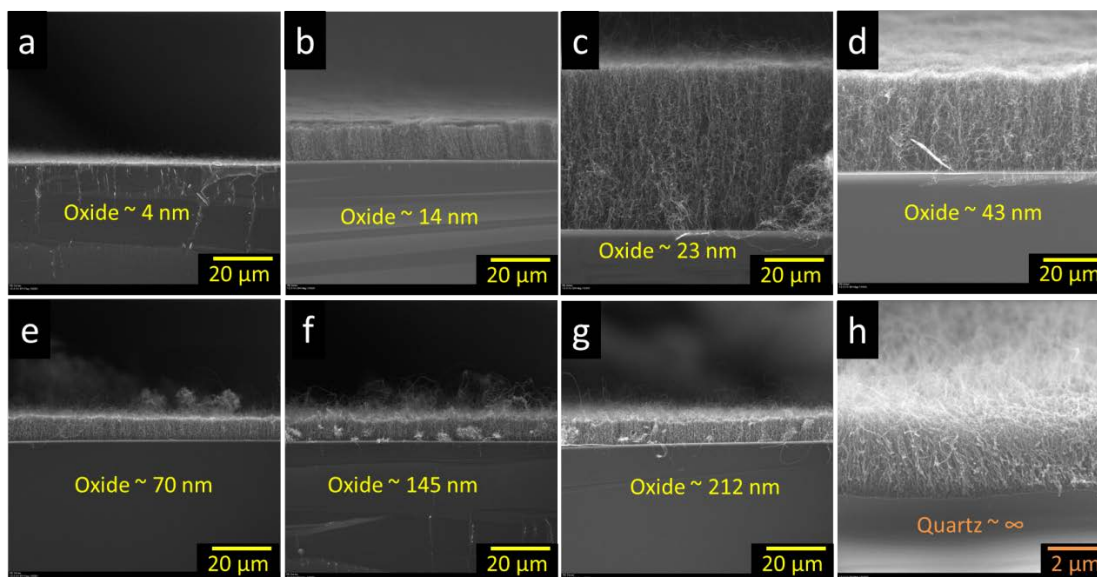
Figure 57 CNTs Grown on Various Plasma Silica Thickness Deposited on Standard Carbon Samples
a) ~4nm, b) ~14 nm, c) ~23 nm, d) ~43 nm, e) ~70 nm, f) ~145, g) ~212 nm, g) fused quartz.
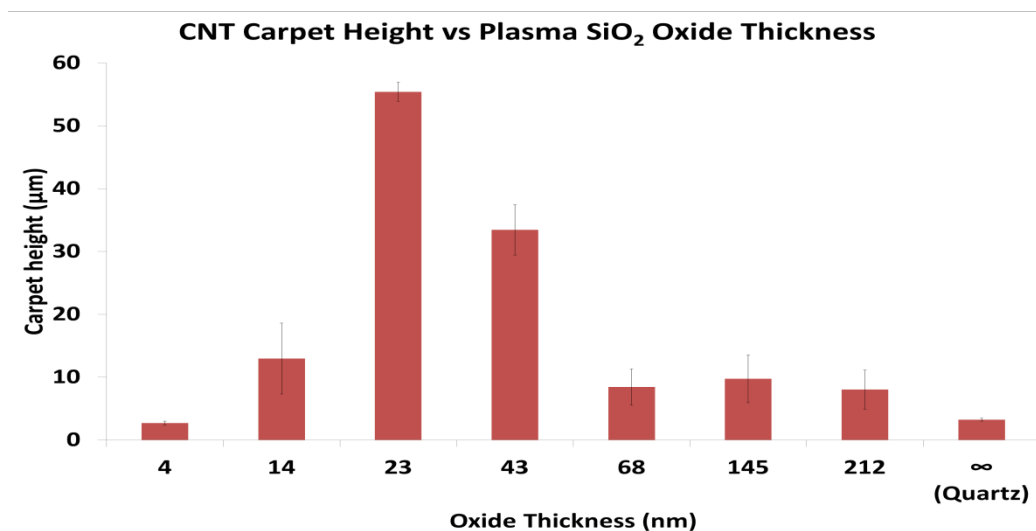
Figure 58: Chart Showing the CNT Carpet Height vs. Plasma Oxide Thickness

6.4.4.3 Oxide Thickness Effect Summary

It was observed that both alumina and silica buffer layers each have an optimal oxide thickness that allows CNTs to grow the fastest. For alumina this thickness is around 10 nm Figure 56 and for silica it is about 23 nm Figure 58. One possible reason that this optimal oxide thickness is different for different oxides might have to do with ionic surface difference. This ionic surface is related to the driving force behind CNT nucleation and growth kinetics, as a result different oxides have their own optimal oxide thickness. This point is supported by an earlier observation, Section 6.4.3, that samples with alumina and silica have different nucleation rate. The results show that samples with alumina buffer layer nucleated CNT faster, and that the optimal oxide thickness is thinner than silica buffer layer. However, alumina samples were plagued with adhesion issues that should be investigated in future studies if stronger adhesion is desired. For this study, the weak adhesion is problematic for thermal applications, and therefore samples with alumina oxide will not be used for samples intended for thermal analysis.

This is not the first time that CNT carpet heights influenced by oxide thickness were observed. In an earlier study, Cao et al., reported that varying the thermally grown SiO_2 on Si from 3.5 nm – 24 nm resulted in carpet height differences [69]. More specifically, Cao reported that an oxide thickness of 5 nm is required for CNT to grow, and that as the oxide thickness increases so does the carpet height [69]. This investigation uses ALD alumina and plasma silica, with oxide thickness > 24 nm, which was maximum used by Cao et al. It was observed that CNT growth beyond 24 nm resulted in a shorter CNT carpet height.

The effect of oxide buffer layer for CNT growth can be explained by the following.
1. When the oxide was too thin/incomplete
    a. Not enough film coverage was provided to allow dense catalyst seeding, which leads to a limited amount of CNT growth. It was observed that in the previous chapter that when CNTs has a lower growth density they tend to have more growth direction freedom. As a result shorter vertical height was achieved. At this point it is unknown if shorter tube or shorter vertical growth was resulted.
2. When the oxide was thick enough

a. Diffusion of iron particles into substrate is effectively blocked, which leads to full growth potential. As a result we observed taller CNTs grown as oxide thickness increases to about 23 nm.

3. When the oxide was too thick

It was observed that CNT carpet height was reduced after reaching certain oxide thickness. In order to find out the root cause one needs to investigate the following

a. The thickness of the oxide layer, beyond certain thickness, it might be possible that the thermal and electrical hot spots in some substrates become an issue. These hot spots might prevent efficient and effective CNT growth and should be considered for investigation in future studies.

b. It is also possible that iron particles continues to diffuse into the depth of porous silica, as a result carbon sources can no longer react with catalyst particle to facilitate CNT growth. When this happens, CNT growth ceased to continue.

4. Investigating in these areas could be very beneficial in multilayer component device. It will allow someone to design specific CNT height using oxide thickness as the controlling variable. Assuming CNT growth rate is constant, it is possible to control CNT height by varying growth time. If controllable CNT carpet height were achievable it can be very beneficial for conducting thermal testing. Therefore growth time was investigated in the following section.

6.4.5 Growth Time Effect

6.4.5.1 ALD alumina Growth Time Effect

Many studies have reported that, catalyst activity or poisoning, is one major factor in determining the duration of CNT growth and the ultimate carpet height achieved. In order to find out where the limitation is, CNTs were grown with discrete growth time of 20 minutes and 40 minutes on sample coated with 5 nm of ALD alumina. Figure 59 shows the result of ALD alumina coated samples that were treated with and without RIE prior to the oxide coating. It was observed that when the surface roughness is less than RMS = 0.59 nm, increase in growth time from 20 minutes to 40 minutes, results in increases of carpet heights. However, when the surface roughness is > RMS = 0.59 nm increase in growth time does not continue to increase in carpet height. This suggests that there is a limitation in growth time for samples that uses 5 nm of ALD alumina.
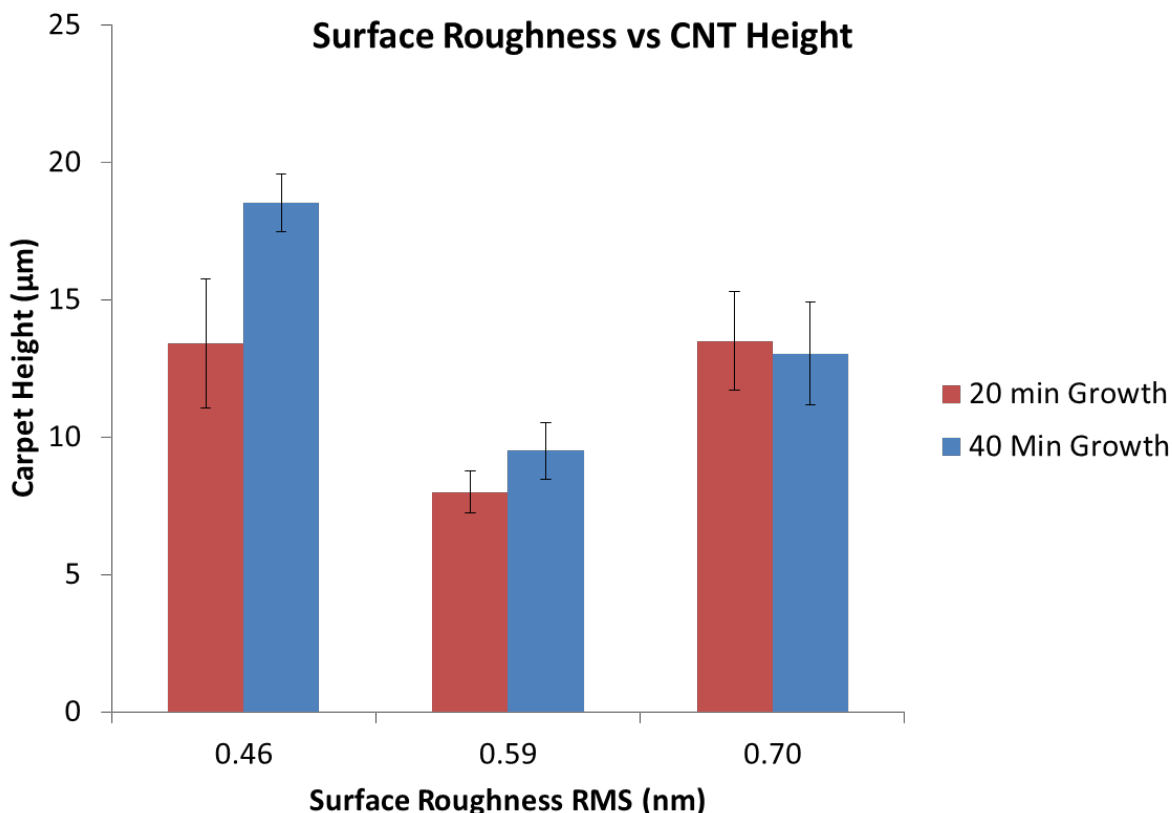
Figure 59: CNT Carpet Height on RIE Treated/Untreated Samples with ALD Alumina, Growth Time Variance

6.4.5.2 Plasma SiO_2 Growth Time Effect

Similarly, CNT growths were conducted on sample deposited with 23 nm of plasma silica, where the growth time parameter was changed from 1 minute to 120 minutes. Figure 60shows the cross-sectional SEM images of the samples grown at each corresponding time, these images shown are taken at the same magnification. The measured carpet heights were plotted in a chart shown in Figure 61, however this chart is missing the data point from 1 minute growth. The carpet height from 1 minute growth was too small to have a conclusive measurement. The result shows that the CNT array height increases linearly with growth time. In addition, the result shows that the growth continued for up to 120 minutes. Therefore the physical possible height limit for this growth is currently unknown. However is has been reported before that due to deactivation of catalyst source a termination in CNT growth was resulted. Therefore it is possible that termination of CNT growth will happen at some point. Furthermore it might be possible to model this growth trend to something similar to population growth. Figure 48 shows that accountable growth did not happen until 5 minutes, which suggest that growth happen less than 5 minutes was very low. Growth time longer than 5 minutes follows exponential rule until a carrying capacity is met. It is unknown when and where the carrying capacity is for this growth, but once the carrying capacity is met the growth will plateau. This investigation shows that time variable can be used as a controlling parameter for CNT growth.
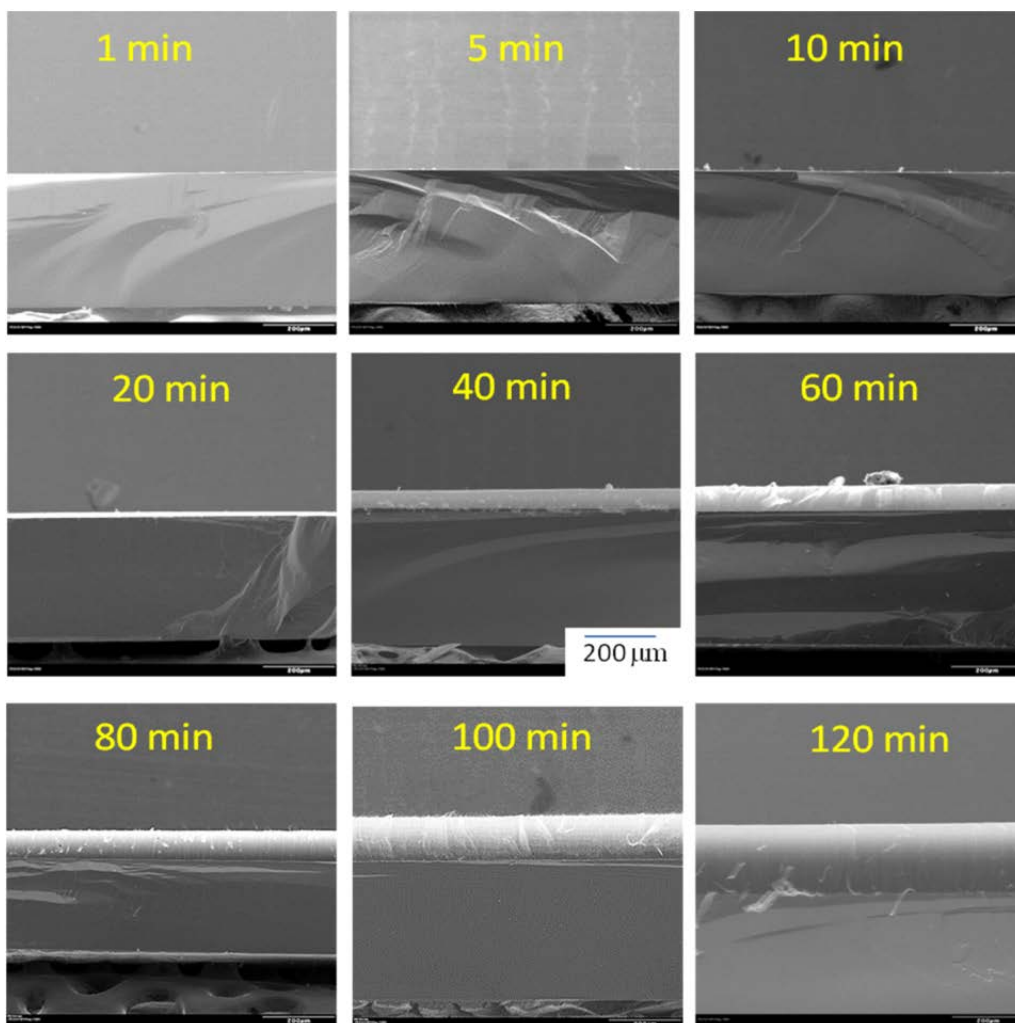
Figure 60: X-section Image of Samples Coated with 5 nm Plasma SiO₂, Grown for Various Growth Times

(Samples shown are the same magnification with scale bar showing 200 μm.)
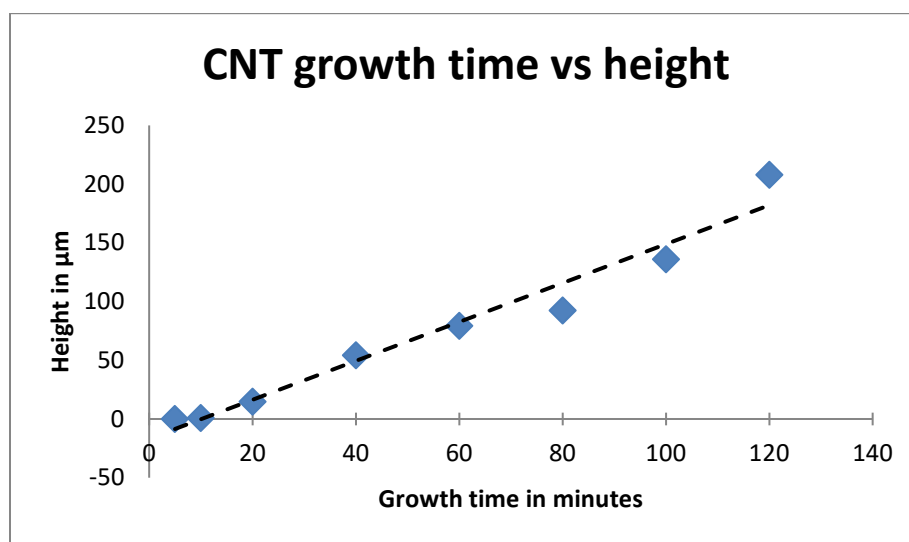
Figure 61: Plot of CNT Array Height vs. Growth Time

80

DISTRIBUTION STATEMENT A: Approved for public release. Distribution is unlimited.

6.4.5.3 Growth Kinetics

When it comes to CNT growth kinetics several parameters needs to be considered. CNT growth is a balance between the driving forces that allows CNT to growth vs resistances that prevents CNT from growing. The parameter that allows CNTs to grow is the driving force behind CNT growth rate, which includes concentration of gas source, catalyst source, and temperature. The parameter that prevents CNT from growing includes the following: ability for carbon source to diffuse through growing CNT carpets and reaching the catalyst source, catalyst source life-time, resistance associated with incorporating carbon source to the growing CNT, resistance associated with activation energy to nucleate CNT from catalyst source.

Keeping the above mentioned in mind, a simplified CNT growth kinetic equation can be seen in Equation 5, which is similar to ones reported by In et al. [155].

Equation 5 CNT Growth Kinetic

$$v_{CNT(growth)} = \frac{\frac{\Delta\mu}{kT} N_0 \omega}{R_1 + R_2 + R_3}$$

Where $\frac{\Delta\mu}{kT}$, is oxide specific driving force for the reaction, and N_0 is the initial concentration of catalyst active sites, ω is kinetic coefficient and R_1 is growth resistance related to diffusion of gas/molecules through the growing CNT forest to the catalyst sites, R_2 is growth resistance related to carbon adsorption and catalyst deactivations, and R_3 is growth resistance related to CNT nucleation.

It should be noted that each resistance is not contributing in equal weight throughout the CNT growth. For example, when CNT growth was > 10 minutes, the growth was slower because majority of growth resistance was contributed by the rate/ability at which catalyst particles can settle on the surface of substrate, follow by diffusion of carbon source through the catalyst source and reaching beyond the activation energy required for CNT nucleation. Once the ideal amount of catalyst particle is present on the substrate surface and the majority of CNT has nucleated, the growth rate become linear and is mostly limited by the diffusion rate of carbon source through the catalyst particle. This was observed in Figure 61, where CNT growth is linearly proportional to growth time, when growth was > 10 minutes. Furthermore, initial contribution associated with resistance from catalyst deactivation (R_2) is negligible, and it would only become significant after certain amount of CNT growth time has been achieved. However, in this study, deactivation of catalyst was not observed for sample that used silica as buffer layer, since CNT growth continued upto 120 minute of growth time. For sample that used alumina, the resistance associated with catalyst deactivation or carbon absorption was larger, since CNT growth has taper off around 40 min of growth time. This was observed in Figure 59, where the CNT carpet height at 20 minutes was similar to ones that were grown for 40 minutes.

6.4.6 TEM analysis: CNT and catalyst morphology

Figure 62 shows that CNTs grown in this study resulted in multiple walls regardless of the type of oxide used as buffer layers. Numerous articles have stated that catalyst particle size determines the tube diameter and growth rate for CNTs [96], [109], [110]. As seen in Figure 62, there were two different morphologies for catalytic particles: spherical or cylindrical. Spherical particles seemed to have less uniformity in terms of the size of residual particles and resulting CNT diameters, whereas cylindrical particles seem to yield more uniform CNT diameters. The

images revealed that the samples made with silica favored the spherical shapes, while the samples made with ALD Al_2O_3 favored the cylindrical shapes. The white arrows in Figure 62 point to the catalyst particles, and the dashed white arrows points to a few of the larger CNTs shown in the inserts of the figures, located on the top right corners.
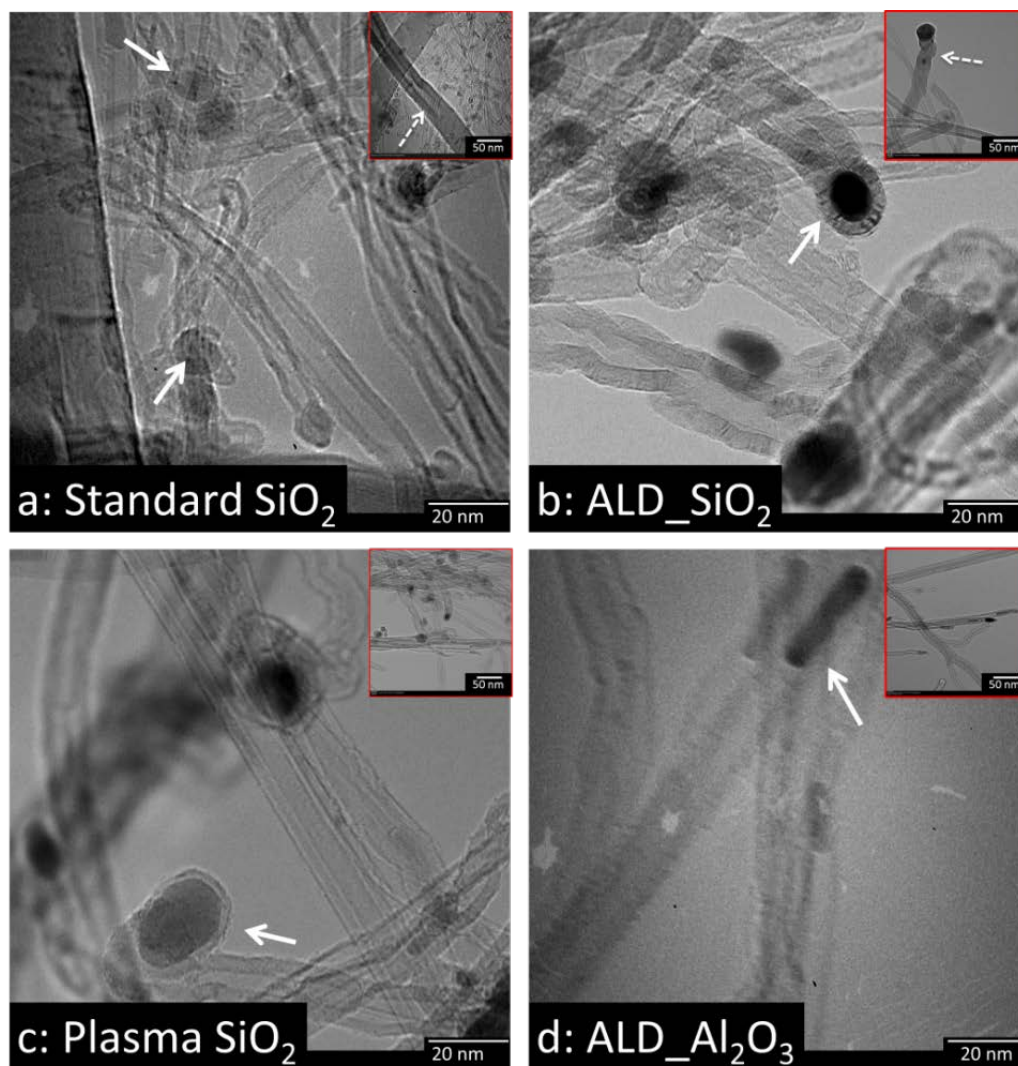
Figure 62: TEM Images that Show Particle and CNT Morphology
(Morphologies are for (a - c) SiO₂, and (d) Al₂O₃ buffer layer samples.)

It was observed that after one minute the particle sizes on all the samples were relatively the same; however, it was later found that CNTs grown via the SiO_2 buffer layer had larger variances than ones grown with the Al_2O_3 buffer layer. It was also observed that the CNT initiation rate was different between the two oxides. This difference may be the cause for the particle morphology differences observed in Figure 62, where samples grow using Al_2O_3 resulted in elongated catalyst shape, while ones using SiO_2 has more spherical shaped catalyst. CNT growth initiated earlier in samples with the ALD Al_2O_3 buffer layer; therefore, the particle sizes remained smaller and more uniform size. The early nucleation process may have stopped the nanoparticles from enlarging, but it may have elongated the particles.

It is unclear if the morphology of the catalyst particle is formed prior to CNT growth or after. However the study done by Schaper et al. showed the particle morphology can change during CNT growth, due to the catalyst particle being in a quasi-liquid state.[156] Therefore, even if the starting catalyst particles at 1 minute are similar in shape and size, it is possible that the morphology of the particles changes during CNT formation and growth. Several papers have suggested that it is possible to have nanometer size transition metals in a liquid state even if the temperature is several hundred degrees below the bulk melting point.[89], [157] Compounding this with the possibility that the catalytic particles can be in the form of a carbide, instead of α-iron, which would also lower the melting point temperature. If too much carbon was introduced during CNT growth, this may lead to supersaturation of carbon with carbide formation [156]. Although it is not possible to determine if any of the iron particles were in the liquid phase or in a carbide form, Figure 62 shows that the catalytic particle morphology is different when different oxide composition were used.

The particles that are elongated have similar cross-sectional areas. As a result, samples that grew with elongated particles have tube diameters that are comparable in size. However, for the SiO_2 samples, the CNT nucleation took longer to initiate, which could allow the catalyst particles to continue to grow. In other words, it is possible that the delayed CNT growth on SiO_2 surfaces allowed the catalysts more time to grow in size, resulting in larger variations in catalyst size and CNT diameter. Figure 63 schematically indicates two possibilities that would allow iron particle sizes to enlarge on the SiO_2 buffer layer. The particles can grow by agglomeration with nearby particles, or by absorption of iron from the condensed catalytic source. In a floating catalyst technique, where the catalyst source is present in the precursor gases, it is not possible to separate the contribution of each of these possibilities. It is possible that both are occurring simultaneously to create larger catalytic particles on SiO_2 buffer layers.
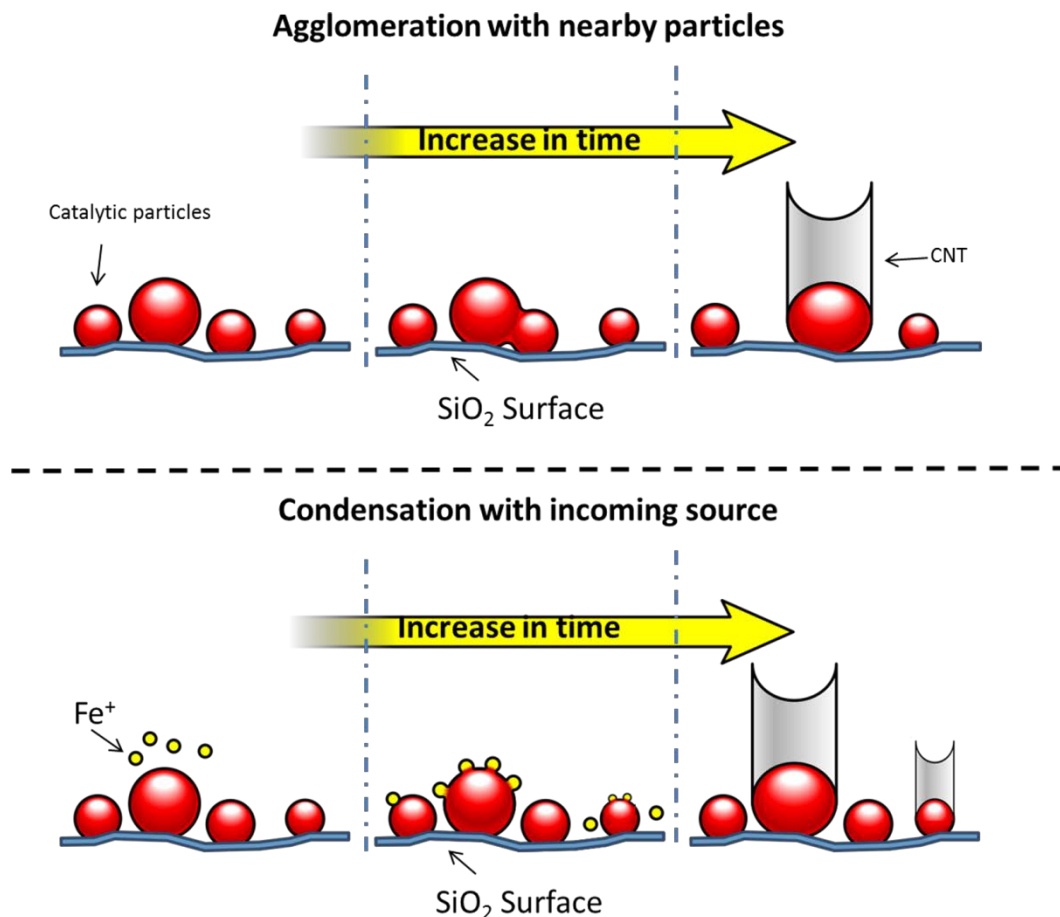
Figure 63: Schematic Representing Two Ways that Particles may Increase in Size

6.4.7 Summary table

Table 1 below summarizes the observations of this study. The different categories compared are as follows: surface roughness of the oxide buffer layer, CNT nucleation rate, carpet height achieved after extended growth, tube diameter uniformity, buffer layer to model carbon layer strength, and other noticeable characteristics. This is a comparison; therefore, the descriptions used in each column are what were observed when comparing one sample to another sample in the study. It is important to point out that the observations may be specific to the chemicals and the deposition performed in this study, and that if other chemicals are used the outcome may be different.

Table 1: A Comparison Table Highlighting Some of the Characteristics Observed in this Study

	BL SiO$_2$	ALD SiO$_2$	Plasma SiO$_2$	ALD Al$_2$O$_3$
Surface Roughness	low (0.21 ± 0.034 nm)	mid (1.469 ± 0.256 nm)	high (3.861 ± 0.136 nm)	low ((0.405 ± 0.017 nm)
(CNT Count) /CNT nucleation rate	(15/μm^2)/slow	(40/ μm^2) / mid	(49/μm^2)/mid	(454/μm^2)/fast
Carpet Height	Shortest (15.03 ± 0.91 nm)	Mid(21.46 ± 0.64 nm)	Tallest (34.71 ± 1.81 nm)	Mid (20.82 ± 0.47 nm)
Comments	The buffer layer was on Si substrate without carbon, and CNT diameters were observed to have large variances	Carbon degradation by precursors was observed, and CNT diameters have some variances	Most promising and scaleable method with good buffer layer to carbon adhesion and low CNT diameter variances	Oxide detachment issues were observed in some areas, but CNT diameters were very uniform

6.5 Conclusions

It was observed in Chapter 5 that oxides can enhance CNT growth density. The object for this chapter is to identify how oxides influence CNT growth differently so that better growth controllability can be achieved.

Two different oxide compositions, alumina and silica, have been compared, and the results shows that oxides can influence CNT growth in the following ways: CNT nucleation rates, CNT growth rates, and nanocatalyst particle morphologies. It also shows that CNT growth is controllable via growth time. In addition, the study shows that certain features associated with surface morphology, such as surface roughness and oxide thickness, can influence CNT growth density and carpet height. Furthermore the study identified that due to CTE mismatch, certain oxides have adhesion issues associated with the substrate, which can be important depending on the intended application.

The study result shows that samples with an Al$_2$O$_3$ buffer layer resulted in faster CNT nucleation and elongated residual nanocatalyst particles. In contrast, those with SiO$_2$ buffer samples showed a slower nucleation rate and more spherical particle morphologies. The study shows that the surface roughness of the sample is an important parameter and should be considered in sample design. It shows that catalyst particle density increased linearly with surface roughness, and that surface roughness can proportionately increase the CNT carpet height. In addition, it was observed that, oxide thickness has an effect on the CNT growth rate, and that there is an optimal oxide thickness if fastest CNT growth rate is desired.

It was demonstrated that samples that uses alumina oxides have growth limitation, up to 40 minutes, while samples that uses plasma SiO$_2$, the growth continues through 120 minutes with no tapering observed. Therefore, resistance associated with ability to grow is larger with alumina oxide comparing to silica oxide. The growth rate was related to equation 5, where it shows that the growth kinetic is driven by oxide specific driving force. Furthermore, this study shows that growth time can be used for growing controllable CNT array height when plasma silica was used.

This research emphasizes that growing CNTs on carbon substrates requires careful selection of the oxide buffer layer. Depending on the actual application, a carefully engineered buffer layer should be able to provide control over CNT growth density and array characteristics. Among the buffer oxides investigated in this study, the ALD Al$_2$O$_3$ buffer layer provides the fastest CNT nucleation and most uniform catalyst size distribution, but samples with oxide were plagued by adhesion issues, which may limit future applications. This issue should be further investigated in future studies. Perhaps other oxides that are more suitable and provide better substrate adhesion

for the application can be found. Plasma SiO_2 offers a slower initial nucleation rate, but appears to be the most stable, controllable and scalable, which is why Plasma SiO_2 has been selected as the buffer layer that will be used for growing samples used for thermal analysis in the next chapter.

CHAPTER 7: Thermal investigation of CNT arrays on carbon substrate

It was established earlier that buffer layer material is required in order to enhance CNT growth on graphite substrate. Then it was demonstrated that CNT array height is linearly related to growth time, when samples of same oxide thickness was used. This means that CNT carpet height is controllable by controlling growth time.

This opens up the opportunity to design samples with tailorable carpet heights, which would be essential for investigation the effect of length/thickness on the thermal properties of the sample. Thermal property investigations involving CNT has shown improvements when loose CNTs were added into the matrix in a random orientation [1]. It was believed that configuration with aligned carpets of CNT attached directly to carbon substrate would further improve the thermal performances by minimizing contact resistance.   Therefore samples configured with aligned CNT carpet directly grown on HOPG substrates, were prepared for the thermal investigation. As a result of this thermal investigation, parametric modeling equations, Equation 7 and Equation 8 in Section 7.4.7, were created to better understand how the variables affect the thermal resistance properties of CNT carpets. The variables include the following: CNT array height, density, and diameter.

7.1 Objective: Evaluate the thermal properties of CNT array

The objective of this study is to understand how some of the controllable CNT variables have on the thermal property of the CNT array. To accomplish this, CNT array of different heights were fabricated and tested using laser flash apparatus.

7.2 Background

One of the driving forces behind nanotechnology research is their potential to miniaturize electronic devices. As these devices shrink in size and enable more components to be packed into smaller spaces, efficient dissipation of waste heat generated through smaller volumes becomes more challenging to accomplish. Excess heat, if not rapidly dissipated away from the nanoscale electronic components, can lead to signal instabilities and/or premature device degradation. One common issue is failure at the device/substrate interfaces due to thermal expansion mismatch between different interface material compositions. Therefore, optimizing thermal transport through the interface is necessary to ensure stable performance. This calls for new strategies of integrating emerging materials and/or material combinations for future thermal management devices.

Commercially available thermal interface materials (TIM) products, such as solder and thermal grease, have known thermal resistance (R) values of 0.07 x 10^{-4} and 0.14 x 10^{-4} m^2K/W, respectively [1]. However, these materials have limited use in many future aerospace applications due to their high densities, tendency to harden and crack after prolong usage, and/or environmental degradation [2,3]. Therefore it is becoming very important to investigate lightweight and robust architectures for TIM that can support the emerging power electronic devices for aerospace use.

Graphene and carbon nanotubes (CNTs) are potential candidates for future microelectronic device packaging materials due to their excellent thermal and mechanical properties. In addition, these carbon materials are tailorable and can be fabricated into highly flexible films that supports mechanical compliance in certain electronic packaging materials [4,5]. Carbon materials have lower coefficients of thermal expansion (CTE) values, 1.1×10^{-6} m/(m-K), compared to other commonly used materials for electronics packaging: copper has a CTE value of $\sim 16.6 \times 10^{-6}$ m/(m-K). In addition, CNTs array can be engineered into a highly flexible films [4,5]. Carbon materials can address failures due to CTE mismatch while adding mechanical strength and flexibility to the components. In addition these kinds of components can withstand prolong thermal cycling and are less prone to failure due to interfacial delamination. Furthermore, carbon materials are chemically inert, which allows these components to operate in more extreme conditions such as corrosive environments.

Thermal analysis involving CNT arrays has been reported extensively, but there are currently no uniform testing standards due to a lack of standardization in CNT fabrication. The reported data on thermal conductivity vary over a wide range depending on the test samples and testing conditions. For example, using a dynamic modeling technique, the thermal conductivity (κ) value of a single walled CNT (SWNT) was reported to be 6,600 W/m-K [6]. Others have reported κ values with results ranging from 8 to 10,000 W/m-K [7–13] for SWNTs, and 0.145 to 3000 W/m-K for multi-walled CNTs (MWNTs) [7,11,14–20]. The wide range of values is a result of differences in the morphology of CNTs tested.

From electronic packaging standpoint, an understanding of the thermal transport properties of an array of CNTs orientated in the same direction is more applicable than those of individual CNT or masses of randomly orientated CNTs. Thermal conductivity values of free standing CNTs arrays have been reported to be 1.9 W/m-K for SWNT arrays [7], and 3 to 15 W/m-K for MWNT arrays[17]. Thermal analysis on free standing CNTs array may be ideal, in terms of the intrinsic thermal properties of the CNTs; but in practical devices, CNT arrays will need to be attached to a substrate that supports the device. Therefore, a thermal analysis of samples comprised of CNTs arrays attached to their growth substrate is more realistic but also more challenging.

The majority of reported CNT array growth is on electronic grade silicon substrates, and reported thermal conductivity (κ) value ranges from 8.3 to 15 W/m-K [16,21]. Others have reported values of 27 W/m-K with the addition of a metallized bonding layer on the CNT array[19]. More recently, studies have reported success with growing CNT arrays on graphite substrates [2,22–24]. It has also been suggested that three-dimensional structure consisting of CNTs joined perpendicular to graphene may be suitable as a high performance TIM [2]. That study involved CNT arrays of a fixed length 25 µm grown on thin graphite foil, and laser flash analysis (LFA) was used to measure the thermal resistance of the CNT layer. The CNTs were reported to be branched and having bamboo-like structures. Assuming their thermal conductivity to be 7 W/m-K, interfacial resistance was estimated to be about 6 mm^{2}K/W, which showed promise for future applications .

The objective of this investigation is to perform thermal measurements on a series of precisely controlled CNT arrays having different carpet lengths grown on highly oriented pyrolytic graphite (HOPG) substrates coated with thin silica buffer films. Success of this growth technique and details of CNT array quality have been reported in earlier publications [22-24]. In this study, LFA was used to measure the thermal transport properties of these samples in the

transverse (through thickness) direction, of the sample. To the best of our knowledge, this is the first study reported having 3 different CNT array length conducting thermal analysis to this extent. A 1-D thermal resistance model was incorporated to investigate the influence of CNT array variables (diameter, array height, and density) on the thermal transport properties of an all carbon system for electronics packaging applications.

7.3 Experimental

7.3.1CNT Growth:

Floating catalyst chemical vapor deposition (FCCVD), mentioned in Section 3.5.3.3.2, was used to grow CNT array films on (1 x 1 x 0.1 cm) highly oriented HOPG samples purchased from SPI, Inc. The growth time was varied from 60 min to 120 minutes in order to produce CNT with various carpet heights. The HOPG substrates were first coated with a thin film of SiO_2 (< 200 nm) as a buffer layer. Using methods similar to the ones documented in Pulikoll's dissertation[26], the SiO_2 was deposited using a microwave plasma CVD, where the silicon source was hexamethyldisiloxane. The resulting samples were analyzed by scanning electron microscopy (SEM), transmission electron microscopy (TEM), Raman spectroscopy, and LFA. In this investigation, even though the thermal analysis testing temperature ranges from room temperature to 110 °C, for the analysis and comparisons portion of the study, only the diffusivity values measured at room temperature was used to calculate thermal conductivity value, and ultimately the thermal resistance values. Table 2 show the samples prepared for the investigation.

Table 2: Sample Properties

Samples	units	Bottom Layer			Cap	Top Layer		
		HOPG 1	HOPG 2	HOPG 3	HOPG Cap	CNT I (482µm)	CNT II (199µm)	CNT III (75µm)
x	mm	1 cm x 1 cm (nominal sample size)						
y	mm							
z	mm	1.23±.01	1.37±.01	1.42±.01	1.15±.01	0.482±8e-4	0.199±7e-4	0.075±6e-4
Weight	g	0.2518	0.3060	0.3148	0.2363	4.20E-03	2.10E-03	1.90E-03
(Average Sample Density)	g/cm³	2.16±0.1				0.091	0.102	0.248

7.3.2 Microscopy:

SEM and TEM analysis was performed to characterize the CNTs in relation to morphology, packing density, and interface composition. The TEM foils were prepared using focused ion beam (FIB) extraction and thinning techniques described in Chapter 3. The samples were protected with a layer of sputtered platinum in order to help preserve the CNTs and the cross-sectional area of interest. The resulting foil was extremely delicate and easily damaged by the high intensity TEM beam. Hence, images of regions of interest had to be quickly taken after all the focusing adjustments were made on an adjacent area of the specimen. Electron energy loss spectroscopy (EELS) was used for iron and silicon identification at the CNT/HOPG interface, Figure 65 .

7.3.3 Raman spectroscopy analysis:

Raman spectroscopy data was collected and it was found that the samples did not have a peak at (200 cm^{-1}), therefore the CNT samples grown were MWCNTs.

7.3.4 Thermal analysis:

A Netzsch LFA 457 laser flash apparatus was used to measure the thermal property of the samples. Samples were loaded into 1 cm^2 sample holder and were placed on the testing stage. Essential data values (dimensions, density, weight, specific heat, and testing temperature range)

were entered into the system prior to testing of a one layer sample. The system only measures the diffusivity value of one unknown layer at a time. To measure the diffusivity value of a multi-layer sample, data values mentioned above plus the diffusivity value of the known layers must be entered prior to multi-layer analysis. LFA measures the thermal diffusivity value of the unknown layer as a function of temperature. The thermal diffusivity, α (mm^2/s), was first defined by Parker et al. [30] for laser flash analysis as

$$\alpha = 0.138 \frac{l^2}{t_{1/2}} \quad \text{or } \alpha = \frac{k}{\rho * c_p} \quad \text{with a unit of (mm}^2\text{/ second), shown in Equation 4.}$$

where l is the length/thickness of the specimen and $t_{1/2}$ is the time needed for the rear surface temperature to reach half its maximum value. The equipment can measure the diffusivity of a sample that ranges from 0.01 to 1000 mm^2 /s with reproducibility of ±3%. The values reported in this study uses one σ standard error.

In this work, single, and two-layer analysis were conducted to analyze the thermal diffusivity values for HOPG substrates, and CNT array films. Such sample is constructed with CNT on HOPG substrate as lamellar composites. The thermal resistance of each layer and each interface was calculated using a 2-step testing procedure, as shown in the results section. For details of calculation please see Appendix D.

7.4 Results and Discussion

Figure 64a, shows the cross-sectional schematic of the 2-layer samples used for thermal analysis. Figure 64b is a 3-D representation of the 2-lyaer sample. The 2-layer model configuration is indicated where CNT array is labeled as the top layer and the oxide coated substrate as the bottom layer. Equations that correspond to the thermal resistance contributed from each layer are shown. R_{HOPG} is the thermal resistance of the substrate layer, and R_{array} is the thermal resistance of the CNT array. It is important to note that $R_{interface}$ incorporated many of the thermal resistance values that are not experimentally measured in this study. $R_{interface}$ value is a combine thermal resistance value that incorporated the following: thermal resistance of the catalyst particles, and the thermal interface resistance resulting from the interface between the oxide and the substrate. The physical properties of the HOPG layer and the CNT layer are listed in Table 2. The weights of CNTs were obtained by weighing the HOPG samples before and after CNT growth. These physical property values were entered in the laser flash system for the thermal analysis.
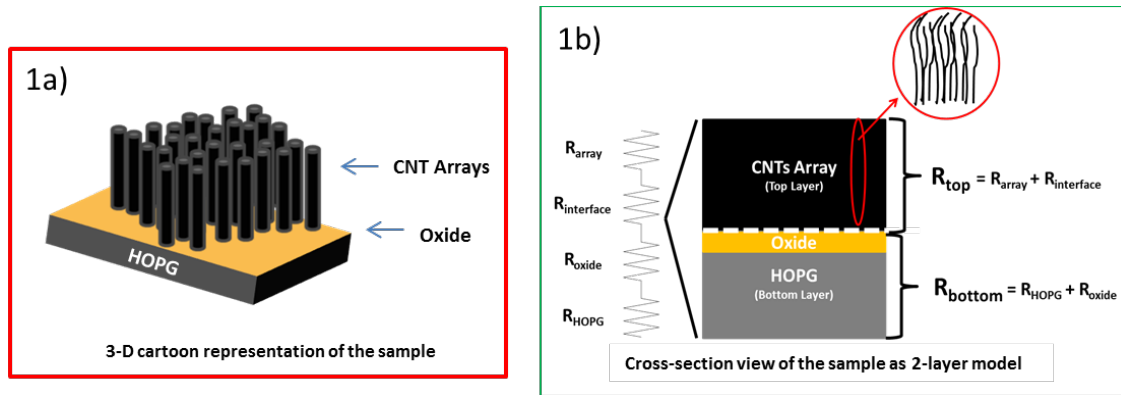
Figure 64: 1a) 3-D Cartoon Representation of the Sample, 1b) Cartoon Representation of the Sample for a 2-layer Thermal Analysis Model
**Figures are not drawn to scale

7.4.1 Microscopy and characterization:

An overall measure of CNT content in the samples can be obtained from the weight, i.e. the difference in weight before and after CNT growth on the solid. In order to assure that CNT growth was only on the top surface and not on the sides, the sides of the HOPG substrates were masked off prior to deposition of the oxide buffer layer. It has been clearly demonstrated in the past that there is minimal growth of CNT without a buffer oxide layer on the carbon substrate surface [22,24,31,32].

More details of CNT growth, such as number of nanotubes per unit area of substrate, and their length (carpet height) can be obtained from their SEM images. The CNT growth density can be estimated using the SEM image depth of field and count the number of CNTs visible in an image area. In this study, the number of CNTs was measured to be 77 ± 6 CNTs/μm^2 or 7.7 x 10^9 CNTs/cm^2. Several studies have attempted to measure CNT density in arrays grown on different types of substrates using different deposition techniques [7,33,34], which show a wide range from about 8 X 10^9 to 5 X10^{11} CNTs/cm^2. It must be pointed out that this is an estimate only, and there is a possibility of underestimating the total number of CNT in a given area because a SEM image can only capture objects within the line of sight, and this can lead to some unaccounted CNTs that fall outside of the field of view or are hidden behind a visible CNT. Secondly, it is assumed that the number of CNTs stays the same from the interface of the sample to the CNT tips. This may not be true, since it is possible for new CNTs to grow some distance away from the interface. Therefore using SEM to estimate the number of CNTs leads to a number that represents minimum numbers of CNTs in an area. This value was used in the parametric modeling analysis, Equation 7.

Each component within the thermal interface can affect the thermal pathway, and thereby increase the overall thermal resistance. Therefore it is important to examine the interface in order to determine if any obstructions are in the thermal pathway. Figure 65 is a set of TEM images taken from the CNT/HOPG interface. The inset in Figure 65b is an SEM image prior to the TEM alteration, and shows that the CNTs used for thermal measurements were uniform and aligned before FIB processing. Figure 65e is a merged image that shows the location of the Fe catalyst particles in relation to the oxide at the interface. In theory, the particles should have some thermal resistance contributions; however due to their size being small in scale (10 nm), it is expected that the contribution would be small as well. Hence, these particles were not treated as a separate component/layer in the thermal analysis portion of this study.

To make TEM foils, FIB process was used. This technique requires pre-coating the area of interest with sputtered platinum, thereby filling the voids between CNTs and coating the CNT during the process. Once the coating is in place, an ion beam was used to etch away excess material, allowing the area of interest to be lifted for TEM and electron energy loss spectroscopy analyses. Figure 65b is a representation of unaltered CNTs with a higher magnification image as an insert. This image shows that the CNTs used for thermal measurements were uniform and aligned before FIB processing.
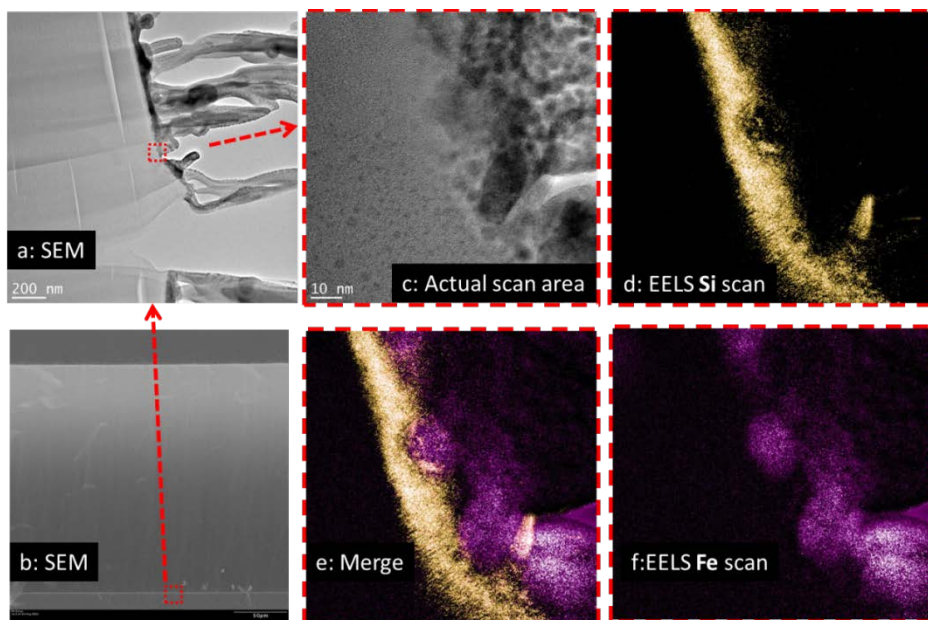
Figure 65: SEM and TEM Images of the CNT/HOPG Interface
(The TEM uses EELS technique to find the oxide layer and the iron catalyst particles.)

7.4.2 Raman spectroscopy:

Based on the absence of a peak in the radial breathing zone (~200 cm^{-1}), it was concluded that the bulk of CNTs were multi-walled. The D-peak to G-peak ratios were measured and the values ranged from 0.46 to 0.79. Hence, the grown CNTs have more graphitic structures than defects sites. The Raman values suggested that CNTs has good morphology, more graphitic features, which should correlates to high thermal conductivity values.

7.4.3 Thermal Analysis:

The LFA system uses a laser pulse to deposit energy on the front face of a sample, and a detector measures the temperature response of the rear face. LFA uses validated models from literature to determine the thermal diffusivity, α, of the sample or layer in question. Once the diffusivity is determined, both the thermal conductivity (κ), and the thermal resistance (R), can be calculated. To calculate the thermal conductivity of the sample, equation 2 can be used

$$\kappa = \alpha * \rho * c_p$$

where ρ (g/cm^3) and C_p (J/g °C) are density and specific heat, respectively. The specific heat for the sample was validated using differential scanning calorimetry (DSC). To determine the thermal resistance value (R) of an area, Equation 6 is used. This thermal resistance equation is more favorably used for thermal interface material. As seen from the equation, the thermal interface layer is independent of area.

$$R = \frac{l}{\kappa}, \text{ with the unit of } \frac{m^2 K}{W}$$

Equation 6 Thermal Resistance, Dewitt et al. [2]

where l is the thickness of the thermal layer within the sample.

7.4.4 Thermal Analysis of the Substrate (HOPG):

The HOPG sample is an excellent sample to be measured by the LFA system because it is made of graphite and nontransparent to the IR detector. Figure 66 shows the average thermal diffusivity values of HOPG samples measured over the temperature range of (25 - 100 °C).
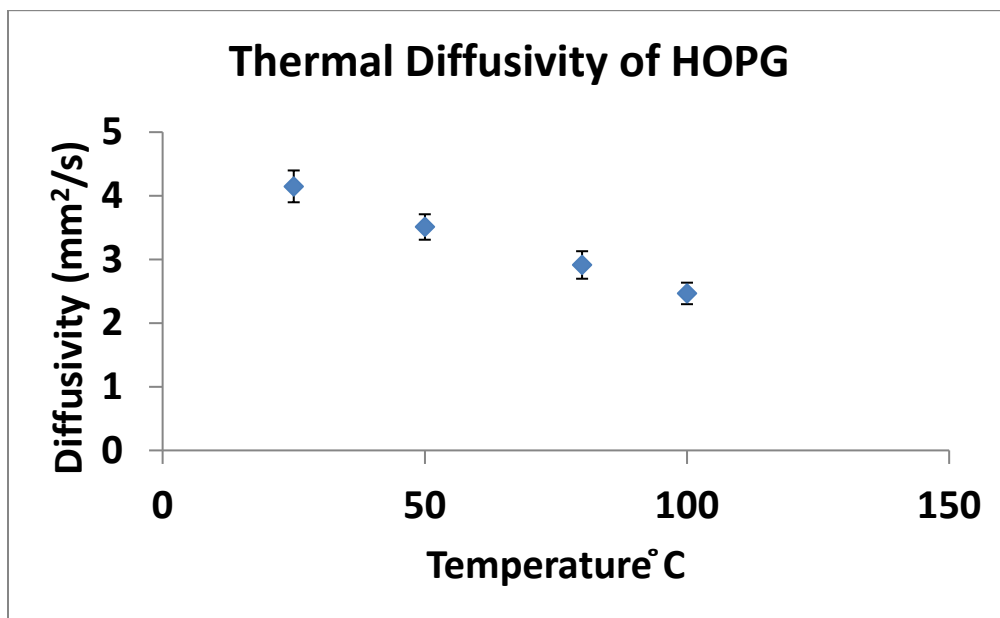
Figure 66: Diffusivity Values for Uncoated HOPG Samples

7.4.5 Thermal Analysis of Substrates with a Buffer Layer:

Diffusivity values were obtained for HOPG samples coated with a SiO_2 buffer layer. It was determined that the oxide layer was too thin for the LFA system to measure the diffusivity contributions. Namely, the measured diffusivity value for the SiO_2 coated HOPG samples were essentially the same as those measured of the baseline HOPG sample, Figure 66. Using a referenced thermal conductivity value for silica, 1.4 W/m-K, the thermal resistance of the silica oxide layer was estimated. It shows that the thermal resistance value for the silica buffer layer is indeed expected to be several orders of magnitude smaller, 5.21×10^{-8} m^2K/W, than that of the HOPG substrate layer about 2.5×10^{-4} m^2K/W. Therefore it is safe to assume that the oxide buffer layer has negligible thermal resistance contribution, as indicated in Table 3.

7.4.6 Thermal Analysis of Substrates with a Buffer Layer and CNT Array Film:

In this investigation, CNT arrays were grown as a uniform film on the oxide coated HOPG samples. The oxide coated HOPG substrate was considered the bottom layer of the composite, and the CNT film and the corresponding $R_{interface}$ were treated as the top layer. The previously obtained thermal diffusivity value and corresponding physical properties of the bottom layer of each sample (HOPG 1, 2 and 3) was first entered as a known value in the Netzcsh LFA two-layer analysis. The resulting average diffusivity values for the top layer of each sample (CNT I (482 µm), II (199 µm), and III (75 µm)) are listed in Table 2. The thermal diffusivity value for the top layer was converted/calculated to thermal resistance value using Equation 3 and Equation 6, in order to compare the thermal resistance contributions from each of the layers.

Table 3: Thermal Analysis Results

Samples	units	Bottom Layer			Top Layer		
		HOPG 1	HOPG 2	HOPG 3	CNT I (482µm)	CNT II (199µm)	CNT III (75µm)
α	mm^2/s	3.864±0.06	4.053±0.08	4.177±0.09	6.099±0.04	3.088±0.04	0.558±0.03
C_p	J/(g*K)	0.63±0.01					
k	W/mK	5.23	5.52	5.71	0.351	0.199	0.087
$R_{bottom} = R_{sub}+R_{oxide}$	m^2 K/W	2.35E-04	2.48E-04	2.49E-04			
R_{oxide}	m^2 K/W	5.21E-08					
$R_{top} = R_{array} + R_{interface}$	m^2 K/W				1.37E-03	1.00E-03	8.61E-04
$R_{interface}$ (Figure 5)	m^2 K/W				7.59E-04		
k_{array} (Figure 5)	W/mK				7.91E-01		
R_{array}	m^2 K/W				6.09E-04	2.52E-04	9.48E-05

Figure 67, R_{top} is plotted and it is the value for the sum of CNT array and the $R_{interface}$. It can be seen that, there is a linear trend between R_{array} and the height of the CNT arrays. Since all of the samples use the same growth parameters (other than growth time), it was assumed that the CNT/HOPG interface resistance, $R_{interface}$, for all samples were the same. Therefore, the contribution of $R_{interface}$ to the combined resistance of R_{top} can be obtained by a linear line extrapolated to the y-axis intercept. Based on this y-intercept, inherent $R_{interface}$ was measured to be 7.59 x 10^{-4} m^2 K/W. R_{array} values for each of the three samples were calculated by subtracting $R_{interface}$ from the respective R_{top} values. The thermal conductivity value of the CNT array was then calculated to be 7.91 x 10^{-1} W/m-K, from the inverse of the slope of the trend line.

Figure 67 also indicated two noteworthy points. When the carpet height is short, the dominating thermal resistance contribution is from the $R_{interface}$. When the carpet height becomes nominally tall the dominating thermal resistance contribution is coming from R_{array}.

One area to keep in mind when selecting optimal carpet height for the TIM application is to consider the balance between thermal resistance and the thermal mechanical compliance properties that CNTs can offer. On one hand longer CNTs can provide flexibility to a thermal interface that is otherwise rigid, on the other hand the length of CNT carpet can increase thermal resistance.
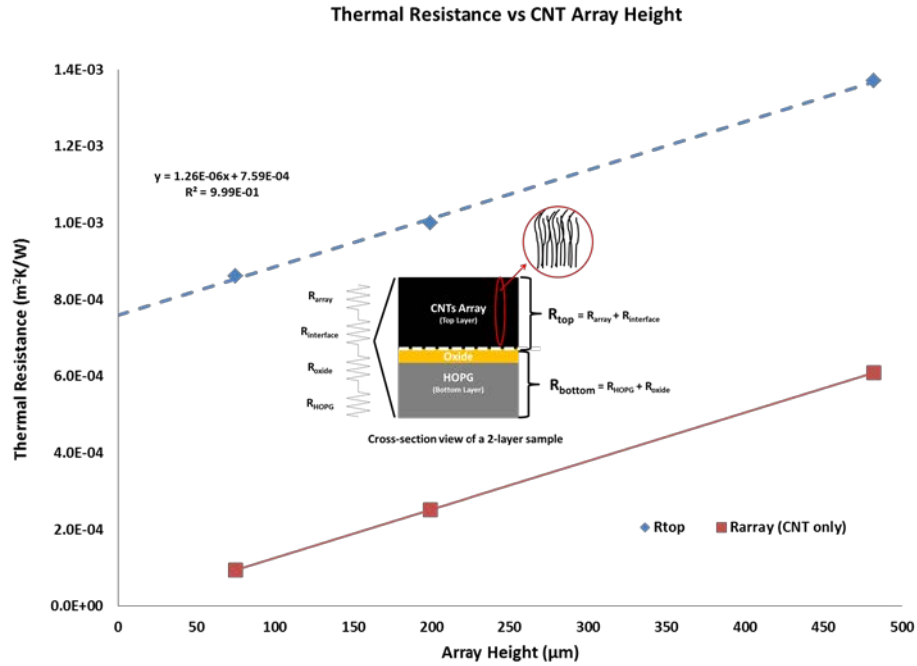
Figure 67: Thermal Resistance of Samples with Different CNT Height

7.4.7 CNT Thermal Conductivity Analysis:

Using the array thermal conductivity calculated above, it is also possible to calculate the thermal conductivity value of a single CNT (κ_{CNT}). To accomplish this, an equation was formulated using simplified assumptions about the CNT array. It was assumed that all individual CNTs in the array are solid cylinders and they are all uniform in material composition (morphology, tube diameter, and height). In addition, the CNTs are in parallel with each other and occupy a certain volume fraction, 8.5% in this case. Furthermore, the thermal conductivity value of each CNT in the array is equal to each other and is constant along the length of CNT, Figure 68. If the number of CNTs per area and the diameter of the CNT are known, then the thermal conductivity value of a CNT, κ_{CNT}, can be calculated using Equation 7.

$$\kappa_{cnt} = \frac{\dfrac{L}{R_{array}} - \left(\kappa_{air} * \left(1 - \left(N * \dfrac{\pi}{4} * d^2\right)\right)\right)}{N * \dfrac{\pi}{4} * d^2}$$

Equation 7 Thermal Conductivity of Parametric Comparisons

where d is the average diameter of the CNTs and N is the number of CNTs per area.
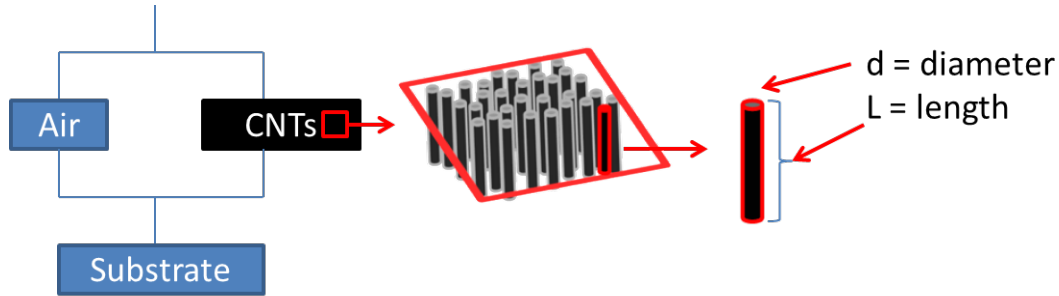
Figure 68: Modeling CNT Array in Parallel with Air and Image of Ssimplified CNT

Using the SEM images, the average CNT diameter was measured to be 19 ± 5 nm, and the growth density was measured to be 7.7 ± 0.6 x 10^{13} CNTs/m^2. Using equation 4, the thermal conductivity of a CNT, κ_{CNT}, was calculated to be 35.09 W/m-K. Note that this is the average thermal conductivity of the CNT assuming the CNT to be a solid cylinder. In reality, the CNT is a hollow cylinder having inner diameter about 7 nm and outer diameter about 19 nm. While this is not the highest thermal conductivity value reported for carbon nanotubes, it is an excellent value. As discussed in the introduction, the reported thermal conductivity of CNT ranges from 0.145 – 3000 W/m-K depending on the quality of CNT, sample configuration and testing methods.   From the engineering point of view, 35 W/m-K is the experimentally measured conductivity of these nanotube cylinders, which is superior to many commercially available thermal interface material (thermal grease, or epoxy bond etc.) used today [175]. This value shows the possibility of using samples in such configuration (aligned and attached CNTs on HOPG) as new TIM for certain electronic applications.

7.4.8 Thermal Resistance Analytical Model:

Since there is a limitation on controllable CNT growth, in terms of (areal density, alignment, and tube sizes), modeled equation has been developed to help with understanding some of the tunable variables that should be further investigated.

Equation 8 (parameter sensitivity analysis) was created, by rearranging Equation 7, to help to predict the effect of CNT morphology and growth density on thermal resistivity of the array

$$R_{array} = \frac{L}{\left(N * \kappa_{cnt} * \frac{\pi}{4} * d^2\right) + \left(\kappa_{air} * \left(1 - \left(N * \frac{\pi}{4} * d^2\right)\right)\right)}$$

Equation 8 Thermal Resistance of Parametric Comparisons

This model was used to investigate the effect of CNT growth density and CNT diameter on R_{array}. Figure 69, shows that if the number of CNTs per area is increased, R_{array}, would decrease, as expected. However there is a limitation on how much improvement can be achieved, since R_{array} convenes to an asymptote. This suggests that once a critical CNT growth density is reached, any additional increases do not greatly improve the thermal resistance. The result also shows that the effect of CNT length diminishes as the density of CNT increases, suggesting that CNT growth density is the dominant factor affecting the thermal resistance. There will also be a practical limit set by the density at which the individual nanotubes touch each other, and cannot be grown any closer together. In this investigation is believed that a theoretical maximum is achieved when closed pack density of 90% is reached. This simple model underscores that through CNT growth optimization, the thermal resistance of the array can be further reduced.

Using the thermal conductivity value of 35 W/ m-K, the best possible thermal resistance achievable will be about 2 x 10^{-6}, if pristine samples of CNT with 90 % growth coverage were fabricated. This value places samples in such configuration (CNTs growth on HOPG substrate) on par with many commercially available TIM samples.
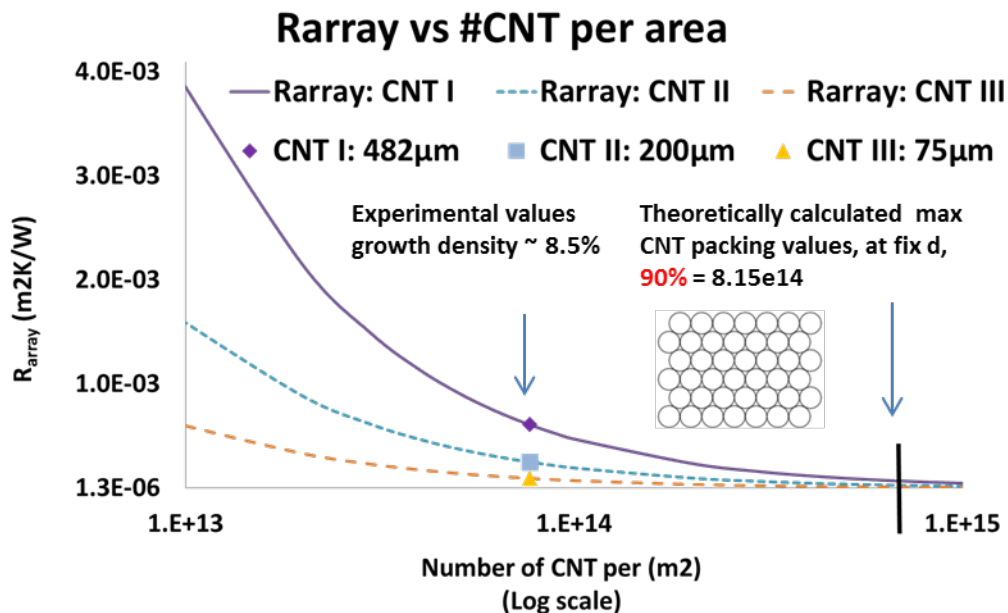
Figure 69: How the Variable (#CNT/area) would Change Thermal Resistance Using the Model Equation
(The experimental values are marked in each of the lines.)

The uniqueness about this study is the sample substrate is made almost entirely out of carbon, which CNT was grown on HOPG. In this configuration, CNT on HOPG, thermal resistance of the interface $R_{interface}$ value was extrapolated, which are often missing when testing sample consisted of CNT bundles or single CNT. In addition, R_{array} = 9.48 x 10^{-5} m^2 K/W is the measure thermal resistance value for the shortest CNT carpet of 75 μm. This value is comparable with commercially available product such as solder, silicon grease, and epoxy, with thermal resistance value that ranges from 0.01 x 10^{-4} - 7 x 10^{-4} m^2 K/W. In addition this value is slightly higher then reported thermal resistance value of 6 x $10^{-6}$by Ganguli et al. However, in that report it was reported that an estimated CNT growth density was 20%. The model used in this study shows that an absolute minimum thermal resistance R_{array} reachable if ideal CNT can be fabricated is a value of 1.3 x 10^{-6} W/mK. Furthermore, this study demonstrates this is one technique that one can use to provide precision control over the thickness of TIM used with uniform coverage, which is often a difficult task to accomplish when using commercial grade thermal grease.

7.5 Conclusion

In this investigation, carpet-like arrays of carbon nanotubes (CNT) were attached to oxide coated HOPG substrates, and direct bonding between CNT and the oxide layer was achieved at the interface. It was shown by high resolution TEM images that the catalyst particles were imbedded in the oxide layer. Using the height of CNT array as the variable, the thermal properties of these all carbon samples were determined. The result shows that R_{array} is linearly related to the CNT array height. It was also calculated that the thermal conductivity value for a CNT was about 35 W/m-K. Furthermore, this investigation provided a simple analytical model

DISTRIBUTION STATEMENT A: Approved for public release. Distribution is unlimited.

to determine the effect of different CNT variables on thermal resistance. The model suggests that if pristine CNT with maximum packing density can be achieved, an optimally low thermal resistance value of about $2x\ 10^{-6}\ m^2$ K/W is obtainable in the array. This value placed the thermal resistance of CNT, in such configuration (CNT on HOPG), on par with current commercially available TIM material, with the added benefit of all carbon system that is strong, durable, compliant and will not suffer from drying out or thermal cycling issues.

Section IV: Future and Conclusions
(Ideas for Future Studies, and Concluding Remarks)

CHAPTER 8: Future Work and Future Applications

The results from the study revealed that there are of study that can use more investigation in order to understand and to address some of the issues that have risen during the research. Such areas are mentioned here.

8.1 Future work:

8.1.1 Optimization of CNT array height with plasma silica oxide thickness:

In Section 7.2.3 shows that oxide thickness has an effect on CNT array length. If optimization investigation were conducted in this area, it is possible to use oxide thickness as a variable to obtain desired CNT carpet thickness.

8.1.2 Address the "lift-off" issue associated with CNT growth using ALD alumina oxide:

"Lift-off" is an undesirable side effect of CNT growth with ALD alumina. This incident suggested that the bonding between the oxide and the substrate is weak. Such weakness is a problem for many applications that requires strong attachment for energy transfer. It is crucial to address problem in order to develop a robust device.

8.1.3 Surface functionalization:

Although the current CNT/graphite configuration has a strong interface attachment between the CNT and the substrate, problem still remains at the interface form between the tip of CNT and the surface that it attaches to. One way to address this issue is to functionalize the tips of CNT to allow better interface attachment. A few initial investigations were done to explore the feasibility of surface functionalization. The two tests done were electroless plating and metallic ALD coating.

8.1.3.1 Electroless plating

The electroless plating method was a wet chemistry method where it requires multiple steps in order for the metal particles to adhere to the surface of CNT. The steps used was developed by Fan et al. [174], which includes the following steps: acetone wash, sensitization, activation, and coating. It wasn't clear how fast the surface of the CNT can be coated with the metallic particles so the experiment. The experiment was stopped every minute in order for images analysis to be taken. The total metal deposition process was 6 minutes. Figure 70 showing the results gather from this experiment.

8.1.3.1.1 Electroless plating
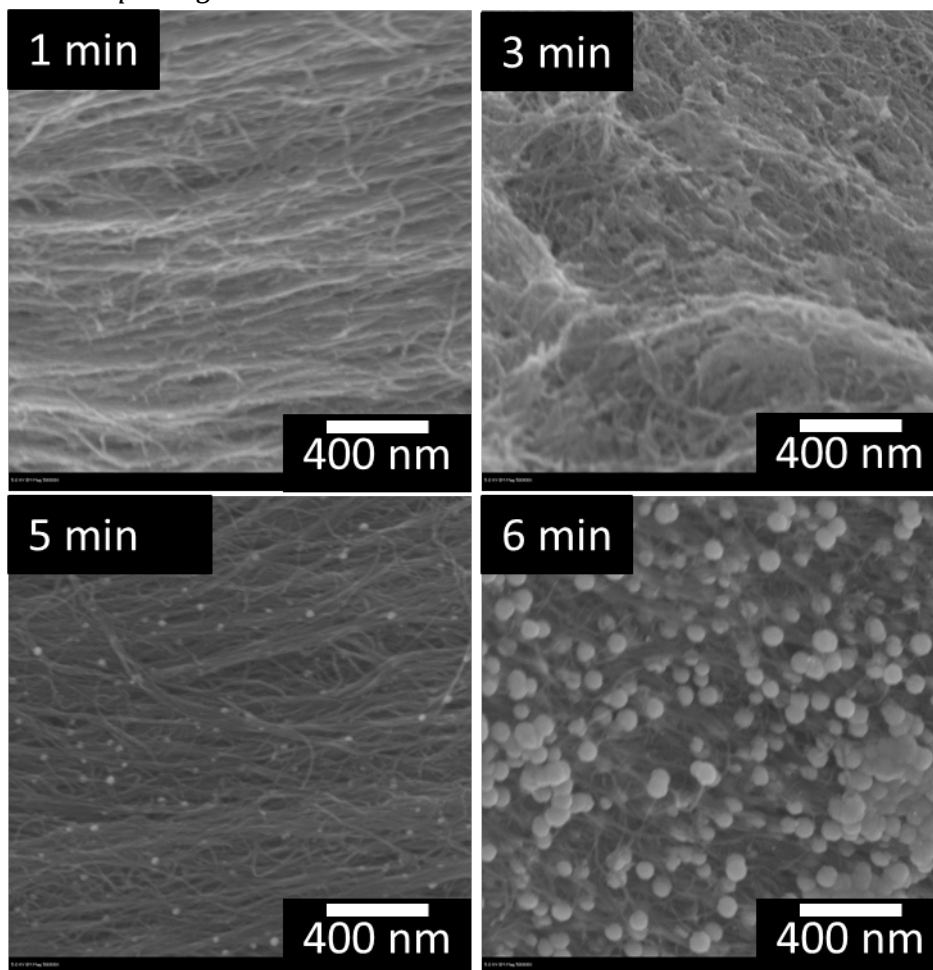
Figure 70: Electroless Nickel Plating at Various Time Intervals
A) 1 min, B) 3 min, C) 5 min, D)6 min.

Figure 70 revealed that the earliest detectable nucleation process starts at around 5 minute. The particle rapidly grows after that. It appears that the metal particles are much larger than CNT at 6 minutes into the coating process. The coating does not coat individual CNT, but rather taking up the void spaces between the tubes.

8.1.3.1.2 ALD Pt:

The ALD metal plating process uses (Trimethyl)methylcyclopentadienylplatinum(IV) and remote O_2 plasma to deposit the platinum thin film. The growth chamber was set at 270 °C with a deposition rate of 0.7 Å/cycle. Figure 71shows the result after ALD pt treatment.
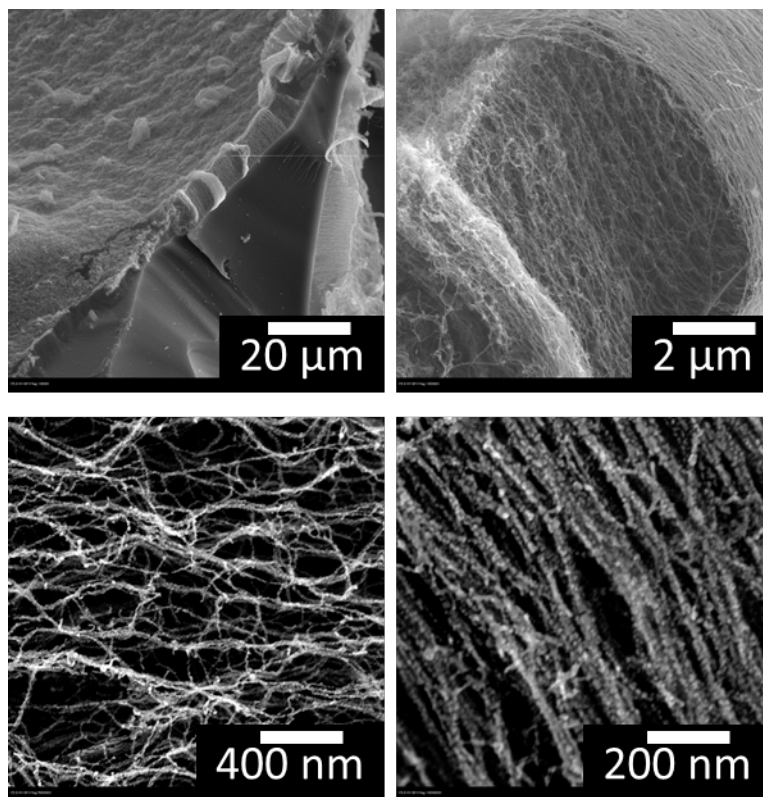
Figure 71: Metal Coating Using ALD Platinum

The result shown in Figure 71 indicated two major noticeable differences between electroless plating and ALD coating method. First the alignment and carpet morphology in the ALD sample is preserved, and second the particle sizes found in ALD are much smaller and actually coats individual CNT.

8.1.4 Super growth:

During the initial investigation, it was observed that certain CNTs would grow up to two orders of magnitude longer than the rest, Figure 72. The samples used were silica coating on silicon wafers. It wasn't clear why this phenomenon was happening, but it suggests that faster growth is achievable. This area should be further investigated if rapid growth is one of the design parameter.
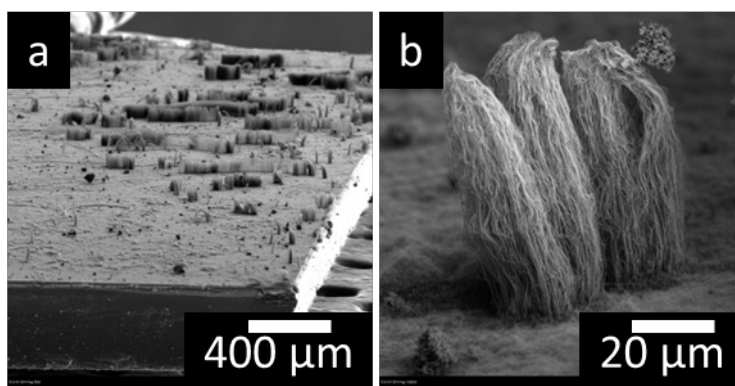
Figure 72: Examples of Super Long Growth on Thermal SiO₂ Samples

Carbon configurations such as the ones developed in this investigation are very versatile and can potentially be used in broader ranges of applications. A few examples of other applications that can benefit from lightweight carbon applications include the following.

8.2 Future applications

8.2.1 Thermal interface material:

An ideal thermal interface is the one that have two sides of material that forms a uniform connection with the opposite side. However these kinds of interface seldom exist. Therefore materials such as thermal interface material (TIM) are used in order to enhance the connection while filling in any voids created by joining of the two sides. Figure 73 is an image showing non-uniform contacts from joining two substrates, where the voids are created.
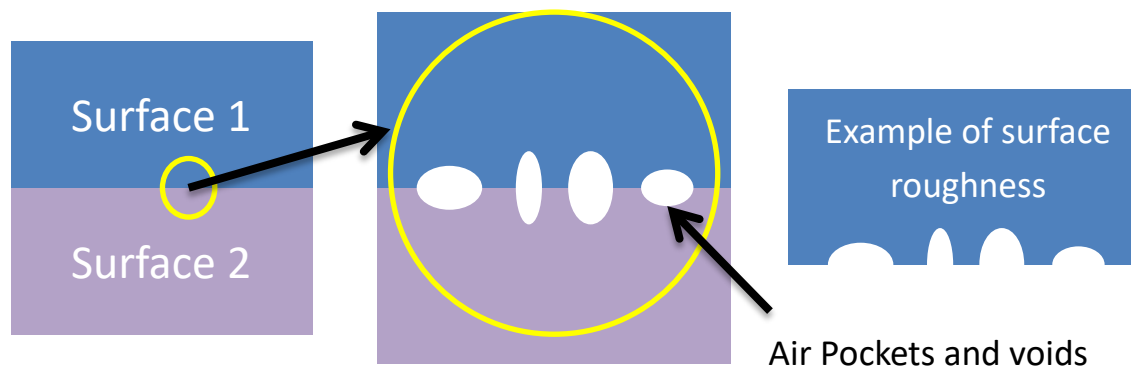
Figure 73: Representation of an Interface

To address the voids there are many commercial products available to help minimize these imperfections while increase thermal conductivities across two surfaces Figure 73. However many commercial products available currently can suffer failure through environment contributions or shelve life. Therefore CNT provides an alternative to some of the commercial products. Figure 74 listed some of the advantages and disadvantages from some of the common TIM materials.

TIM		ADVANTAGES	DISADVANTAGES
Thermal Greases		• High thermal conductivity • Thin joint with low thermal resistance • No curing time • No delamination • Low cost	• Phase separation during thermal cycling • Messy to work with • Dry out over time • Hard to achieve uniform thickness • Possible for excess greases
Filled Polymers		• Not messy • Uniform application thickness • Good dielectric properties • Low modulus • Easily cut to size	• Need curing time • Lower thermal conductivity than greases • Delamination problems • Permanent clamping needed • Higher cost than greases
Phase changing material	Polymeric	• Easier application and handling • No curing time • No dry-out • No delamination	• Surface resistance can be greater than greases • Constant pressure required • Voids can result with thermal cycles
	Low Melting Alloy	• Easy to apply • all metal path • No curing time	• Dry-out and creat voids at the interface • intermetallic growth • Oxidation/Corrosion at elevated temperatures

Figure 74: Common TIM Material and Their Comparisons

8.2.2 Lightweight composites

One of the benefits of exploring CNT growth on carbon substrates is the ability to create a lightweight composite. These composites can provide grate benefits to space and aerospace industries, where weight saving is critical to the success of the mission.

8.2.3 Electrical applications

CNT is known to have excellent thermal, electrical and mechanical properties. In this investigation, only thermal properties were investigated extensively. It is possible that such carbon configuration can be beneficial for electrical applications as well.

CHAPTER 9: Conclusion

This dissertation was focused on investigation and characterization of growth and tailoring of dense aligned carbon nanotube (CNT) carpets on a variety of carbon substrates. The combination of high thermal transport materials is expected to be very beneficial for high power electronic applications. To achieve the goal of creating such material combination and to test its feasibility as high power electronic devices, five detailed investigations were performed and summarized below.

In the first investigation, CNTs forests were grown on synthetic diamond substrates using three different CVD growth methods. The result shows that each method produces CNTs with a distinctly different diameter, morphology, graphitic purity, and interfacial characteristics. Of the different growth methods, FCT-CVD has the advantage of being a one-step CNT growth method that does not need a separate catalyst deposition step, yet produces dense uniform CNTs. This technique is also not limited to line of sight growth. This is beneficial for growing samples having complex geometry. In addition, this technique provided the finest CNT diameter, and intermediate diamond/graphite ratio in the Raman signal. This method does produce some excess metal particles due to continuous catalyst nucleation. However, this issue can be addressed in the future if needed, by stopping the catalytic source after a certain growth time.

Due to the scalability and versatility of FCCVD growth methods, it was selected for the next study: growth of CNT on (sp^2) graphitic carbon. Initial investigation showed that due to the inert surface of sp^2 carbon a low density of dispersed CNT bundles were formed. This result prompted a detailed investigation to identify surface modification techniques that can enhance CNT growth on graphitic carbon. It was found that oxide buffer layer is the key to improve CNT growth density.

Investigation three was designed study the influence of oxide buffer layers on the growth of CNT arrays on graphitic carbon. Two different oxide compositions, alumina and silica, have been compared on flat pyrolytic carbon film, and the results show very different CNT nucleation rates, growth rates, and nanocatalyst particle morphologies. Samples with an Al_2O_3 buffer layer resulted in faster CNT nucleation and elongated residual nanocatalyst particles. In contrast, those with SiO_2 buffer samples showed a slower nucleation rate and more spherical particle morphologies. For samples using SiO_2 as a buffer layer, three different growth techniques have been investigated, which showed that surface roughness of the buffer layer may be an important property to control. Catalyst particle density increased linearly with surface roughness, which proportionately increased the CNT carpet height. This research emphasizes that growing CNTs on carbon substrates requires careful selection of the oxide buffer layer. Depending on the actual application, a carefully engineered buffer layer should be able to provide control over CNT growth density and array characteristics. Among the buffer oxides investigated in this study, the ALD Al_2O_3 buffer layer provides the fastest CNT nucleation and most uniform size distribution, but is plagued by adhesion issues, which may limit future applications. Plasma SiO_2 offers a slower initial nucleation rate, but the tallest carpet height in the same growth time, and appears to be the most stable and scalable.

In investigation four key factors for CNT array height were investigated. Silica oxide thickness and growth time were investigated as a means to increase CNT growth rate and controllability. It was observed that CNT growth was initially increased by an increase of oxide

thickness. However, after a certain thickness, further increase in oxide thickness actually negatively impacted the CNT height. It was also observed that, at a selected barrier oxide thickness, CNT carpet height follows a linear trend with growth time. This study demonstrates that CNT can be fabricated on HOPG substrates, and the CNT array height is controllable with growth time.

Finally, the thermal properties of CNT arrays were evaluated using Laser Flash Analysis. The result shows that thermal resistance of the CNT array, R_{array}, is linearly related to the CNT array height. This, along with structural information, could be used to estimate the thermal conductivity of the multi-walled CNT, and was found to be about 35 W/m-K. Furthermore, this investigation leads to a simple analytical model for determining the effect of different CNT variables on thermal resistance. These studies indicate that carbon-CNT system can be an excellent candidate towards development of advanced thermal interface materials. The limitation would be the interface contact between the tips of the CNT array.

In conclusion, this investigation throws new light on Carbon-CNT hybrid materials and approaches to control sever key factors necessary for their use in power electronic devices.

References

[1]   S. Berber, Y. Kwon, and D. Tomanek, "Unusually high thermal conductivity of carbon nanotubes," *Phys. Rev. Lett.*, vol. 84, no. 20, pp. 4613–6, May 2000.

[2]   J. Hone, "Carbon Nanotubes : Thermal Properties," *Dekker Encyclopedia of Nanoscience and Nanotechnology*. CRC Press, pp. 603–611, 2004.

[3]   D. J. Yang, Q. Zhang, G. Chen, S. F. Yoon, J. Ahn, S. G. Wang, Q. Zhou, Q. Wang, and J. Q. Li, "Thermal conductivity of multiwalled carbon nanotubes," *Phys. Rev. B*, vol. 66, no. 16, p. 165440, 2002.

[4]   T. Tong, Y. Zhao, L. Delzeit, A. Kashani, M. Meyyappan, and A. Majumdar, "Dense Vertically Aligned Multiwalled Carbon Nanotube Arrays as Thermal Interface Materials," *IEEE Trans. Components Packag. Technol.*, vol. 30, no. 1, pp. 92–100, 2007.

[5]   P. R. Bandaru, "Electrical Properties and Applications of Carbon Nanotube Structures," *J. Nanosci. Nanotechnol.*, vol. 7, no. 3, pp. 1–29, 2007.

[6]   B. I. Yakobson and P. Avouris, "Mechanical Properties of Carbon Nanotubes," *Top. Appl. Phys.*, vol. 80, pp. 287–327, 2001.

[7]   J. Wang, "Carbon-Nanotube Based Electrochemical Biosensors : A Review," *Eectroanalysis*, vol. 17, no. 1, pp. 7–14, 2005.

[8]   A. K. Karumuri, "Hierarchical Porous Structures Functionalized with Silver Nanoparticles : adaptation for antibacterial applications," Wright State University, 2014.

[9]   E. I. Maurer, "Surface Modification of Carbon Structures For biological Applications," Wright State University, 2010.

[10]   A. Maleszewski, "The Functionalization and Characterization of Adherent Carbon Nanotubes with Silver Nanoparticles for Biological Applications," Wright State University, 2014.

[11]   T. A. Elwi, H. M. Al-Rizzo, D. G. Rucker, E. Dervishi, Z. Li, and A. S. Biris, "Multi-walled carbon nanotube-based RF antennas.," *Nanotechnology*, vol. 21, no. 4, pp. 1–10, Jan. 2010.

[12]   A. K. Karumuri, D. P. Oswal, H. a. Hostetler, and S. M. Mukhopadhyay, "Silver Nanoparticles Attached to Porous Carbon Substrates: Robust Materials for Chemical-Free Water Disinfection," *Mater. Lett.*, vol. 109, pp. 83–87, Oct. 2013.

[13]   H. Vijwani, "Hierarchical Porous Structures with Aligned Carbon Nanotubes as Efficient Adsorbents and Metal-Catalyst Supports," Wright State University, 2015.

[14]   L. Ci, J. Suhr, V. Pushparaj, X. Zhang, and P. M. Ajayan, "Continuous Carbon Nanotube Reinforced Composites," *Nano Lett.*, vol. 8, no. 9, 2008.

[15]   E. Bekyarova, E. T. Thostenson, A. Yu, H. Kim, J. Gao, J. Tang, H. T. Hahn, T. Chou, M. E. Itkis, and R. C. Haddon, "Multiscale Carbon Nanotube - Carbon Fiber Reinforcement for Advanced Epoxy Composites," no. 4, pp. 3970–3974, 2007.

[16]   K. L. Kepple, G. P. Sanborn, P. a. Lacasse, K. M. Gruenberg, and W. J. Ready, "Improved fracture toughness of carbon fiber composite functionalized with multi walled carbon nanotubes," *Carbon*, vol. 46, no. 15, pp. 2026–2033, 2008.

[17]   K. H. Hung, W. S. Kuo, T. H. Ko, S. S. Tzeng, and C. F. Yan, "Processing and tensile characterization of composites composed of carbon nanotube-grown carbon fibers," *Compos. Part A Appl. Sci. Manuf.*, vol. 40, no. 8, pp. 1299–1304, 2009.

[18]   F. An, C. Lu, Y. Li, J. Guo, X. Lu, H. Lu, S. He, and Y. Yang, "Preparation and characterization of carbon nanotube-hybridized carbon fiber to reinforce epoxy composite," *Mater. Des.*, vol. 33, no. 2012, pp. 197–202, 2012.

[19]   H. Vijwani, "Highly Active Porous Catalysts Fabricated By Attachment of Palladium Nanoparticles on Hierarchical Carbon Structures," Wright State University, 2011.

[20]   S. Ganguli, A. K. Roy, R. Wheeler, V. Varshney, F. Du, and L. Dai, "Superior thermal interface via vertically aligned carbon nanotubes grown on graphite foils," *J. Mater. Res.*, vol. 28, no. 07, pp. 933–939, Dec. 2012.

[21]   M. J. Biercuk, M. C. Llaguno, M. Radosavljevic, J. K. Hyun, A. T. Johnson, and J. E. Fischer, "Carbon nanotube composites for thermal management," *Appl. Phys. Lett.*, vol. 80, no. 15, pp. 2767–2769, 2002.

[22]   A. J. McNamara, Y. Joshi, and Z. M. Zhang, "Characterization of nanostructured thermal interface materials – A review," *Int. J. Therm. Sci.*, vol. 62, no. 2012, pp. 2–11, 2012.

[23]   M. Hu, P. Keblinski, J.-S. Wang, and N. Raravikar, "Interfacial thermal conductance between silicon and a vertical carbon nanotube," *J. Appl. Phys.*, vol. 104, no. 8, p. 083503, 2008.

[24]   R. V. Pulikollu, "Nano-Coatings on Carbon Structures for Interfacial Modification," *Phd dissertation*, 2005.

[25]   I. T. Barney, "Hierarchical Carbon Nanostructures," Wright State University, 2012.

[26]   D. Takagi, Y. Kobayashi, and Y. Homma, "Carbon nanotube growth from diamond.," *J. Am. Chem. Soc.*, vol. 131, no. 20, pp. 6922–3, May 2009.

[27]   L. T. Sun, J. L. Gong, Z. Y. Zhu, D. Z. Zhu, S. X. He, Z. X. Wang, Y. Chen, and G. Hu, "Nanocrystalline diamond from carbon nanotubes," *Appl. Phys. Lett.*, vol. 84, no. 15, pp. 2901–2903, 2004.

[28]   Q. Yang, S. Yang, C. Xiao, and A. Hirose, "Transformation of carbon nanotubes to diamond in microwave hydrogen plasma," *Mater. Lett.*, vol. 61, pp. 2208–2211, May 2007.

[29]   G. a. Slack and S. F. Bartram, "Thermal expansion of some diamondlike crystals," *J. Appl. Phys.*, vol. 46, no. 1975, pp. 89–98, 1975.

[30]   P. Hidnert and W. T. Sweeney, "Thermal Expansion of Graphite," *Technol. Pap. Bur. Stand.*, vol. 21, 1927.

[31]   J. R. Davis, *Metals Handbook Desk Edition*, vol. 2. 1998.

[32]   M. Endo, S. Iijima, and M. S. Dresselhaus, *Carbon Nanotubes*, 1st ed. Pergamon, 1996.

[33]   M. Terrones, "S CIENCE AND T ECHNOLOGY OF THE T WENTY -F IRST C ENTURY : Synthesis, Properties, and Applications of Carbon Nanotubes," *Annu. Rev. Mater. Res.*, vol. 33, no. 1, pp. 419–501, Aug. 2003.

[34]   T. Ebbesen, *Carbon nanotubes, preparation and properties*. CRC Press, 1996.

[35]   S. Iijima, "© 1991 Nature Publishing Group," *Nature*, vol. 354, pp. 56–58, 1991.

[36]   A. Oberlin, M. Endo, and T. Koyama, "Filamentous Growth of Carbon through Benzene Decomposition," *J. Cryst. Growth*, vol. 32, pp. 335–349, 1976.

[37]   J. Mintmire, B. Dunlap, and C. White, "Are fullerene tubules metallic?," *Phys. Rev. Lett.*, vol. 68, no. 5, pp. 631–634, Feb. 1992.

[38]   C. Dekker, "Carbon Nanotubes As Molecular Quantum Wires," *Phys. Today*, vol. 52, no. 5, p. 22, 1999.

[39]   H. Zhang, E. Liang, P. Ding, and M. Chao, "Layered growth of aligned carbon nanotube arrays by pyrolysis," *Phys. B-CONDENSED MATTER*, no. 337, 2003.

[40]   W. Z. Li, J. G. Wen, and Z. F. Ren, "Effect of temperature on growth and structure of carbon nanotubes by chemical vapor deposition," *Appl. Phys. A*, vol. 402, pp. 397–402, 2002.

[41]   W. Z. Li, J. G. Wen, Y. Tu, and Z. F. Ren, "Effect of gas pressure on the growth and structure of carbon nanotubes by chemical vapor deposition," *Appl. Phys. A*, vol. 264, pp. 259–264, 2001.

[42]   C. Gommes, S. Blacher, C. Bossuot, P. Marchot, J. B.Nagy, and J.-P. Pirard, "Influence of the operating conditions on the production rate of multi-walled carbon nanotubes in a CVD reactor," *Carbon*, vol. 42, no. 8–9, pp. 1473–1482, Jan. 2004.

[43]   A. C. Dillon, K. E. H. Gilbert, P. A. Parilla, J. L. Alleman, G. L. Hornyak, K. M. Jones, and M. J. Heben, "HYDROGEN STORAGE IN CARBON SINGLE-WALL NANOTUBES," *US DOE Hydrog. Progr. Rev.*, pp. 1–18, 2002.

[44]   J. Bonard, H. Kind, T. Stockli, and L. Nilsson, "Field emission from carbon nanotubes : the first five years," *Solid. State. Electron.*, vol. 45, 2001.

[45]   R. Signorelli and J. G. Kassakian, "Electrochemical Double-Layer Capacitors Using Carbon Nanotube Electrode Structures," *Proc. IEEE*, vol. 97, no. 11, 2009.

[46]   L. SangWook, E. Anders, S. AbdelrahimA., and C. EleanorE., "Carbon-nanotube-based Nano Electromechanical Switches," *J. Korean Phys. Soc.*, vol. 55, no. 31, p. 957, Sep. 2009.

[47]   G. U. Sumanasekera, B. K. Pradhan, C. K. W. Adu, R. E. Romero, and P. C. Eklund, "CARBON NANOTUBES AS A CHEMICAL SENSOR," *Prepr pap Am Chem Soc Div Fuel Chem*, vol. 49, pp. 885–886, 2004.

[48]   M. S. Saito, R., Fujita, M., Dresselhaus, G., Dresselhaus, "Electronic structure of chiral graphene tubules," *Appl. Phys. Lett.*, vol. 60, no. 18, pp. 2204–2206, 1992.

[49]   Z. Kordrostami, M. H. Sheikhi, and R. Mohammadzadegan, "Modeling Electronic Properties of Multiwall Carbon Nanotubes," *Fullerenes, Nanotub. Carbon Nanostructures*, vol. 16, no. 1, pp. 66–77, Jan. 2008.

[50]   M. Terrones, W. Hsu, H. Kroto, and D. Walton, *Nanotubes: A rrevolution in materials science and electronics*. springer-verlag berlin, 1999.

[51]   P. Kim, L. Shi, a. Majumdar, and P. L. McEuen, "Thermal Transport Measurements of Individual Multiwalled Nanotubes," *Phys. Rev. Lett.*, vol. 87, no. 21, p. 215502, Oct. 2001.

[52]   M. M. J. Treacy, T. W. Ebbesen, and J. M. Gibson, "Exceptionally high young's modulus observed for individual carbon nanotubes," *NatureNature*, no. 381, p. 678, 1996.

[53]   M. R. Falvo, G. Clary, A. Helser, S. Paulson, R. M. T. Ii, V. Chi, F. P. Brooks, S. Washburn, and R. Superfine, "Nanomanipulation Experiments Exploring Frictional and Mechanical Properties of Carbon Nanotubes," *Microsc. Microanal.*, no. 4, pp. 504–512, 1999.

[54]   H. Schneider, J. S. J. Achard, L. Inpt, and T. Cedex, "The diamond for power electronic devices," *Power Electron. Appl.*, vol. 3, no. 1, pp. 1–9, 2005.

[55]   C. Varanasi, J. Petry, L. Brunke, B. T. Yang, W. Lanter, J. Burke, H. Wang, J. S. Bulmer, J. Scofield, and P. N. Barnes, "Growth of high-quality carbon nanotubes on free-standing diamond substrates," *Carbon*, vol. 48, no. 9, pp. 2442–2446, Aug. 2010.

[56]   V. Varshney, S. S. Patnaik, A. K. Roy, G. Froudakis, and B. L. Farmer, "Modeling of Thermal Transport in Pillared-Graphene Architectures," *ACS Nano*, vol. 4, no. 2, pp. 1153–1161, 2010.

[57]   C. Du and N. Pan, "CVD growth of carbon nanotubes directly on nickel substrate," *Mater. Lett.*, vol. 59, no. 13, pp. 1678–1682, Jun. 2005.

[58]   D. Mata, M. Ferro, a. J. S. Fernandes, M. Amaral, F. J. Oliveira, P. M. F. J. Costa, and R. F. Silva, "Wet-etched Ni foils as active catalysts towards carbon nanofiber growth," *Carbon*, vol. 48, no. 10, pp. 2839–2854, Aug. 2010.

[59]   N. K. Reddy, J.-L. Meunier, and S. Coulombe, "Growth of carbon nanotubes directly on a nickel surface by thermal CVD," *Mater. Lett.*, vol. 60, no. 29–30, pp. 3761–3765, Dec. 2006.

[60]   C. E. Baddour, F. Fadlallah, D. Nasuhoglu, R. Mitra, L. Vandsburger, and J.-L. Meunier, "A simple thermal CVD method for carbon nanotube synthesis on stainless steel 304 without the addition of an external catalyst," *Carbon*, vol. 47, no. 1, pp. 313–318, Jan. 2009.

[61]   C. Masarapu and B. Wei, "Direct growth of aligned multiwalled carbon nanotubes on treated stainless steel substrates.," *Langmuir*, vol. 23, no. 17, pp. 9046–9, Aug. 2007.

[62]   S. Pacheco Benito and L. Lefferts, "The production of a homogeneous and well-attached layer of carbon nanofibers on metal foils," *Carbon*, vol. 48, no. 10, pp. 2862–2872, Aug. 2010.

[63]   S. Talapatra, S. Kar, S. K. Pal, R. Vajtai, L. Ci, P. Victor, M. M. Shaijumon, S. Kaur, O. Nalamasu, and P. M. Ajayan, "Direct growth of aligned carbon nanotubes on bulk metals.," *Nat. Nanotechnol.*, vol. 1, no. 2, pp. 112–6, Nov. 2006.

[64]   T. Hiraoka, T. Yamada, K. Hata, D. N. Futaba, H. Kurachi, S. Uemura, M. Yumura, and S. Iijima, "Synthesis of single- and double-walled carbon nanotube forests on conducting metal foils.," *J. Am. Chem. Soc.*, vol. 128, no. 41, pp. 13338–9, Oct. 2006.

[65]   L. Martínez-Latorre, P. Ruiz-Cebollada, A. Monzón, and E. García-Bordejé, "Preparation of stainless steel microreactors coated with carbon nanofiber layer: Impact of hydrocarbon and temperature," *Catal. Today*, vol. 147, pp. S87–S93, Sep. 2009.

[66]   X. Lepró, M. D. Lima, and R. H. Baughman, "Spinnable carbon nanotube forests grown on thin, flexible metallic substrates," *Carbon*, vol. 48, no. 12, pp. 3621–3627, Oct. 2010.

[67]   J. M. Simmons, B. M. Nichols, M. S. Marcus, O. M. Castellini, R. J. Hamers, and M. A. Eriksson, "Critical Oxide Thickness for Efficient Single-Walled Carbon Nanotube Growth on Silicon Using Thin SiO2 Diffusion Barriers," *Small*, vol. 2, no. 7, pp. 902–909, 2006.

[68]   J. García-Céspedes, S. Thomasson, K. B. K. Teo, I. a. Kinloch, W. I. Milne, E. Pascual, and E. Bertran, "Efficient diffusion barrier layers for the catalytic growth of carbon nanotubes on copper substrates," *Carbon.*, vol. 47, no. 3, pp. 613–621, Mar. 2009.

[69]   A. Cao, P. M. Ajayan, G. Ramanath, R. Baskaran, and K. Turner, "Silicon oxide thickness-dependent growth of carbon nanotubes," *Appl. Phys. Lett.*, vol. 84, no. 1, pp. 109–111, 2004.

[70]   C. J. H. Wort and R. S. Balmer, "Diamond as an electronic material," *Mater. Today*, vol. 11, no. 1–2, pp. 22–28, 2008.

[71]   A. Inayat, H. Freund, T. Zeiser, and W. Schwieger, "Determining the specific surface area of ceramic foams: The tetrakaidecahedra model revisited," *Chem. Eng. Sci.*, vol. 66, no. 6, pp. 1179–1188, Mar. 2011.

[72]   Nanoprobes, "HOPG." [Online]. Available: http://nanoprobes.aist-nt.com/apps/HOPG info.htm.

[73]   H. Wang, J. Lin, C. H. a. Huan, P. Dong, J. He, S. H. Tang, W. K. Eng, and T. L. J. Thong, "Controlled synthesis of aligned carbon nanotube arrays on catalyst patterned silicon substrates by plasma-enhanced chemical vapor deposition," *Appl. Surf. Sci.*, vol. 181, no. 3–4, pp. 248–254, Sep. 2001.

[74]   Y. Homma, Y. Kobayashi, T. Ogino, D. Takagi, R. Ito, Y. J. Jung, and P. M. Ajayan, "Role of Transition Metal Catalysts in Single-Walled Carbon Nanotube Growth in Chemical Vapor Deposition," *J. Phys. Chem. B*, vol. 107, pp. 12161–12164, Nov. 2003.

[75]   H. W. Zhu, C. L. Xu, D. H. Wu, B. Q. Wei, R. Vajtai, and P. M. Ajayan, "Direct synthesis of long single-walled carbon nanotube strands.," *Science*, vol. 296, no. 5569, pp. 884–6, May 2002.

[76]   B. Q. Wei, R. Vajtai, Y. Jung, J. Ward, R. Zhang, G. Ramanath, and P. M. Ajayan, "Assembly of Highly Organized Carbon Nanotube Architectures by Chemical Vapor Deposition," *Chem. Mater.*, vol. 15, no. 20, pp. 1598–1606, 2003.

[77] P. Jadaun, S. K. Banerjee, L. F. Register, and B. Sahu, "Density functional theory based study of graphene and dielectric oxide interfaces.," *J. Phys. Condens. Matter*, vol. 23, no. 50, p. 505503, Dec. 2011.

[78] S. M. Mukhopadhyay, R. V. Pulikollu, and a. K. Roy, "Surface modification of a microcellular porous solid: carbon foam," *Appl. Surf. Sci.*, vol. 225, no. 1–4, pp. 223–228, Mar. 2004.

[79] R. V Pulikollu and S. M. Mukhopadhyay, "Nanoscale coatings for control of interfacial bonds and nanotube growth," *Appl. Surf. Sci.*, vol. 253, pp. 7342–7352, 2007.

[80] S. Mukhopadhyay, P. Joshi, and R. Pulikollu, "Thin Films for Coating Nanomaterials," *Tsinghua Sci. Technol.*, vol. 10, no. 6, pp. 709–717, Dec. 2005.

[81] M. Kumar and Y. Ando, "Chemical Vapor Deposition of Carbon Nanotubes: A Review on Growth Mechanism and Mass Production," *J. Nanosci. Nanotechnol.*, vol. 10, pp. 3739–3758, Jun. 2010.

[82] Y. Li, W. Kim, Y. Zhang, M. Rolandi, D. Wang, and H. Dai, "Growth of Single-Walled Carbon Nanotubes from Discrete Catalytic Nanoparticles of Various Sizes," *J. Phys. Chem. B*, vol. 105, no. 46, pp. 11424–11431, Nov. 2001.

[83] J. Sehested, P. L. Hansen, S. Helveg, C. Lo, B. S. Clausen, J. R. Rostrup-nielsen, and F. Abild-pedersen, "Atomic-scale imaging of carbon nanofibre growth," *Lett. to Nat.*, vol. 427, pp. 427–429, 2004.

[84] R. T. K. Baker, M. A. Barber, P. S. Harris, F. S. Feates, and R. J. Waite, "Nucleation and Growth of Carbon Deposits from the Nickel Catalyzed Decomposition of Acetylene," *J. Catal.*, vol. 26, pp. 51–62, 1972.

[85] M. Wilson, K. Kannangara, G. Smith, M. Simmons, and B. Raguse, *Nanotechnology basic science and emerging technologies*. Chapman and Hall, CRC, 2002.

[86] A. Szabó, C. Perri, A. Csató, G. Giordano, D. Vuono, and J. B. Nagy, "Synthesis methods of carbon nanotubes and related materials," *Materials (Basel).*, vol. 3, no. 5, pp. 3092–3140, 2010.

[87] I. Cheap Tubes, "Carbon Nanotubes, Production Methods for Carbon Nanotubes Including Arc Discharge, Laser, Chemical Vapor Depsition and Ball Milling by Cheap Tubes Inc." [Online]. Available: http://www.azonano.com/article.aspx?ArticleID=1561.

[88] R. L. Vander Wal, G. M. Berger, and T. M. Ticich, "Carbon nanotube synthesis in a flame using laser ablation for in situ catalyst generation," *Appl. Phys. A Mater. Sci. Process.*, vol. 77, no. 7, pp. 885–889, Dec. 2003.

[89] M. Kumar, "Chapter 8: Carbon Nanotube Synthesis and Growth Mechanism," in *Carbon Nanotubes - Synthesis, characterizationo, application*, S. Yellampalli, Ed. In Tech, 2011, p. 148.

[90] B. L. Crossley, N. E. Glauvitz, B. T. Quinton, R. A. Coutu, and P. J. Collins, "Characterizing Multi-Walled Carbon Nanotube Synthesis for Field Emission Applications," in *InTech*, 2011, pp. 105–126.

[91] Y. M. Wong, W. P. Kang, J. L. Davidson, B. K. Choi, W. Hofmeister, and J. H. Huang, "Field emission triode amplifier utilizing aligned carbon nanotubes," *Diam. Relat. Mater.*, vol. 14, no. 11–12, pp. 2069–2073, Nov. 2005.

[92] I. T. Barney, "Fabrication and Testing of Hierarchical Carbon Nanostructures for Multifunctional Applications," Wright State University, 2012.

[93] M. H. Rümmeli, F. Schäffel, M. Löffler, C. Kramberger, D. Adebimpe, T. Gemming, P. Ayala, B. Rellinghaus, L. Schultz, B. Büchner, and T. Pichler, "Unifying catalyst size dependencies in floating catalyst and supported catalyst carbon nanotube synthesis," *Phys. Status Solidi*, vol. 205, no. 6, pp. 1386–1390, Jun. 2008.

[94] R. T. K. Baker, "CATALYTIC GROWTH of Carbon Filaments," *Carbon*, vol. 27, no. 3, pp. 315–323, 1989.

[95] a. Gohier, C. P. Ewels, T. M. Minea, and M. a. Djouadi, "Carbon nanotube growth mechanism switches from tip- to base-growth with decreasing catalyst particle size," *Carbon*, vol. 46, no. 10, pp. 1331–1338, Aug. 2008.

[96] S. B. Sinnott and R. Andrews, "Model of carbon nanotube growth through chemical vapor deposition," *Chem. Phys. Lett.*, vol. 315, pp. 25–30, 1999.

[97] Y. Wang, Z. Luo, B. Li, P. S. Ho, Z. Yao, L. Shi, E. N. Bryan, and R. J. Nemanich, "Comparison study of catalyst nanoparticle formation and carbon nanotube growth: Support effect," *J. Appl. Phys.*, vol. 101, no. 12, p. 124310, 2007.

[98] C. T. Wirth, S. Hofmann, and J. Robertson, "State of the catalyst during carbon nanotube growth," *Diam. Relat. Mater.*, vol. 18, pp. 940–945, May 2009.

[99] J. H. Lin, C. S. Chen, M. H. Rümmeli, A. Bachmatiuk, Z. Y. Zeng, H. L. Ma, B. Büchner, H. W. Chen, and H. R. Mark, "Growth of Carbon Nanotubes Catalyzed by Defect-Rich Graphite Surfaces," *Chem. Mater.*, vol. 23, no. 7, pp. 1637–1639, Apr. 2011.

[100] S. M. Mukhopadhyay, R. V. Pulikollu, E. Ripberger, and A. K. Roy, "Surface modification of graphitic foam," *J. Appl. Phys.*, vol. 93, no. 2, pp. 878–882, 2003.

[101] H. Wang, Q. Cai, C.-L. Chen, D. Wang, and Z. Ren, "Growth of aligned carbon nanotubes on ALD-Al2O3 coated silicon and quartz substrates," *J. Exp. Nanosci.*, vol. 6, no. 5, pp. 464–472, Oct. 2011.

[102] B. Fultz and J. Howe, *Transmission Electron Microscopy and Diffractometry of Materials*, 3rd ed. Springer-

verlag berlin, 2007.

[103] B. T. Quinton, P. N. Barnes, C. V. Varanasi, J. Burke, B.-H. Tsao, K. J. Yost, and S. M. Mukhopadhyay, "A Comparative Study of Three Different Chemical Vapor Deposition Techniques of Carbon Nanotube Growth on Diamond Films," *J. Nanomater.*, vol. 2013, pp. 1–9, 2013.

[104] W. J. Parker, R. J. Jenkins, C. P. Butler, and G. L. Abbott, "Flash method of determining thermal diffusivity, heat capacity, and thermal conductivity," *J. Appl. Phys.*, vol. 32, no. 9, pp. 1679–1684, 1961.

[105] L. Delzeit, C. V. Nguyen, B. Chen, R. Stevens, A. Cassell, J. Han, and M. Meyyappan, "Multiwalled Carbon Nanotubes by Chemical Vapor Deposition Using Multilayered Metal Catalysts," *J. Phys. Chem. B*, vol. 106, no. 22, pp. 5629–5635, Jun. 2002.

[106] J. Robertson, S. Hofmann, M. Cantoro, A. Parvez, C. Ducati, G. Zhong, R. Sharma, and C. Mattevi, "Controlling the Catalyst During Carbon Nanotube Growth," *J. Nanosci. Nanotechnol.*, vol. 8, no. 4, pp. 1762–1774, 2008.

[107] M. Cantoro, S. Hofmann, S. Pisana, V. Scardaci, A. Parvez, C. Ducati, A. C. Ferrari, A. M. Blackburn, K. Wang, J. Robertson, E. Engineering, V. Di, V. Uni, and C. Cb, "Catalytic Chemical Vapor Deposition of Single-Wall Carbon Nanotubes at Low Temperatures," 2006.

[108] W. H. Chiang and R. M. Sankaran, "In-flight dimensional tuning of metal nanoparticles by microplasma synthesis for selective production of diameter-controlled carbon nanotubes," *J. Phys. Chem. C*, vol. 112, no. 46, pp. 17920–17925, 2008.

[109] K. Bartsch and a Leonhardt, "An approach to the structural diversity of aligned grown multi-walled carbon nanotubes on catalyst layers," *Carbon*, vol. 42, no. 8–9, pp. 1731–1736, Jan. 2004.

[110] Y. C. Choi, Y. M. Shin, Y. H. Lee, B. S. Lee, G.-S. Park, W. B. Choi, N. S. Lee, and J. M. Kim, "Controlling the diameter, growth rate, and density of vertically aligned carbon nanotubes synthesized by microwave plasma-enhanced chemical vapor deposition," *Appl. Phys. Lett.*, vol. 76, no. 17, p. 2367, 2000.

[111] Y. Zhang, Q. Yu, X. Wang, and Y. Tian, "A new understanding of carbon nanotube growth: Activation and deactivation of a catalyst," *Appl. Surf. Sci.*, vol. 298, no. 2014, pp. 221–224, 2014.

[112] P. B. Amama, C. L. Pint, F. Mirri, M. Pasquali, R. H. Hauge, and B. Maruyama, "Catalyst–support interactions and their influence in water-assisted carbon nanotube carpet growth," *Carbon.*, vol. 50, no. 7, pp. 2396–2406, Jun. 2012.

[113] J. L. Lauer, *Handbook of Raman Spectroscopy from the Research Laboratory to the Process Line*, 1st ed. West Yorkshire: Marcel Dekker, Inc, 2001.

[114] M. J. Behr, E. A. Gaulding, K. A. Mkhoyan, and E. S. Aydil, "Hydrogen etching and cutting of multiwall carbon nanotubes," *J. Vac. Sci. Technol. B Microelectron. Nanom. Struct.*, vol. 28, no. 6, pp. 1187–1194, 2010.

[115] M. Lin, J. P. Y. Tan, C. Boothroyd, K. P. Loh, E. S. Tok, and Y. L. Foo, "Dynamical observation of bamboo-like carbon nanotube growth," *Nano Lett.*, vol. 7, no. 8, pp. 2234–2238, 2007.

[116] S. H. Lim, Z. Luo, Z. Shen, and J. Lin, "Plasma-assisted synthesis of carbon nanotubes," *Nanoscale Res. Lett.*, vol. 5, no. 9, pp. 1377–1386, 2010.

[117] L. Lindsay, D. A. Broido, and N. Mingo, "Diameter dependence of carbon nanotube thermal conductivity and extension to the graphene limit," *Phys. Rev. B - Condens. Matter Mater. Phys.*, vol. 82, no. 16, pp. 4–7, 2010.

[118] M. S. Dresselhaus, G. Dresselhaus, R. Saito, and A. Jorio, "Raman spectroscopy of carbon nanotubes," *Phys. Rep.*, vol. 409, no. 2, pp. 47–99, Mar. 2005.

[119] M. S. Dresselhaus, a Jorio, a G. Souza Filho, and R. Saito, "Defect characterization in graphene and carbon nanotubes using Raman spectroscopy.," *Philos. Trans. A. Math. Phys. Eng. Sci.*, vol. 368, no. 1932, pp. 5355–77, Dec. 2010.

[120] L. C. O'brien, R. L. Kubicek, and J. J. O'brien, "Laser Raman Spectroscopy of Diamond," *Highlights*, vol. 71, no. 9, pp. 759–760, 1994.

[121] G. Zhang, P. Qi, X. Wang, Y. Lu, D. Mann, X. Li, and H. Dai, "Hydrogenation and hydrocarbonation and etching of single-walled carbon nanotubes.," *J. Am. Chem. Soc.*, vol. 128, no. 18, pp. 6026–7, May 2006.

[122] M. B. Jakubinek, M. A. White, G. Li, C. Jayasinghe, W. Cho, M. J. Schulz, and V. Shanov, "Thermal and electrical conductivity of tall, vertically aligned carbon nanotube arrays," *Carbon*, vol. 48, no. 13, pp. 3947–3952, 2010.

[123] A. A. Mikhalchan, V. A. Lysenko, N. S. Muradova, D. A. Zhiteneva, E. V. Saklakova, and A. A. Lysenko, "Carbon nanotubules: morphology and properties," *Fibre Chem.*, vol. 42, no. 5, pp. 287–292, 2011.

[124] H. Fan, K. Zhang, and M. M. F. Yuen, "Effect of defects on thermal performance of carbon nanotube investigated by molecular dynamics simulation," *IEEE Electron. Mater. Packag.*, 2006.

[125] A. Gohier, T. M. Minea, M. A. Djouadi, and A. Granier, "Impact of the etching gas on vertically oriented

single wall and few walled carbon nanotubes by plasma enhanced chemical vapor deposition," *J. Appl. Phys.*, vol. 101, no. 5, 2007.

[126] V. Shanov, Y. Yun, and M. J. Schulz, "SYNTHESIS AND CHARACTERIZATION OF CARBON NANOTUBE MATERIALS (REVIEW)," *J. univerisity Chem. tehcnology Metall.*, vol. 41, no. 4, pp. 377–390, 2006.

[127] F. Rao, T. Li, and Y. Wang, "Growth of 'all-carbon' single-walled carbon nanotubes from diamonds and fullerenes," *Carbon*, vol. 47, no. 15, pp. 3580–3584, Dec. 2009.

[128] Q. Yang, Y. Tang, S. L. Yang, Y. S. Li, and a. Hirose, "Simultaneous growth of diamond thin films and carbon nanotubes at temperatures ⩽550°C," *Carbon*, vol. 46, no. 4, pp. 589–595, Apr. 2008.

[129] P. B. Amama, C. L. Pint, S. M. Kim, L. McJilton, K. G. Eyink, E. a Stach, R. H. Hauge, and B. Maruyama, "Influence of alumina type on the evolution and activity of alumina-supported Fe catalysts in single-walled carbon nanotube carpet growth.," *ACS Nano*, vol. 4, no. 2, pp. 895–904, Feb. 2010.

[130] J. H. Lin, C. S. Chen, M. H. Rummeli, A. Bachmatiuk, Z. Y. Zeng, H. L. Ma, B. Buchner, and H. W. Chen, "Growth of Carbon Nanotubes Catalyzed by Defect-Rich Graphite Surfaces," *Chem. Mater.*, vol. 23, pp. 1637–1639, 2011.

[131] T. de los Arcos, M. Gunnar Garnier, P. Oelhafen, D. Mathys, J. Won Seo, C. Domingo, J. Vicente García-Ramos, and S. Sánchez-Cortés, "Strong influence of buffer layer type on carbon nanotube characteristics," *Carbon.*, vol. 42, pp. 187–190, Jan. 2004.

[132]   a Lahmar, N. Hmina, Y. Scudeller, and J. . Bardon, "Correlation between the adhesion and the thermal contact resistance: effects of substrate surface ion bombardment etching," *Thin Solid Films*, vol. 325, no. 1–2, pp. 156–162, Jul. 1998.

[133] C. Schrank, C. Eisenmenger-Sittner, E. Neubauer, H. Bangert, and a Bergauer, "Solid state de-wetting observed for vapor deposited copper films on carbon substrates," *Thin Solid Films*, vol. 459, no. 1–2, pp. 276–281, Jul. 2004.

[134] T. Ohashi, R. Kato, T. Tokune, and H. Kawarada, "Understanding the stability of a sputtered Al buffer layer for single-walled carbon nanotube forest synthesis," *Carbon.*, vol. 57, pp. 401–409, Jun. 2013.

[135] G. D. Nessim, A. J. Hart, J. S. Kim, D. Acquaviva, J. Oh, C. D. Morgan, M. Seita, J. S. Leib, and C. V Thompson, "Tuning of Vertically-Aligned Carbon Nanotube Diameter and Areal Density through Catalyst Pre-Treatment," *Nano*, vol. 8, no. 11, pp. 3587–3593, 2008.

[136] B. T. Quinton, Q. Zhang, J. Burke, K. Leedy, B. Tsao, J. Scofield, J. N. Merrett, K. Yost, and S. M. Mukhopadhyay, "The Effects of Surface Treatments on the Growth of CNTs on 3-Dimensional Carbon Foam Structures .," *Procedding Nanotechnol. Conf.*, pp. 2–5, 2013.

[137] S. M. Mukhopadhyay, A. Karumuri, and I. T. Barney, "Hierarchical nanostructures by nanotube grafting on porous cellular surfaces," *J. Phys. D. Appl. Phys.*, vol. 42, no. 19, p. 195503, Oct. 2009.

[138] E. I. Maurer, K. K. Comfort, S. M. Hussain, J. J. Schlager, and S. M. Mukhopadhyay, "Novel platform development using an assembly of carbon nanotube, nanogold and immobilized RNA capture element towards rapid, selective sensing of bacteria.," *Sensors*, vol. 12, no. 6, pp. 8135–44, Jan. 2012.

[139] H. Vijwani and S. M. Mukhopadhyay, "Applied Surface Science Palladium nanoparticles on hierarchical carbon surfaces : A new architecture for robust nano-catalysts," *Appl. Surf. Sci.*, vol. 263, pp. 712–721, 2012.

[140] Q. Zhang, J. Liu, R. Sager, L. Dai, and J. Baur, "Hierarchical composites of carbon nanotubes on carbon fiber: Influence of growth condition on fiber tensile properties," *Compos. Sci. Technol.*, vol. 69, no. 5, pp. 594–601, Apr. 2009.

[141] Rodriguez-Reino and F. So, "The role of carbon materials in the heterogeneous catalysis," *Carbon.*, vol. 36, no. 3, pp. 159–175, 1998.

[142] Z. Fan, J. Yan, L. Zhi, Q. Zhang, T. Wei, J. Feng, M. Zhang, W. Qian, and F. Wei, "A three-dimensional carbon nanotube/graphene sandwich and its application as electrode in supercapacitors," *Adv. Mater.*, vol. 22, no. 33, pp. 3723–3728, 2010.

[143] L. Gao, A. Peng, Z. Y. Wang, H. Zhang, Z. Shi, Z. Gu, G. Cao, and B. Ding, "Growth of aligned carbon nanotube arrays on metallic substrate and its application to supercapacitors," *Solid State Commun.*, vol. 146, no. 9–10, pp. 380–383, Jun. 2008.

[144] S. Fan, M. Chapline, N. Franklin, T. Tombler, A. Cassell, and H. Dai, "Self-oriented regular arrays of carbon nanotubes and their field emission properties," *Science*, vol. 283, no. 5401, pp. 512–4, Jan. 1999.

[145] B. Liu, D. M. Tang, C. Sun, C. Liu, W. Ren, F. Li, W. J. Yu, L. C. Yin, L. Zhang, C. Jiang, and H. M. Cheng, "Importance of oxygen in the metal-free catalytic growth of single-walled carbon nanotubes from SiOx by a vapor-solid-solid mechanism," *J. Am. Chem. Soc.*, vol. 133, pp. 197–199, 2011.

[146] B. Liu, W. Ren, C. Liu, C.-H. Sun, L. Gao, S. Li, C. Jiang, and H.-M. Cheng, "Growth velocity and direct

length-sorted growth of short single-walled carbon nanotubes by a metal-catalyst-free chemical vapor deposition process.," *ACS Nano*, vol. 3, no. 11, pp. 3421–3430, 2009.

[147] B. Liu, W. Ren, L. Gao, S. Li, S. Pei, C. Liu, C. Jiang, and H. M. Cheng, "Metal-catalyst-free growth of single-walled carbon nanotubes," *J. Am. Chem. Soc.*, vol. 131, pp. 2082–2083, 2009.

[148] Y. Chen and J. Zhang, "Diameter controlled growth of single-walled carbon nanotubes from SiO 2 nanoparticles," *Carbon*, vol. 49, no. 10, pp. 3316–3324, 2011.

[149] A. Stiles, "Catalyst Supports and Supported Catalysts Theoretical and Applied Concepts," *AlChE*, vol. 34, no. 1, pp. 174–175, 1988.

[150] S. M. George, "Atomic layer deposition: an overview.," *Chem. Rev.*, vol. 110, no. 1, pp. 111–31, Jan. 2010.

[151] B. Liu, W. Ren, L. Gao, S. Li, Q. Liu, C. Jiang, and H. Cheng, "Manganese-Catalyzed Surface Growth of Single-Walled Carbon Nanotubes with High Efficiency," *J. Phys. Chem. C*, vol. 112, pp. 19231–19235, 2008.

[152] Y.-Q. Xu and R. H. Hauge, "Growth of Single-Walled Carbon nanotubes on a Nanorough Surface," *J. Phys. Chem. C*, vol. 111, pp. 9142 – 9145, 2007.

[153] M. Xu, D. N. Futaba, M. Yumura, and K. Hata, "Alignment control of carbon nanotube forest from random to nearly perfectly aligned by utilizing the crowding effect," *ACS Nano*, vol. 6, no. 7, pp. 5837–5844, 2012.

[154] Y. Xuan, Y. Q. Wu, T. Shen, M. Qi, M. A. Capano, J. A. Cooper, and P. D. Ye, "Atomic-layer-deposited nanostructures for graphene-based nanoelectronics," *Appl. Phys. Lett.*, vol. 92, no. 1, p. 013101, 2008.

[155] J. Bin In, C. P. Grigoropoulos, A. A. Chernov, and A. No, "Growth Kinetics of Vertically Aligned CNT Arrays in Clean Oxygen-Free Conditions," *ACS Nano*, vol. 5, no. Suppl, p. 9602, 2012.

[156] A. K. Schaper, H. Hou, A. Greiner, and F. Phillipp, "The role of iron carbide in multiwalled carbon nanotube growth," *J. Catal.*, vol. 222, no. 1, pp. 250–254, Feb. 2004.

[157] A. Moisala, A. G. Nasibulin, and E. I. Kauppinen, "The role of metal nanoparticles in the catalytic production of single-walled carbon nanotubes—a review," *J. Phys. Condens. Matter*, vol. 15, no. 42, pp. S3011–S3035, Oct. 2003.

[158] F. Sarvar, D. Whalley, and P. Conway, "Thermal Interface Materials - A Review of the State of the Art," *2006 1st Electron. Syst. Technol. Conf.*, pp. 1292–1302, 2006.

[159] F. P. Incropera and D. P. DeWitt, *Fundamental of Heat and Mass Transfer*, 5th ed. New York, NY: John Wiley & Sons, 2002.

[160] M. Akoshima, K. Hata, D. N. Futaba, K. Mizuno, T. Baba, and M. Yumura, "Thermal diffusivity of single-walled carbon nanotube forest measured by laser flash method," *Jpn. J. Appl. Phys.*, vol. 48, no. 5 PART 3, p. 05EC07, 2009.

[161] J. Hone, M. Whitney, C. Piskoti, and a. Zettl, "Thermal conductivity of single-walled carbon nanotubes," *Phys. Rev. B*, vol. 59, no. 4, pp. R2514–R2516, Jan. 1999.

[162] K. Sato, T. Shiraiwa, T. Maruyama, and S. Naritsuka, "Effect of buffer thickness on single-walled Carbon Nanotube Growth Using Aluminum Oxide Buffer Layer with Alcohol Gas Source Method," *J. Nanosci. Nanotechnol.*, vol. 10, pp. 3929 – 3933, 2010.

[163] W. Ma, T. Miao, X. Zhang, L. Yang, A. Cai, Z. Yong, and Q. Li, "Thermal performance of vertically-aligned multi-walled carbon nanotube array grown on platinum film," *Carbon*, vol. 77, pp. 266–274, 2014.

[164] M. Fujii, X. Zhang, H. Xie, H. Ago, K. Takahashi, T. Ikuta, H. Abe, and T. Shimizu, "Measuring the Thermal Conductivity of a Single Carbon Nanotube," *Phys. Rev. Lett.*, vol. 95, no. 6, p. 065502, 2005.

[165] C. Yu, L. Shi, Z. Yao, D. Li, and A. Majumdar, "Thermal conductance and thermopower of an individual single-wall carbon nanotube.," *Nano Lett.*, vol. 5, no. 9, pp. 1842–6, 2005.

[166] Q. Li, C. Liu, X. Wang, and S. Fan, "Measuring the thermal conductivity of individual carbon nanotubes by the Raman shift method.," *Nanotechnology*, vol. 20, no. 14, p. 145702, 2009.

[167] I. Ivanov, A. Puretzky, G. Eres, H. Wang, Z. Pan, H. Cui, R. Jin, J. Howe, and D. B. Geohegan, "Fast and highly anisotropic thermal transport through vertically aligned carbon nanotube arrays," *Appl. Phys. Lett.*, vol. 89, no. 22, pp. 174–177, 2006.

[168] W. Lin, J. Shang, W. Gu, and C. P. Wong, "Parametric study of intrinsic thermal transport in vertically aligned multi-walled carbon nanotubes using a laser flash technique," *Carbon*, vol. 50, no. 4, pp. 1591–1603, 2012.

[169] X. Wang, Z. Zhong, and J. Xu, "Noncontact thermal characterization of multiwall carbon nanotubes," *J. Appl. Phys.*, vol. 97, no. 6, pp. 1–5, 2005.

[170] S. Shaikh, L. Li, K. Lafdi, and J. Huie, "Thermal conductivity of an aligned carbon nanotube array," *Carbon*, vol. 45, no. 13, pp. 2608–2613, 2007.

[171] B. T. Quinton, K. D. Leedy, J. W. Lawson, B. Tsao, J. D. Scofield, J. N. Merrett, Q. Zhang, K. Yost, and S. M. Mukhopadhyay, "Influence of oxide buffer layers on the growth of carbon nanotube arrays on carbon substrates," *Carbon*, vol. 87, pp. 175–185, 2015.

111

[172]   I. T. Barney, S. Ganguli, A. K. Roy, and S. M. Mukhopadhyay, "Improved Thermal Response in Encapsullated Phase change materials by nanotube Attachment on Encapsulating Solid," *J. Nanotechnol. Eng. Med.*, vol. 3, no. 3, 2012.

[173]   D. N. Futaba, K. Hata, T. Namai, T. Yamada, K. Mizuno, Y. Hayamizu, M. Yumura, and S. Iijima, "84% Catalyst Activity of Water-Assisted Growth of Single Walled Carbon Nanotube Forest Characterization By a Statistical and Macroscopic Approach.," *J. Phys. Chem. B*, vol. 110, no. 15, pp. 8035–8, 2006.

[174]   Y. F. Zou, Y. Haibann, H. Zhu, X. Liu, M. Li, Y. Ou, N. Yang, Y. Fan, H. Yang, H. Zhu, X. Liu, M. Li, Y. Qu, N. Yang, and G. Zou, "Metallization of Carbon Fibers with Nickel by Electroless Plating Technique.," *Metall. Mater. Trans. Part A*, vol. 38, no. 9, pp. 2148–2152, 2007.

[175] S. M. Mukhopadhyay,"Nanoscale multifunctional Materials: Science and Applications" Wiley 2012, New Jersey

Appendix A: List of Publications

- *Betty T. Quinton, et al. "Controllable CNT growth with SiO$_2$ buffer layer" submitting soon!*
- *Betty. T Quinton, et al "Thermal analysis of multi layer carbon structure" submitting soon!*
- Betty T. Quinton, Kevin Leedy, Jacob W. Lawson, Bang Tsao, James D. Scofield, Joseph N. Merrett, Qiuhong Zhang, Kevin Yost, and Sharmila M. Mukhopadhyay. "Influence of Oxide Buffer Layers on the Growth of Multi-Walled Carbon Nanotubes on Carbon Substrate." Carbon 2015
- Betty T. Quinton, Paul N. Barnes, Chakrapani V. Varanasi, Jack Burke, Bang-Hung Tsao, Kevin J. Yost, and Sharmila M. Mukhopadhyay. "A Comparative Study of Three Different Chemical Vapor Deposition Techniques of Carbon Nanotube Growth on Diamond Films." Journal of Nanomaterials 2013
- Betty T. Quinton, Q. Zhang, J. Burke, K. Leedy, B. Tsao, J. Scofield, J.N. Merrett, K. Yost, J. Lawson, S. M. Mukhopadhyay. "The Effect of Surface Treatments on the Growth of CNTs on 3-Dimensional Carbon foam Structure." NSTI-Nanotech 2013
- C. Varanasi, J. Petry, L. Brunke, B.T.Yang, W. Lanter, J. Burke, H. Wang, J.S. Bulmer, J. Scofield, P.N. Barnes. "Growth of high quality carbon nanotubes on free standing diamond substrates." Carbon 48, 9, 2010

Appendix B: Preliminary Thermal analysis on carbon samples

B.1: Initial Thermal Testing

In addition to the thermal analysis conducted on HOPG samples, Chapter 8, thermal analysis were also conducted on other carbon structure samples. However, these samples were only evaluated initially and were never used in the later part of the investigation. Appendix B will show the result from the thermal analysis conducted on these samples.

Before that CNT carpet can be controlled with confidence some thermal analysis was conducted as preliminary tests. These tests were conducted with two purposes. It was a way to understand how to operate laser flash equipment and to see if sample geometry is proper for the testing equipment. The thermal analysis investigations were conducted on different carbon substrates including: diamond, carbon foam and pressed graphite.

B.1.1 Laser Flash analysis (LFA) on Diamond

Figure 75 shows the thermal conductivity results taken from diamond substrate samples, using the LFA method. The samples tested for comparison are as the following: standard diamond sample, diamond sample coated with 5 nm nickel on diamond with CNT growth, and 10 nm nickel coated on diamond with CNT growth. The result shows that the samples with CNT did have a higher thermal conductivity value then ones that do not have CNT.
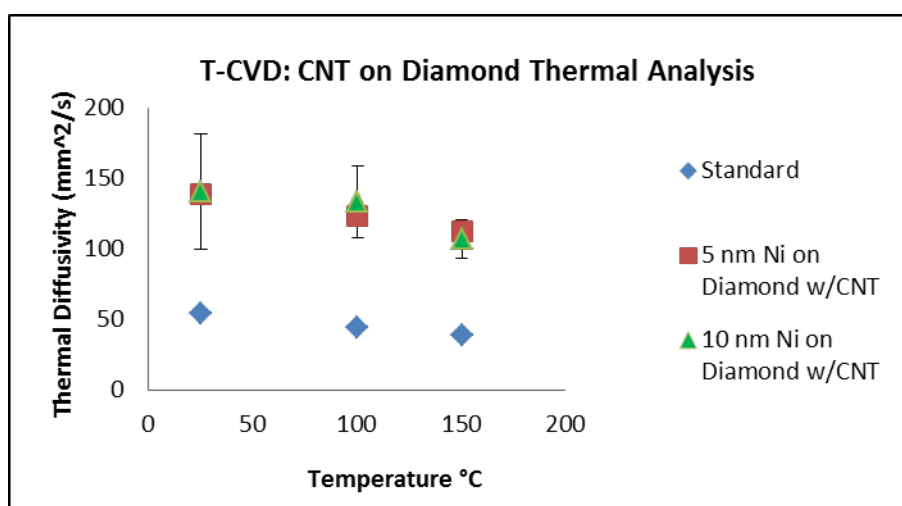

Figure 75: LFA Result on Diamond Samples

B.1.2 LFA on Foam

The porosity of the foam is usually filled by air, which is low in thermal conductivity and a poor measurement median. Therefore, in order to measure the thermal property of a carbon foam sample, with and without CNT, it was filled with epoxy prior to thermal testing. The samples shown in Figure 76 were tested as the following, a piece of epoxy, RVC foam filled with epoxy and RVC foam with CNT that is filled with epoxy. The result showed that samples with CNT did have a higher thermal diffusivity value than ones without.
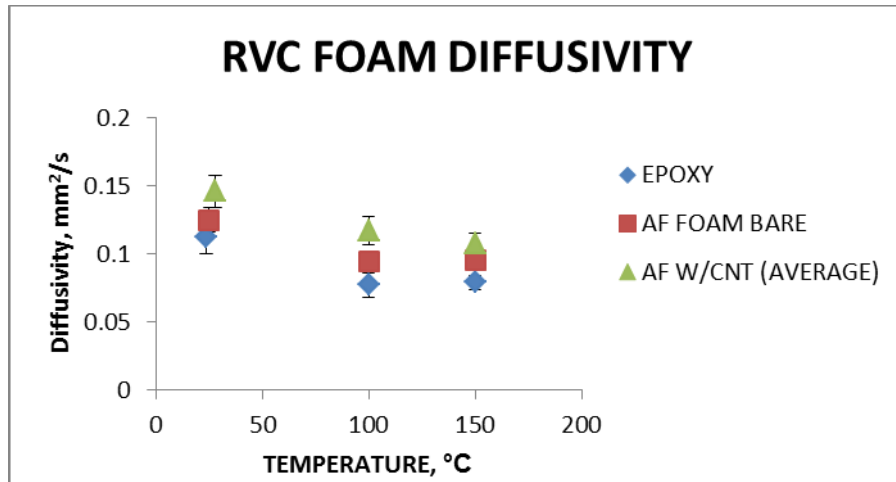
DISTRIBUTION STATEMENT A: Approved for public release. Distribution is unlimited.

Figure 76: LFA Result on RVC Samples

B.1.3 LFA on pressed graphite

The foam samples have complex geometry and high in porosity, therefore it is difficult to accurately measure thermal conductivity value contributed from the foam. One way to test thermal conductivity of the sample is by testing it on a flat sample with materials that are the same chemically. Hence pressed graphite substrates were chosen as a flat model for this test. Figure 77 shows the result measured on pressed graphite. The result shows the graphite sample with CNT have slightly higher thermal diffusivity value than samples without the CNT, however more test will be needed to see if it is significantly different.
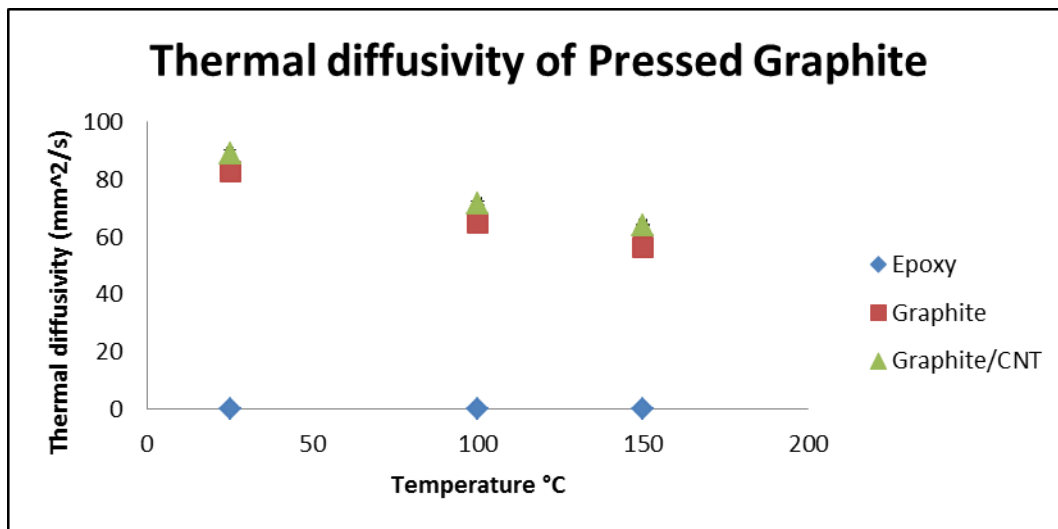

Figure 77: LFA Results on Pressed Graphite Samples

B.1.4 LFA on HOPG sandwich

It was envisioned that when CNTs are used in an application it will be in some forms of interface layer much like a thermal interface material. Because of this, sandwich configurations with CNTs imbedded in the middle was fabricated; see Figure 78 for a cross section configuration. The samples (with and without CNTs) were fabricated with oxides and the CNT sides facing each other. This way the CNT layer will be the only changing variable for the evaluation.

115

Three different sandwiches were made and they are the following:

SPI = two SPI HOPG facing each other.
SPI/Al$_2$O$_3$ = Two SPI HOPG each ALD with 10nm of Al$_2$O$_3$. The sandwich were made with Al$_2$O$_3$ facing each other.
SPI/Al$_2$O$_3$/CNT = Two SPI HOPG each ALD with 10nm of Al$_2$O$_3$ and CNTs were grown on the Al$_2$O$_3$.
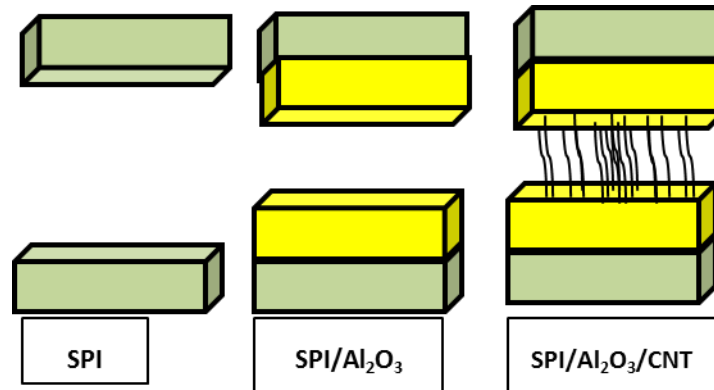The sandwich was made with CNTs facing each other.

Figure 78: LFA Results on HOPG Sandwiches

Appendix C: Thermal analysis on samples with very short CNTs

It was thought that samples with shorter CNT carpets would have better thermal resistance value. Therefore, in addition to the samples tested in section 8.2, there was another sample made for evaluation. This sample has the shortest CNT array height among the entire sample tested. Using the growth time as the control variable, the height of the array fabricated on HOPG was only 23 µm in length. Due to the shortness of the sample, accurate analysis of the sample becomes a challenge. First the amount of weight gain cannot be measured with confidence. This is because the amount of weight gain was within the measuring error of the equipment (±0.3mg). The weight of the sample is crucial for the thermal analysis since it uses this value to find the density related to the sample. The density of the sample is used by the LFA equipment for thermal diffusivity measurement. Because of this relationship, the resulting thermal diffusivity values were not measured with confidence.

Appendix D: Thermal Analysis Calculation

Nomenclature	Definition	Units
α	Thermal Diffusivity	$\dfrac{mm^2}{s}$
C_p	Specific Heat	$\dfrac{J}{g\,^{\circ}C}$
g	Mass	g
ρ	Density	$\dfrac{g}{cm^3}$
ɭ	Length	m
κ	Thermal Conductivity	$\dfrac{W}{mK}$
$κ_{array}$	Thermal Conductivity of an array of CNTs	$\dfrac{W}{mK}$
$κ_{CNT}$	Thermal Conductivity of a CNT	$\dfrac{W}{mK}$
R	Thermal Resistance with normalized area	$\dfrac{m^2K}{W}$
R_{HOPG}	Thermal Resistance of the HOPG layer	$\dfrac{m^2K}{W}$
R_{oxide}	Thermal Resistance of the oxide layer	$\dfrac{m^2K}{W}$
R_{array}	Thermal Resistance of an array of CNT	$\dfrac{m^2K}{W}$
N	# of CNT per area	$\dfrac{\#CNT}{m^2}$
d	Diameter of CNT	m

Measured
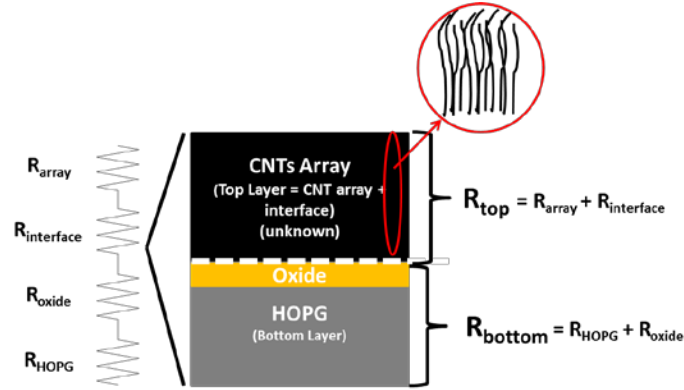- Thermal diffusivity
- Specific heat
- Mass
- Length

Equations:
- Established equations
  - $κ = \alpha * c_p * \rho$
  - $R = \dfrac{ɭ}{κ}$

- Equation used for thermal resistance layers defined

• $R_{Top} = R_{array} + R_{interface}$

• $R_{Bottom} = R_{HOPG} + R_{oxide}$

Cross-section view of a 2-layers sample

- Equation related to the investigation
• $\kappa_{Top} = \alpha_{Top} * c_{p_{Top}} * \rho_{Top}$

• $R_{Top} = \dfrac{l}{\kappa_{Top}}$

• $R_{array} = R_{Top} - R_{interface}$

- Modeled equations
• $R_{array} = \dfrac{l}{\left(N * \kappa_{cnt} * \frac{\pi}{4} * d^2\right) + \left(\kappa_{air} * \left(1 - \left(N * \frac{\pi}{4} * d^2\right)\right)\right)}$

$\kappa_{cnt} = \dfrac{\dfrac{l}{R_{array}} - \left(\kappa_{air} * \left(1 - \left(N * \frac{\pi}{4} * d^2\right)\right)\right)}{N * \frac{\pi}{4} * d^2}$

DISTRIBUTION STATEMENT A: Approved for public release. Distribution is unlimited.